DOKTORARBEIT

The Weak Coupling Method for Coupling Continuum Mechanics with Molecular Dynamics

Dissertation

zur

Erlangung des Doktorgrades (Dr. rer. nat.)

der

Mathematisch-Naturwissenschaftlichen Fakultät

der

Rheinischen Friedirch-Wilhelms-Universität Bonn

Vorgelegt von

Konstantin Fackeldey

aus

Berlin

Bonn, Februar 2009

Angefertigt mit Genehmigung der Mathematisch-Naturwissenschaftlichen Fakultät der
Rheinischen Friedirch-Wilhelms-Universität Bonn

Für meinen Stern.
Maktub.

Zusammenfassung

Für das globale Verhalten von Festkörpern in der Strukturmechanik bei nichtlinearen Prozessen sind lokale Effekte auf atomarer Ebene von wesentlicher Bedeutung. Oftmals ist eine direkte numerische Simulation des makroskopischen Verhaltens durch vollständige Auflösung der Mikroskala aus Aufwandsgründen nicht möglich.

In den letzten Jahren wurden Methoden zur Mehrskalensimulationen entwickelt, die sowohl atomistische als auch kontinuierliche Modelle innerhalb eines Simulationsgebietes verwenden. Zeitgleich können somit auf der Markoebene Finite Elemente und auf der Mikroebene eine Moleküldynamiksimulation benutzt werden.

Einer der wichtigsten Aspekte in der Mehrskalensimulation ist dabei die Konstruktion von geeigneten Transferoperatoren welche entsprechend Informationen zwischen den beiden Skalen transportieren. In dieser Doktorarbeit wird ein neuartiger schwacher Kopplungsoperator ("weak coupling operator") entwickelt, der eine Brücke zwischen atomistischen Prozessen und kontinuierlichen Modellen schafft.

Zunächst werden die Newtonschen Bewegungsgleichungen in der Moleküldynamik und die der Kontinuumsmechanik mit den jeweiligen Hamiltonschen und Lagrangeschen Energiebegriffen vorgestellt. Anschließend werden die fundamentalen Unterschiede in der Modellierung der beiden Skalen und den damit verbundenen Problemen diskutiert.

Die in der Literatur über Mehrskalenmethoden häufig beschriebenen Reflexionen ("spurious reflections"), werden untersucht und deren Ursachen erläutert. Eine Identifikation der strukturellen Merkmale der in der Literatur bisher existierenden Mehrskalenmethoden erlaubt es, eine neue Klassifikation einzuführen. Diese hebt hervor, dass alle bisherigen Mehrskalenmethoden einen punktweisen Ansatz verfolgen.

Der in dieser Arbeit entwickelte neue Kopplungsoperator basiert nicht auf einer punktweisen Auswertung sondern auf einer Mittelung. Dazu werden lokale Gewichtsfunktionen, mittels einer Partition der Eins, konstruiert. Dieser Ansatz erlaubt es nun, das Mikroskalenverschiebungsfeld mit Hilfe einer L^2 Projektion in einen hochfrequenten und niederfrequenten Teil aufzuteilen.

Mit dieser Skalendekomposition und dem neuen Transferoperator betrachten wir zunächst eine vollständige Überlappung, bei der das Gebiet mit der atomaren Modellierung eine Teilmenge des Gebietes mit der kontinuumsmechanischen Modellierung ist. Hierzu werden numerische

Beispiele in $1d$ und $2d$ präsentiert.

Alternativ zu diesem Ansatz stellen wir eine teilüberlappende Zerlegung vor, bei der die moleküldynamische und die kontinuumsmechanische Simulation in einem Teilgebiet koexistieren. Dabei werden die Freiheitsgrade aus der atomaren und die der kontinuumsmechanischen Simulation über zusätzliche Lagrange Multiplikatoren, die die Einhaltung der Nebenbedingung garantieren, gekoppelt. Der schwache Kopplungsansatz erlaubt es uns dabei, die Nebenbedingungen im Funktionenraum zu interpretieren. Dies resultiert in einer sehr effizienten Kopplung zwischen den beiden Skalen, was in $1d$, $2d$ und $3d$ Simulationen gezeigt wird.

Danksagung

Contents

Introduction

Various phenomena in material science involve processes over a wide range of length scales from the atomistic to the continuum. A deeper understanding of solids detect that the multiscale methods, i.e. the coupling of different levels of description are needed, since each individual framework is inadequate on its own at the scale in question.

Here, we consider two scales, which we associate to the continuum mechanics and the molecular dynamics. In continuum mechanics, which we refer to the *coarse* scale, atomistic details are neglected, whereas in molecular dynamics (the *fine* scale) the atoms and their mechanics are accounted for. The continuum mechanics is based on partial differential equations describing the conservation laws and the constitutive relations. This approach is impressively successful in a number of areas like solid mechanics close to equilibrium. However, this description may become inaccurate for problems in which the detailed atomistic processes affect the macroscopic behavior of the material.

Linear elasticity, as a prominent representative of a continuum mechanical description, is inaccurate when the dynamics of the system are too far from equilibrium. One reason for this can be found in the fact that it is assumed in elasticity, that the materials are homogeneous, even at the smallest scales. If the sample is large enough, this approximation is valid, since one can effectively average over the inhomogeneities. Thus, elasticity can be seen as a statistical theory. This averaging in elastic theory becomes inaccurate, if we consider smaller length scales, where the fine grained structure and its effects like thermal fluctuations determine the system inherently. The authors of [RB05] claim, that this inaccuracy appears in sizes smaller than one micro meter. Then, at these length scales, the dynamic of solids far from equilibrium comes into play.

Usually the simulation scene on the fine scale starts with a set of atoms $\mathcal{A}$ which are described as point like masses. The evaluation of this system then can either be done by energy minimization at zero temperature or by Monte Carlo methods, or by molecular mechanics. The absence of an intrinsic time scale makes the Monte Carlo method attractive for the study of equilibrium states. In molecular dynamics, the interaction between the atoms is described by an empirical inter-atomic potential, tailored to reproduce some physical properties of a given material such as the zero temperature lattice parameter and elastic constants. This method is preferable for non-equilibrium states or time dependent quantities.

However a detailed theoretical description of many macroscopic properties down to the atomistic scale, lies far beyond the current possibilities of simulations, since the final properties of

real materials depend on the interplay of chemistry, micro structural evolution, processing history, and others which show extreme complexity. The theoretical understanding of the atomic level mechanisms of deformation and failure leads to the conclusion that atomistic simulation techniques should be the most appropriate tool, representing the "basic" level of description. The drawback of the fine scale simulation is the overwhelming demand on calculation speed and the huge amount of data.

Let us elucidate this problem on an example. In Figures 0.1 an atomistic simulation of a crack can be seen. The figures show, that waves are reflected on the boundary of the simulation domain. At a first attempt one would like to enlarge the computational domain, in order to avoid this unwanted effect. However this approach often is of high computational complexity. Moreover, even a simple enlargement of the domain only delays the occurrence of reflection.
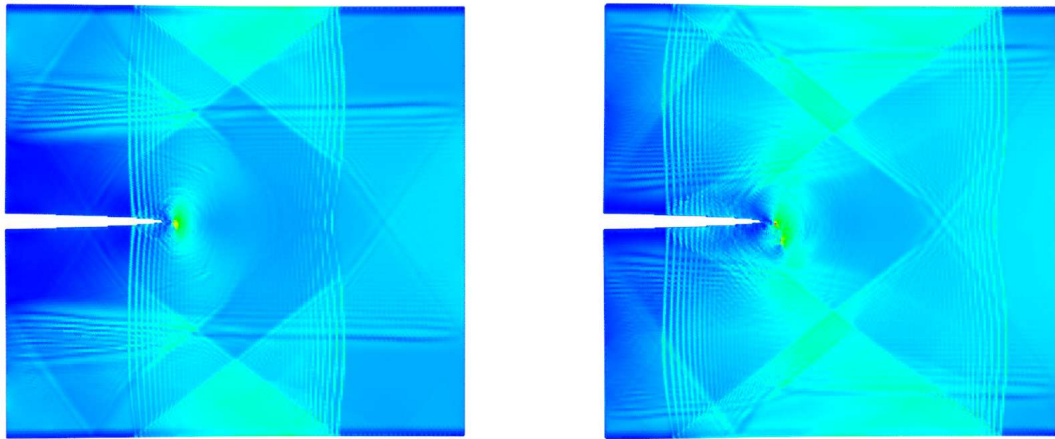
Figure 0.1: *A fully atomistic example of crack propagation in* 2 *dimensions*

Thus, employing a multiscale strategy for an efficient and accurate modelling seems favorable since by separating the problem into two different frameworks, the accuracy of a fine scale model can be combined with the advantages of a computationally efficient model. A comparably small region of atoms surrounding the crack tip is modelled by molecular dynamics. Outside of this region, far from the crack tip, we take advantage of the fact that the displacement is almost homogeneous and can thus be modelled efficiently by a linear elastic continuum dynamical simulation.

In this scenario the atomistic simulation and the continuum mechanics must make contact with each other in order to exchange information. For the decomposition of the computational domain two choices for the design of the transition zone are possible. In the first

approach an interface clearly separates the coarse and the fine scale. In contrast to those interface methods, in handshake approaches the coarse and the fine scale coexists in a subregion.

Clearly, both scales offer fundamentally different descriptions of the matter and they use different simulation methods. Whereas on the continuum scale the finite element method and a function space setting is used, the molecular dynamics is based on the movement of particles in the Euclidean space.

Additionally, dynamical simulations with a transition zone between atomistic systems and the coarser finite element mesh suffer from unwanted (spurious) reflections, since the finite element method can not represent short wave length vibrational modes.

Here we present a completely new approach, which takes advantage of an infinite dimensional function space for the information transfer between the scales. Starting from a handshake region, the key idea is to construct a transfer operator between the different scales. This transfer operator is based on local averaging taken values. In order to construct the local weight functions, a partition of unity is assigned to the molecular degree of freedom. This allows us to decompose the micro scale displacement in the handshake region into a small and large wave number part by means of a weighted L^2 projection.

This thesis is structured as follows. In the first chapter the fine scale and coarse scale is given a precise meaning, by identifying the fine scale with a molecular dynamics structure and the coarse scale with a continuum mechanics structure. A brief introduction into statistical mechanics is given to motivate the classical molecular dynamics, namely the Newton equations of motion, the Hamilton and the Lagrangian. The discussion on the structure preserving properties of the Hamiltonian equations of motion then leads to the time integration scheme. Thereby, the interaction between the atoms is described by an inter-atomic potential.

The second chapter is devoted to the "pathologies" which can occur, when continuum mechanics is coupled with molecular dynamics. More precisely, for the harmonic potential, perturbations in a crystal can be interpreted as a harmonic wave. Based on this from an analytical point of view advantageous formulation, we work out the dispersion relation which gives a relationship between the frequency and the wave number of a wave. Thereby, we explain, that a mismatch of the continuum and atomistic dispersion relation leads to reflection. Based on the harmonic structure, we can determine the amount of reflection, i.e. the reflection coefficient. At the end of Chapter 2, we consider the general problem of imposing boundary conditions in molecular dynamics. Since we confine the molecular dynamics to a bounded domain, for an atomistic simulation, non reflecting boundary conditions have to be imposed.

Outgoing from the knowledge of the two different scales from the foregoing chapters, we develop a new classification of multiscale methods. This classification is based on the

observation, that for a characterization of a multiscale method, the design of the respective handshake region or interface is crucial. As it turns out, all existing multiscale methods, coupling molecular dynamics with continuum mechanics, interpret the displacement fields in the coupling regions pointwise.

The drawbacks of a point wise approach for the coupling between the continuum mechanics and the molecular dynamics in the transition region and the great success of a weak formulation in the theory of Domain Decomposition methods, is the starting point of our method in Chapter 4. The key idea of our new method is to construct a transfer operator on the basis of weighted local averaging instead of pointwise taken values. However, this new method requires that the atomistic displacements have to be interpreted in a function space. Therefore, we assign a partition of unity to the molecular degrees of freedom.

In Chapter 5, we exploit this function space oriented interpretation of the atomistic displacement in the context of a completely overlapping decomposition. More precisely, we consider the case, when domain of the handshake region is conform with the domain of the molecular dynamics. In order to identify the displacements pertaining to the atomistic or continuum level respectively, we employ a multiscale decomposition. In particular, we decompose the micro scale displacement into a "low frequency" and a "high frequency" part in a weak sense. Several numerical examples at the end of this chapter show the good performance of this method.

In the last chapter, we match the coarse and the fine scale simulation by constraining the two displacements in the handshake region. The key issue in this context is, that our function space oriented approach allows us to interpret the constraints in a weak sense. Moreover we give numerical examples in $1d, 2d$ and $3d$ which show that this approach allows molecular displacements for entering into the continuum domain and the other way round flawlessly.

1 Physical Fundamentals

Real materials have various kinds of mechanical behavior. In the classical context one decides between fluids (liquids and gases) and solid states. In the context of change of volume, both classes show a similar behavior, whereas their behavior in change of the form is quite different. More precisely, in contrast to solids the fluids show much less resistance (viscosity) to a change of form since they flow. However, this difference is only quantitatively, since the solid can also flow on a long time scale, i.e. solids have a higher viscosity. Materials which can not be categorized into fluids or solid states are called "soft matter", an example are emulsions.

In this thesis, we consider the multiscale behavior of solid states. More precisely, we are interested in crystalline materials and their different behavior over a wide range of length scales. This requires the knowledge and understanding of what is happening in a material from the continuum mechanics scale down to the atomistic scale.

In the description of the continuum, details on the atomistic scale are neglected. We refer to this continuum scale as the *coarse scale*.

Since for a multiscale material understanding the mechanics of atoms in the material has to be taken into account, we also consider the atomistic level, to which we refer as the *fine scale*. Here, empirical models are used, in order to describe the interactions between the atoms.

For the further understanding in the coupling of the coarse and the fine scale, in this chapter the fundamental properties of molecular dynamics (MD) and continuum mechanics (CM) are explained. Moreover, since we are interested in the computational problem, we also introduce the respective discretizations.

1.1 Equations of Motion in the Molecular Setting

The material behavior on the micro scale is now modelled by means of an isolated system of atoms or molecules of a crystalline solid. We identify each of the atoms in their reference position with a point $X_\alpha \in \mathbb{R}^d$, $\alpha \in \mathcal{A}$, where $\mathcal{A}$ is an index set. Under the influence of external and internal forces, the atoms displace in space. The position $\hat{X}_\alpha$ of the α-th atom in a deformed configuration is then given as

$$\hat{X}_\alpha = X_\alpha + q_\alpha \,, \tag{1.1}$$

where q_α is the displacement of atom α.

More Approximations
Long Times
Many Empirical Parameters
Classical Dynamics

Continuum Models

Empirical Potentials

Tight Binding

Density Functional Theory

Many Electron Density

Quantum Effects
Less Parameters (Adjustable)
Less Approximations
Short Times
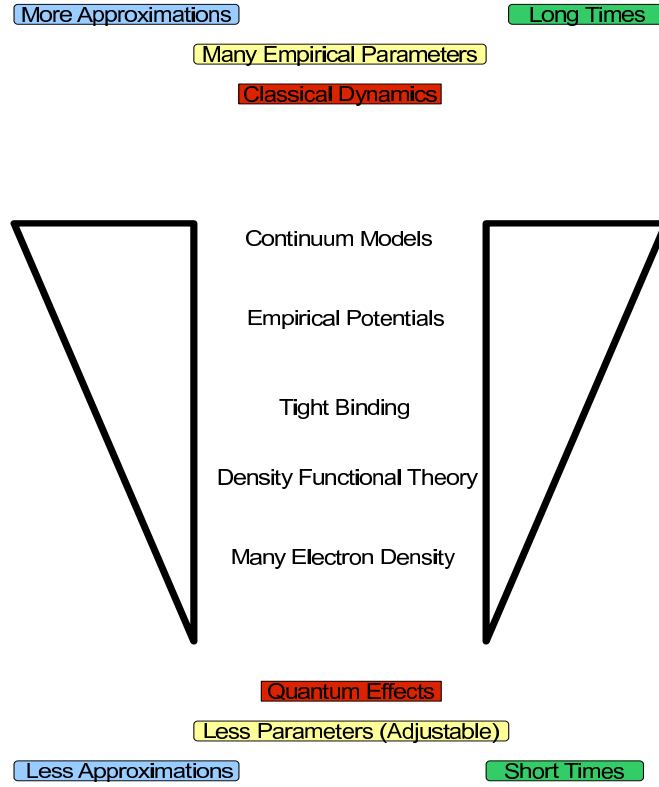
Figure 1.1: *The different physical and modelling scales.*

The atomic displacements $q = (q_\alpha)_{\alpha \in \mathcal{A}}$ are assumed to obey Newton's law of motion

$$M_{\mathcal{A}} \ddot{q} = F^{\text{internal}} + F^{\text{external}}, \qquad (1.2)$$

where F^{internal} and F^{external} are the internal and external forces. With each atom α, we associate the mass $m_\alpha > 0$, such that

$$M_{\mathcal{A}} = \text{diag}(m_\alpha \text{Id}_{\mathbb{R}^{d \times d}})_{\alpha \in \mathcal{A}} \qquad (1.3)$$

is the mass matrix on the micro scale. In case a potential V is given, the internal forces acting on a conservative system can be obtained as $F^{\text{internal}} = -\nabla_{\hat{X}} V(\hat{X})$.

Statistical Mechanics   The system in (1.2) has $d|\mathcal{A}|$ degrees of freedom. For a better further description, we define the *phase space* of the $d|\mathcal{A}|$-body problem as the $2d|\mathcal{A}|$ dimensional set consisting of all possible positions $X = (X_1, ..., X_{|\mathcal{A}|})^T$ and linear momenta

$p = (p_1, ..., p_{|\mathcal{A}|})^T$ of the particles, where the latter are defined by

$$p = M_{\mathcal{A}} \dot{q}.$$

Then a single variable in the phase space Γ is given by

$$z := (q, p)^T,$$

where $q, p \in \mathbb{R}^{|\mathcal{A}|}$ and $z \in \mathbb{R}^{2d|\mathcal{A}|}$.

Let us now assume, that we are not especially interested in the positions and velocities of the system, but macroscopic quantities (e.g. temperature), which are calculated from the atomistic configuration. Then it is adequate to consider only the phase space density $\rho(z)$. It is a probability density, that gives the probability of finding a system of $|\mathcal{A}|$ atoms in a given region of the phase space. For the integration over the whole space, we get

$$\int \rho(z) \, dp dq = 1 \, , \;\; z = (p, q).$$

Since systems of atoms can neither be destroyed nor be created, the total derivative of the density is zero, i.e.

$$\frac{d\rho}{dt} = \frac{\partial \rho}{\partial t} + \sum_{\alpha \in \mathcal{A}} \left(\dot{q}_\alpha \frac{\partial \rho}{\partial q_\alpha} + p_\alpha \frac{\partial \rho}{\partial p_\alpha} \right) = 0.$$

This is also known as the *Liouville theorem*.

Let us consider an *ergodic system*, that is, when the density ρ in every point z in the phase space does not change in time, i.e. $\frac{\partial \rho}{\partial t} = 0$. Then the ergodic hypothesis for such a system states, that the time average is equal to the ensemble average. Here, an ensemble is a collection of points z in the phase space.

As a consequence, for a system in equilibrium, computations either from the time average or from the phase space average can be used. In MD averages are computed from the time average on a comparably long time, whereas Monte Carlo simulations base on the ensemble averaging.

A micro canonical ensemble or NVE ensemble [1] is a closed system with the invariants volume, energy and number of particles. The measurements in classical mechanics are equivalent to the averages over the micro canonical ensemble.

For a subsystem which has an energy exchange, the invariants are the temperature T, the number of particles and the volume (NVT ensemble). For a given temperature T, the probability, that a certain position state of the particles occurs, is proportional to $e^{-E/(Tk_B)}$, where k_B is the Boltzmann constant and E the total energy of the system. For T approaching zero, only the global minimum has a significant density in the ensemble, whereas for increasing T the position states get more equally distributed.

---

[1] Here NVE stems from the notation, since N is the number of particles, V is the volume and E is the energy

The temperature T is given as the average over instantaneous temperature $\hat{T}$

$$\hat{T} = \frac{1}{dnk_B} \sum_{\alpha \in \mathcal{A}} \frac{p_\alpha^2}{m_\alpha}.$$

Remark In many applications, the error induced by neglecting the temperature in the development of a model is not significantly compared to the errors inherent in the model of the inter-atomic potential, which we introduce in the forthcoming.

Hamilton and Lagrange Description   In the Hamiltonian formulation of Newtonian mechanics (1.2) is reduced to a system of first order.

Then, for the Newtonian mechanics, the differential equations

$$\frac{d}{dt}q = M_{\mathcal{A}}^{-1}p \quad \text{and} \quad \frac{d}{dt}p = -\nabla_q V(q), \tag{1.4}$$

are a Hamiltonian system with the *Hamiltonian*

$$\mathcal{H}^{\text{MD}}(q,p) = \mathcal{T}^{\text{MD}} + \mathcal{U}^{\text{MD}} := \frac{p^T M_{\mathcal{A}}^{-1}p}{2} + V(q), \tag{1.5}$$

where the potential part is $\mathcal{U}^{\text{MD}} = V(q)$ and

$$\mathcal{T}^{\text{MD}} := \frac{1}{2}p^T M_{\mathcal{A}}^{-1}p \tag{1.6}$$

is the kinetic part of the energy. This Hamiltonian is constant in time, in the sense, that for solutions along $(q(t), p(t))$ of (1.4) we have

$$\frac{d}{dt}\mathcal{H}^{\text{MD}}(q(t), p(t)) = p^T M_{\mathcal{A}}^{-1}\dot{p}(t) + \dot{q}(t)^T \nabla_q V(q(t)) = 0.$$

In order to rewrite (1.4) in a more compact form, we furthermore introduce the $2|\mathcal{A}| \times 2|\mathcal{A}|$ canonical structure matrix J

$$J := \begin{pmatrix} 0 & I_{|\mathcal{A}|} \\ -I_{|\mathcal{A}|} & 0 \end{pmatrix}.$$

With the above definition we can rewrite the Hamiltonian equation by

$$\frac{d}{dt}z = J\nabla_z \mathcal{H}^{\text{MD}}(z). \tag{1.7}$$

Under the assumption, that the potential energy V is smooth, there exists at least locally through any point $(q^0, \dot{q}^0)$ of the phase space a unique trajectory of the mechanical system, which is the solution of (1.2) with the initial conditions $q(0) = q^0$ and $\dot{q}(0) = \dot{q}^0$. In the phase space, this means, that the exact flow $\Phi_\tau : \Gamma \to \Gamma$ maps the initial conditions $z(0) = z^0$ to $z(\tau) = \Phi_\tau(z^0)$, where $z(t)$ is the initial solution of (1.7) for initial conditions z^0. It is

a main structure preserving invariant, that the flow Φ_τ is *symplectic*, which is defined as the conservation property

$$(D\Phi)^T J (D\Phi) = J \tag{1.8}$$

for all τ and where $D\Phi$ is the Jacobian of the Hamiltonian flow. It can be illustrated or interpreted as "area preserving" (see Figure 1.2).
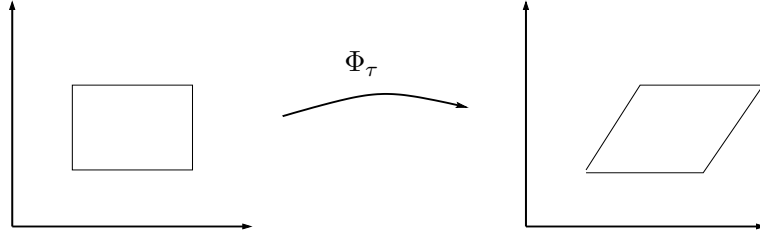
Figure 1.2: *An example of the area preserving property of the mapping Φ_τ.*

Summing up, (1.7) describes a system by its $2|\mathcal{A}|d$ degrees of freedom, the positions and the momenta of each atom in each coordinate direction. Later on in this chapter we will refer to this formulation.

We also introduce another way for describing the atomistic system, namely the Lagrangian. It is defined by

$$\mathcal{L}^{\mathrm{MD}}(q_\alpha(t), \dot{q}_\alpha(t)) = \mathcal{T}^{\mathrm{MD}}(q_\alpha(t), \dot{q}_\alpha(t)) - \mathcal{U}^{\mathrm{MD}}(q_\alpha(t)). \tag{1.9}$$

The Lagrange equations of motion are obtained by Hamilton's principle. It states that the true evolution $q(t)$ of a system between two specified states $q(t_1)$ at time $t = t_1$ and $q(t_2)$ at time $t = t_2$ is a stationary point of the action functional

$$S(q(t)) := \int_{t_1}^{t_2} \mathcal{L}^{\mathrm{MD}}(q(t), \dot{q}(t)) \, dt, \tag{1.10}$$

where $\mathcal{L}^{\mathrm{MD}}(q(t), \dot{q}(t))$ is given by (1.9).

To show this, let $\varepsilon(t)$ be a small perturbation that is zero at the endpoints of the trajectory. A first variation of the action functional gives

$$\delta S = \int_{t_1}^{t_2} \left[\mathcal{L}^{\mathrm{MD}}(q(t) + \varepsilon(t), \dot{q}(t) + \dot{\varepsilon}(t)) - \mathcal{L}^{\mathrm{MD}}(q(t), \dot{q}(t)) \right] dt$$

$$= \int_{t_1}^{t_2} \left(\varepsilon(t) \cdot \frac{\partial \mathcal{L}^{\mathrm{MD}}(q(t), \dot{q}(t))}{\partial q(t)} + \dot{\varepsilon}(t) \cdot \frac{\partial \mathcal{L}^{\mathrm{MD}}(q(t), \dot{q}(t))}{\partial \dot{q}(t)} \right) dt + o(\varepsilon^2),$$

where we have expanded the Lagrangian $\mathcal{L}(q(t), \dot{q}(t), t)$ to first order in the perturbation $\varepsilon(t)$. After integrating by parts, the boundary condition causes the boundary term to vanish and we

obtain

$$\delta S = \int_{t_1}^{t_2} \varepsilon(t) \cdot \left(\frac{\partial \mathcal{L}^{\mathrm{MD}}(q(t), \dot{q}(t))}{\partial q(t)} - \frac{d}{dt} \frac{\partial \mathcal{L}^{\mathrm{MD}}(q(t), \dot{q}(t))}{\partial \dot{q}(t)} \right) dt.$$

As we have already mentioned in Hamiltonian's Principle it is required, that the first variation vanishes for all ε. This is satisfied if and only if

$$\frac{d}{dt} \left(\frac{\partial \mathcal{L}^{\mathrm{MD}}(q_\alpha(t), \dot{q}_\alpha(t), t)}{\partial \dot{q}_\alpha(t)} \right) = \frac{\partial \mathcal{L}^{\mathrm{MD}}(q_\alpha(t), \dot{q}_\alpha(t))}{\partial q_\alpha(t)}, \tag{1.11}$$

which is known as the *Lagrangian equations of motion*. It can be shown, that the Lagrangian equations (1.11) are equivalent to the Hamiltonian (1.5).

Having now introduced the equations of motion and in particular the term symplectic it seems natural to consider the time discretization.

Time integration   Time integration algorithms are based on finite difference methods, where the time is discretized on a finite grid. The distance between the consecutive point on the net is given by Δt. With given value and derivative at time t an integration scheme gives the same quantities at time $t + \Delta t$. However, since this iteration is an approximation of the time evolution truncation and rounding errors are associated with them.

In contrast to the rounding errors, which are associated to a particular implementation of the algorithm, the truncation errors are intrinsic to the algorithm. More precisely, truncation errors are related to finite difference methods, which are usually based on a Taylor expansion truncated at some term.

Here, we only briefly outline the error analysis and address to [DB02] for further details. Of course, in MD the large number of atoms is a challenging task. On the one hand, implicit methods like implicit Runge-Kutta methods are too expensive. On the other hand, for a stable explicit integrator the time step Δt has to be very small.

Moreover, MD also suffer from the *Lyapunov instability*:
For an initial state $z(0)$ and a perturbated intial state $z^*(0)$, the error $\|z(t) - z^*(t)\|$ depends exponentially on the length of the trajectory.

All these facts make the time integration in MD challenging. One important aspect of the Hamiltonian equation of motion is the *symplecticity*. A numerical integrator $\Psi_{\Delta t}$, that is a discretization with time step Δt of Φ_τ is symplectic, if for a one step computation

$$\left(\frac{\partial \Psi_{\Delta t} z(0)}{\partial z(0)} \right)^T J \left(\frac{\partial \Psi_{\Delta t} z(0)}{\partial z(0)} \right) = J,$$

and thus it is area preserving like the continuous flow Φ_τ. Further analysis on the symplectic structure of MD is investigated in [HZ98].

The above observations of the Hamiltonian system have important implications for the numerical treatment of the symplectic structure of Hamiltonian mechanics.

In order to obtain a symplectic method, we decompose the Hamiltonian given by (1.5) into

$$\mathcal{H}_1 = \frac{1}{2}V(q), \qquad \mathcal{H}_2 = \frac{1}{2}p^T M_{\mathcal{A}}^{-1}p, \qquad \mathcal{H}_3 = \frac{1}{2}V(q).$$

For $\mathcal{H}_1$ the associated equations are

$$\dot{p} = -\frac{1}{2}\nabla_q V(q), \qquad \dot{q} = 0$$

which can be solved analytically:

$$p(t) = p(0) - \frac{t}{2}\nabla_q V(q), \qquad q(t) = q(0).$$

It is easy to see, that the flow $\Phi_{\mathcal{H}_1,\Delta t}$ for some time step size Δt is equal to $\Phi_{\mathcal{H}_3,\Delta t}$, thus we consider $\Phi_{\mathcal{H}_2,\Delta t}$:

$$p(\Delta t) = p(0), \qquad q(\Delta t) = q(0) + \tau M_{\mathcal{A}}^{-1}p(0).$$

Applying the conjunction

$$\Phi_{\Delta t} := \Phi_{\Delta t, \mathcal{H}_3} \circ \Phi_{\Delta t, \mathcal{H}_2} \circ \Phi_{\Delta t, \mathcal{H}_1}$$

on some starting point at time step n, which is given by (q^n, p^n) leads to (q^{n+1}, p^{n+1}). This is exactly equivalent to the widely used Störmer-Verlet [Ver67, SABW82] algorithm.

The Störmer-Verlet can be written in the following form:

Algorithm 1.1.1 (Störmer-Verlet)

$$p^{n+1/2} = p^n - \frac{\Delta t}{2}\nabla_q V(q^n)$$

$$q^{n+1} = q^n + \Delta t\, M^{-1}p^{n+1/2}$$

$$p^{n+1} = p^{n+1/2} - \frac{\Delta t}{2}\nabla_q V(q^{n+1}).$$

The evaluation of the three steps in Algorithm 1.1.1 is successive, thus the scheme is completely explicit, since no nonlinear system has to be solved. The velocities in the Störmer-Verlet algorithm can be eliminated to obtain the following two-step method in the displacements q only, i.e.

$$M\frac{q^{n+1} - 2q^n + q^{n-1}}{\Delta t^2} = -\nabla_q V(q^n),$$

which is known as *leap frog* scheme.

For more details in simulating dynamical systems under the aspect of molecular models, we refer to the book [LR04] and to [LRS96].

Potential   So far we have done no further investigation on the potential introduced in (1.2). However, from the atomistic point of view, the inter-atomic interaction is an important issue. The various atomistic methods can be classified by their different calculation of the inter-atomic forces. In the literature several different potentials which describe the inter atomic interactions can be found. These potentials often vary in their accuracy in describing the quantum mechanics. An example of an accurate potential is the density functional theory [Sri97] where the full quantum mechanical equations are solved to calculate the force. However, even with nowadays affordable computer power only very short time scales and very short length scales can be simulated. Thus, it seems reasonable to reduce these models in order to decrease computational complexity.

Most of the multibody potentials are empirical descriptions of the binding on the quantum mechanical level. Here, the potential V is composed of a sum of different heterogeneous nonlinear contributions, which depend on the distances. Moreover, they can vary in their relative intensity and their functional form. More precisely, contributions to the potential can stem from interactions between $(1, 2, .., |\mathcal{A}|)$ particles, i.e.

$$V(X_1, ..., X_{|\mathcal{A}|}) = \sum_{\alpha} V_1(X_\alpha) + \sum_{\alpha,\beta>\alpha} V_2(X_\alpha, X_\beta) + \sum_{\alpha,\beta>\alpha,\gamma>\beta} V_3(X_\alpha, X_\beta, X_\gamma) + ... $$

The advantage of multibody potentials is that their computational burden is by orders of magnitude less than the one in quantum mechanics. More precisely, in classical MD where an empirical potential is assumed, length and time scales in the range of micrometers and nanoseconds can be reached [AWG+02, Abr86]. Of course these length scales are large compared to the quantum mechanical length scales.

In this thesis we are interested in the mechanical properties of materials from the classical MD scale up to the continuum scale. A special class of multibody potentials are the pair potentials. Here, it is assumed, that the force between the atoms can be described by a function which only depends on the distance between the corresponding atoms. In this context we understand the terms local (short range) as a potential which effectively only involves contributions from nearby particles, otherwise we call them long range. It has been understood that for some materials (e.g. argon) and some interactions (e.g. Coulomb interaction) the forces can be best described by pair potentials [Rah64][2]. The authors of [aBKvS90] showed, that even more complex materials like silica can be well described by a pair potential. In general, for pair

---

[2]The reference [Rah64] is also one of the first molecular dynamic studies.

potentials, the potential energy is given by

$$V_2 = \sum_{\beta=1}^{|\mathcal{A}|} V_2(X_\alpha, X_\beta),$$

where $r_{\alpha\beta} = \|q_\alpha - q_\beta\|$ is the absolute separation distance between two particles q_α and q_β.

The harmonic potential   The harmonic potential is probably the simplest radial symmetric body potential. It is given by

$$V(r_{\alpha\beta}) = C(r_{\alpha\beta} - c)^2 \tag{1.12}$$

For small $r_{\alpha,\beta}$ the harmonic potential is a quite accurate approximation of sufficiently smooth pair potentials. This potential is for the simulation of metal improper. For the first an explicit knowledge of the neighborhood is required. For the second, modeling unbounded atoms, we need that the force goes to zero for $r_{\alpha\beta} \to \infty$, whereas in the harmonic potential the attractive forces become infinite.

However it is attractive for analytical reasons, since (1.12) is quadratic and thus linear in the equation of motion formulation. In the next subsection on crystalline structures we exploit this advantageous structure for a rigorous analysis.

The Lennard-Jones Potential   A prominent and widely used example of pair potentials is the Lennard-Jones potential [LJ24]. This short range potential is given by ($\sigma, \varepsilon > 0$)

$$V_{\mathrm{LJ}}(r_{\alpha\beta}) = \varepsilon \left[\left(\frac{\sigma}{r_{\alpha\beta}} \right)^{12} - \left(\frac{\sigma}{r_{\alpha\beta}} \right)^6 \right]. \tag{1.13}$$

Here, σ is called the collision diameter, it is the distance of two atoms, at which $V_{\mathrm{LJ}} = 0$. The value ε corresponds to the minimum of the potential located at the equilibrium distance $r_0 = 2^{1/6}\sigma$. From the physical point of view it can be interpreted as the amount of work, that needs to be done, in order to move the interacting particles apart from the equilibrium distance r_0. The first term in (1.13) is the atomic repulsion, which dominates for small distances ($r_{\alpha\beta} < \sigma$). The second term in the Lennard-Jones potential is the bonding term and is clearly weaker than the other. In Figure 1.3 it can be clearly seen, that the potential is singular where particle positions overlap and the bonding term for e.g. $r/\sigma = 2.5$ is negligible.

In general the interactions in a pair potential include all pairs of atoms, regardless of their distance. However, since the energy decays like r^{-6} the forces outside some critical radius (*cut off radius*) r_{cut} are small and are thus neglected in practice , i.e.

$$V(r_{\alpha\beta}) \approx V_{\mathrm{cut}}(r_{\alpha\beta}) = \begin{cases} \varepsilon \left[\left(\frac{\sigma}{r_{\alpha\beta}} \right)^{12} - \left(\frac{\sigma}{r_{\alpha\beta}} \right)^6 \right] & r_{\alpha\beta} \leq r_{\mathrm{cut}} \\ 0 & r_{\alpha\beta} > r_{\mathrm{cut}} \end{cases}.$$

With a given cut off radius the force acting on particle α for the Lennard-Jones potential is given by

$$F_\alpha \approx 24\varepsilon \sum_{\substack{\alpha=1 \\ 0 < r_{\alpha\beta} \leq r_{\text{cut}}}}^{|\mathcal{A}|} \frac{1}{r_{\alpha\beta}} \left(\frac{\sigma}{r_{\alpha\beta}}\right)^6 \left(1 - 2\left(\frac{\sigma}{r_{\alpha\beta}}\right)^6\right) \mathbf{r}_{\alpha\beta},$$

where $\mathbf{r}_{\alpha\beta} = X_\beta - X_\alpha$.
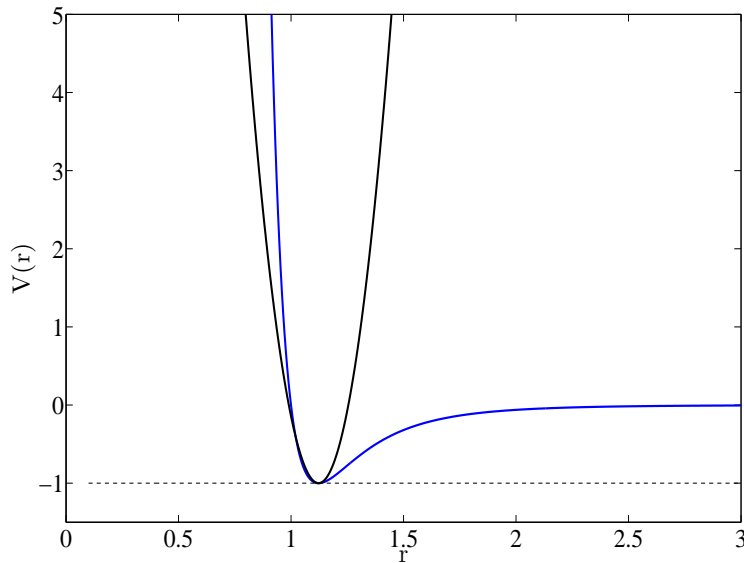
Figure 1.3: *The Lennard-Jones potential (blue) compared with the harmonic potential (black).*

1.2 Crystalline Structures

In many solids, the particles are arranged in regular, systematic patterns. When this happens the solids are said to be in crystalline state, or to be a crystalline solid. Their structure, that is characteristic of the substance is then called crystal structure, formed by a regular repetitive crystal lattice.

A crystal lattice can be described in terms of small repeating three-dimensional segments called unit cells. Arranging these unit cells periodically into space results in plane faces and definite angles between the faces. Such characteristics begin in molecular dimensions and repeat accordingly as the crystal grows up to macroscopic sizes. Common examples are crystals of sodium chloride (table salt), quartz and diamond. Solids that do not present that regularity

(called symmetry) are amorphous solids.

In other words, crystalline solids are a class of solids that have regular or nearly regular crystalline structures. This means that the atoms in these solids are arranged in an orderly manner. Though glass is a solid, it is not crystalline because the silica units are not boned to each other in a regular, uniform, repeatable array. The essence of crystallinity is the description of the regular geometrical arrangement of atoms in space.

In nature the finite regular arrangements of the atoms of crystals is never perfect, however this is neglected to describe the crystals by a lattice. The smallest part of the lattice whose spatial repetition forms the entire lattice is called primitive cell.
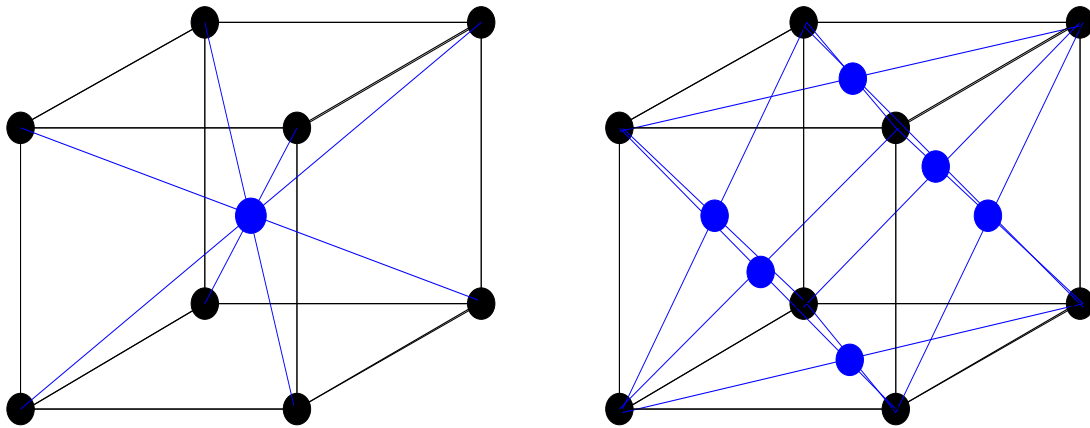
Figure 1.4: *Left: A bcc lattice. Right: A fcc lattice.*

A Bravais lattice is an infinite set of points generated by a set of discrete translation operations. In $d = 3$ we have 14 lattices which are distinguished by the symmetry of their point groups. They are classified into seven different crystal systems. Here we consider the cubic crystal system consisting of three different types, i.e. the simple cubic (sc), the body centered cubic (bcc) and the face centered cubic (fcc). In Table 1.1, some examples for materials, which can be modeled by a bcc or a fcc lattice are shown.

lattice type	Element
bcc	Li (at room temp.), Na, K, V, Cr, Fe, Rb, Nb, Mo, Cs, Ba, Eu, Ta
fcc	Al, Cu, Ni, Sr, Rh, Pd, Ag, Ce, Tb, Ir, Pt, Au, Pb, Th

Table 1.1: *Elements modeled by bcc or fcc lattices*

We remark that there are also materials which can be modeled by a fcc as well as a bcc grid. The total energy of a crystal is the sum over all individual atom-atom interactions in the crystal, however this summation is computationally almost impossible. For example, $1mm^3$ of bulk material contains approximately 10^{19} atoms. Thus, further simplifications have to be done. Under the assumption, that the binding forces of the lattice are small compared to the lattice

Figure 1.5: *Left: A cube with bcc structure. Right: A cube with fcc structure.*

distance, the forces can be considered as *harmonic*. For ease of notation we consider the case, that every cell has one particle. At the temperature of 0 K the average force on each atom is zero, which is equivalent to the equilibrium state. It is defined by

$$
\frac{\partial V}{\partial \mathbf{r}} = \sum_{\alpha,\beta \in \mathcal{A}} \frac{\partial V_{\alpha\beta}}{\partial r_{\alpha\beta}} \frac{\partial r_{\alpha\beta}}{\partial r_0} = 0. \tag{1.14}
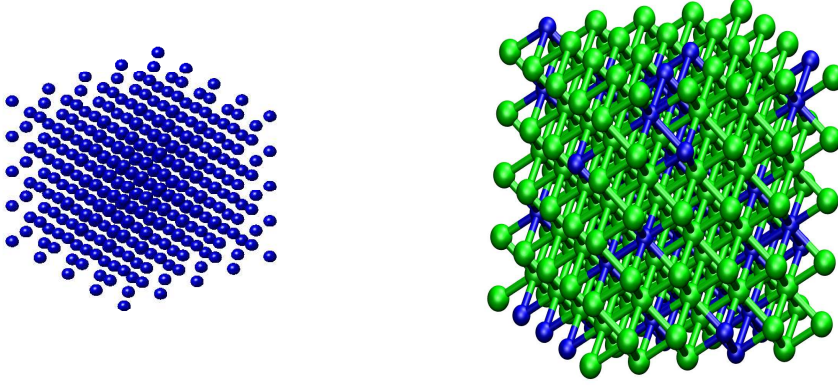$$

Let us recall, that the errors introduced by the temperature assumption are often comparably small to the errors inherent in the inter-atomic potential. If the system is not in equilibrium, the total energy can be expanded in the deviation q_α from the equilibrium position,

$$
V(\mathbf{r}) \approx V(\mathbf{r}) + \sum_{\alpha,d_1} \left.\frac{\partial V}{\partial X_{\alpha,d_1}}\right|_{\hat{X}} q_{\alpha,d_1} + \frac{1}{2} \sum_{\alpha,\beta,d_1,d_2} \left.\left|\frac{\partial^2 V}{\partial X_{\alpha,d_1}\partial X_{\beta,d_2}}\right.\right|_{\hat{X}} q_{\alpha,d_1} q_{\beta,d_2} + ... \tag{1.15}
$$

where α, β are the indices for the particles and d_1, d_2 are the spatial directions.

The second term in (1.15) has to vanish, since in equilibrium the energy attains its minimum, i.e. (1.14). Thus, the third term of (1.15) is the leading one for the force. The component in direction d_1 of the force F_α on particle α is:

$$
\begin{aligned}
F_{\alpha,d_1} = -\frac{\partial V}{\partial q_{\alpha,d_1}} &= -\frac{1}{2}\sum_{\beta,d_2} \left(\left.\left|\frac{\partial^2 V}{\partial X_{\alpha,d_1}\partial X_{\beta,d_2}}\right.\right|_{\hat{X}} q_{\beta,d_2} + \left.\left|\frac{\partial^2 V}{\partial X_{\beta,d_2}\partial X_{\alpha,d_1}}\right.\right|_{\hat{X}} q_{\beta,d_2} \right) \\
&= -\sum_{\beta,d_2} \left.\left|\frac{\partial^2 V}{\partial X_{\alpha,d_1}\partial X_{\beta,d_2}}\right.\right|_{\hat{X}} q_{\beta,d_2} =: -\sum_{\beta,d_2} K_{\alpha\beta,d_1 d_2} q_{\beta,d_2} = \left(-\sum_\beta K_{\alpha\beta} q_\beta \right)_{d_1}.
\end{aligned}
\tag{1.16}
$$

Figure 1.6: *The linear chain in* $1d$.

The symmetric $3|\mathcal{A}| \times 3|\mathcal{A}|$ matrix K is called *harmonic or lattice stiffness matrix*, its components $(K_{\alpha\beta})_{d_1 d_2}$ describe the force constants. The matrix K is positive definite, since the relaxed position is a minimum of $V(\mathbf{r})$ with respect to the variation of all atoms in (small) arbitrary directions.

Due to the translational symmetry, the matrix entries $K_{\alpha\beta,kl}$ only depend on the number of cells between the atoms.

Roughly speaking the entries $(K_{\alpha\beta})_{d_1 d_2}$ depend on the distance and the corresponding cells. Moreover, a displacement q' of the whole crystal in an arbitrary spatial direction d_1', has no effect on the forces, i.e. for $q_{\beta,d_1} = q'\delta_{d_1' d_1}$ the force is $F_{\alpha,d_2} = 0$ and consequently $\sum_{\beta} K_{\alpha\beta,d_2 d_1'} = 0$.

Summing up, we can rewrite the equations of motion by

$$m_\alpha \ddot{q}_\alpha(t) = F_\alpha = -\sum_{\beta} K_{\alpha\beta} q_\beta. \tag{1.17}$$

Under these assumptions we can investigate the harmonic equations of motion in more detail.

The equation of motion in the one-dimensional case Let us assume that we have a linear mono-atomic chain, where each atom has a mass m and a distance of r_0 to its neighbors, see Figure 1.6. Furthermore, $V_s(r_s)$ denotes the energy between the s-th neighbors separated by distance $r_s = sr_0$. Then, in the case of a one dimensional linear chain the potential energy is given by

$$E_s = N \sum_s V_s(sr_0) + \frac{1}{2} \sum_{\alpha,s} \left(\frac{\partial^2 V_s}{\partial q^2} \right)_{r_s = sr_0} (q_\alpha - q_{\alpha+s})^2,$$

where we have neglected the non harmonic terms. The harmonic energy is given by

$$E_{\mathrm{harm},1d} = \frac{1}{2} C_s (q_\alpha - q_{\alpha+s})^2, \tag{1.18}$$

where

$$C_s := \frac{\partial^2 V_s}{\partial q^2} = \left(\frac{\partial^2 V_s}{\partial r_s^2} \right)_{r_s = sr_0}.$$

Here, assume that the two ends of the chain are joined, in order to account for the problem that the atoms $\alpha = 1$ and $\alpha = |\mathcal{A}|$ only have one neighbor each. This is also known as the *Born-von Kármán periodic boundary condition* [BvK12, BvK13].

Then for this one dimensional case the matrix K of (1.17) is simplified to

$$K_{\alpha(\alpha+s)} = \frac{\partial^2 V}{\partial q_\alpha \partial q_{\alpha+p}} = -C_s = \frac{\partial^2 V}{\partial q_{\alpha+s} \partial q_\alpha} = K_{(\alpha+s)\alpha}$$

and

$$K_{\alpha\alpha} = \frac{\partial^2 V}{\partial q_\alpha \partial q_\alpha} = 2C_s \,, \; \frac{\partial^2 V}{\partial q_\alpha \partial q_\beta} = K_{\alpha\beta} = 0 \text{ else.}$$

Inserting this into (1.17) we obtain

$$f_\alpha^{\text{harm}} = m\frac{\partial^2 q_\alpha}{\partial t^2} = -\frac{\partial E_{\text{harm}}}{\partial q_\alpha} = -\sum_p C_p(2q_\alpha - q_{\alpha-p} - q_{\alpha+p}). \tag{1.19}$$

Later on we exploit some advantageous properties of this expression.

Linked Cell Method   The force evaluation for each particle even with a small cut off radius involves all particles within the cut off radius. In general the set $\mathcal{A}$ contains a large number of atoms and a naive approach for summing up the forces is an algorithm with $\mathcal{O}(|\mathcal{A}|^2)$. Here we introduce the linked cell method [GKZC04], which reduces the computational complexity from $\mathcal{O}(|\mathcal{A}|^2)$ to $\mathcal{O}(|\mathcal{A}|)$.

In the linked cell method, the simulation domain is subdivided into uniform subset (cells). The size of the cells is chosen as r_{cut}, such that only the interaction with particles on neighboring cells is considered. The force on particle α in cell Z_j is given given by

$$F_\alpha = \sum_{\substack{\text{cell} Z_i \\ Z_i \in \mathcal{N}(Z_j)}} \sum_{\substack{\beta \in \{\text{Particle of cell } Z_j\} \\ \beta \neq \alpha}} F_{\alpha\beta},$$

where $\mathcal{N}(Z_j)$ denotes the direct neighboring cells and cell Z_j itself. In $3d$ a cell has 26 neighbors. The complexity of the calculation of the forces in the crystal is $C|\mathcal{A}|$ where C depends quadratically on the upper bound of the particles per cell.

The Linked Cell algorithm is given by

Loop over all Z_j
    Loop over all particles α in cell Z_j {
       $F_\alpha \leftarrow 0$ // set F_α zero
         Loop over all cells Z_i of $\mathcal{N}(Z_i)$
           Loop over all particles β in cell Z_i
             if ($\alpha \neq \beta$)
               if ($r_{\alpha,\beta} \leq r_{\text{cut}}$)
                  $F_\alpha \leftarrow F_\alpha + F_{\alpha\beta}$ // add $F_{\alpha\beta}$ on F_α
      }

For implementational details like the particle list management for the particles of each chain and the data structure of the cells we refer to [GKZC04].

1.3 The Equations of Motion in the Continuum Mechanics Setting

The most common way to classical elasticity is the axiomatic introduction of the relevant quantities and the equations of motion (see e.g. [Cia88]). Therein the atomistic structure of the solid is neglected and the motion of the body is described by functions. Let us consider $\Omega \in \mathbb{R}^3$. In classical elasticity it is assumed, that the motion, due to external and internal forces is given by the mapping

$$\phi : \overline{\Omega} \times [0, T] \rightarrow \mathbb{R}^3,$$

such that the deformed configuration at time t of the body is given by

$$\Omega^t = \phi(\Omega, t) \qquad t \geq 0, \tag{1.20}$$

with the displacement $u(t)$

$$u(t) = \phi(X, t) - X \qquad X \in \overline{\Omega}, \, t \geq 0. \tag{1.21}$$

In the forthcoming we denote points of the deformed configuration by

$$x(t) := \phi(X, t)$$

and write x instead of $x(t)$ and u instead of $u(t)$ whenever possible. Furthermore, it is assumed, that ϕ is locally injective in Ω, sufficiently smooth and orientation preserving, which can be expressed by the pointwise inequality

$$\det\left(\frac{\partial \phi_i}{\partial X_j}\right)(X, t) > 0, \, X \in \bar{\Omega}, \, t \geq 0, \, i, j = 1, ..., 3.$$

Let us denote the deformation gradient by F, i.e.

$$F := \left(\frac{\partial \phi_i}{\partial X_j}\right)_{i,j=1,...,d}. \tag{1.22}$$

The mass is given by

$$m(\Omega^t) = \int_{\Omega^t} \varrho(x, t) \, dx,$$

where $\varrho(x, t)$ is the mass density. Here, we assume that the mass is constant in time, which means, that there are no material flows through the boundary of a material subdomain and we do not consider mass to energy conversions. For sake of simplicity the density is given as a

function on $\mathbb{R}^3 \times [0, T]$ by extending $\varrho(\cdot, t) \in L^\infty(\mathbb{R}^3, [0, \infty])$ by zero outside of Ω^t.

The change of square length of the line segment $dx = FdX$ due to the deformation is given by the Green strain tensor:

$$E = \frac{1}{2}(F^T F - I) = \frac{1}{2}(\nabla u^T + \nabla u + \nabla u^T \nabla u).$$

Moreover the Cauchy stress is defined by

$$\sigma n(x)dS = dF = gdS$$

where n is the normal and g is the traction on any surface segment dS. For computational and analytical reasons, we use the Lagrangian description and thus define the first *Piola-Kirchhoff tensor* $\mathcal{P}$, which is a second order tensor, given by

$$\mathcal{P} : [0, T] \times \Omega \to \mathbb{R}^{3\times3}, \ \mathcal{P}(X)ndS^{\text{ref}} = dF = gdS,$$

where dS^{ref} is the surface segment in the undeformed (reference) configuration. The governing equations are then derived by conservation of

- mass

- momentum

- angular momentum.

They are be given by

$$\varrho \frac{\partial v}{\partial t} = \text{div}\mathcal{P} + \varrho b, \tag{1.23}$$

where $v = \dot{u} = \partial u / \partial t$. Here, ϱb is the body force density and $v \in C^1([0, T], C^0(\Omega))$ as well as $\mathcal{P} \in C^0([0, T], C^1(\Omega))$. Let us remark, that for sake of simplicity, we neglected the boundary conditions in our introduction. However, depending on the material model and the pointwise smoothness of the boundary $\partial\Omega$ of Ω, the solutions for u may not be smooth enough to fulfill (1.23).

Thus we introduce the weak formalism. To do so, let $\Omega \subset \mathbb{R}^d$ be measurable. We denote by $L^p(\Omega)$ the space of p-Lebesgue-integrable functions on Ω. Moreover, we denote the standard scalar product by $(\cdot, \cdot)_{L^2(\Omega)}$ and the norm

$$\|u\|_{L^2(\Omega)} := \left(\int_\Omega |u|^2 \, d\Omega\right)^{1/2}.$$

Let α be a multiindex with $\|\alpha\|_1 := \sum_{i=1}^d |\alpha_i|$, Then, for a bounded domain Ω and for $m \in \mathbb{N}, 1 \leq p < \infty$ we denote by $H^{m,p}(\Omega)$ the Sobolev space, given by

$$H^{m,p}(\Omega) := \{u \in L^p(\Omega) \mid \text{there exists } \partial^\alpha u \text{ and } \partial^\alpha u \in L^p(\Omega) \ \forall \|\alpha\| \leq m\}$$

and equipped with the norm

$$\|u\|_{H^{m,p}(\Omega)} := \left(\sum_{\|\alpha\|_1 \leq m} \int_\Omega |\partial^\alpha u|^p d\Omega \right)^{1/p}$$

where the weak derivative (if it exists) is defined by

$$\int_\Omega \partial^\alpha u \varphi \, d\Omega = (-1)^{\|\alpha\|_1} \int_\Omega u \partial^\alpha \varphi \, d\Omega \qquad \forall \varphi \in C_0^\infty(\Omega).$$

Here, $C_0^\infty(\Omega)$ is the set of infinitely differentiable functions with a compact support in Ω. In the forthcoming we omit in the case $p = 2$ the suffix 2, i.e. $\| \cdot \|_{H^m(\Omega)} := \| \cdot \|_{H^{m,2}(\Omega)}$.

Let $\beta \in (0,1)$ then we define

$$|v|^2_{H^\beta(\Gamma)} := \int_\Gamma \int_\Gamma \frac{|v(x) - v(y)|^2}{|x-y|^{3+2\beta}} \, d\Gamma_x d\Gamma_y.$$

We can give a precise meaning to restrictions of components of admissible displacements belonging to $H^1(\Omega)$ to spaces of functions defined on the boundary. For this purpose the trace map is a useful tool.

The trace theorem taken from [Bra97] is a special case of a more general trace theorem and guarantees, that traces are well defined for Sobolev spaces.

Theorem 1.3.1 (Trace Theorem) *Let $\Omega \subset \mathbb{R}^d$ be a bounded Lipschitz domain and $\Gamma = \partial\Omega$, then there exists a unique linear continuous trace mapping*

$$\gamma : H^1(\Omega) \longrightarrow H^{1/2}(\Gamma)$$

such that $\gamma(v) = v|_\Gamma$ for each $v \in H^1(\Omega) \cap C^0(\overline{\Omega})$ and

$$\|\gamma v\|_{H^{1/2}(\Gamma)} \leq c\|v\|_{H^1(\Omega)}.$$

We assume, that Ω is a polygonal domain and $\partial\Omega = \Gamma_N \dot\cup \Gamma_D$ be the disjoint union of the portions Γ_D and Γ_N. Moreover we assume, that $b \in C^0([0,T], L^2(\Omega)), g \in C^0([0,T], L^2(\Gamma_N)), u_D \in C^0([0,T], H^{1/2}(\Gamma_D))$ and the initial displacements $u_0 \in H^1(\Omega)$. Then for the weak formulation of (1.23) we seek for a $u \in C^2([0,T], H^1(\Omega))$ such that $u(\cdot, 0) = u_0, u|_{\Gamma_D} = u_D$ and

$$\int_\Omega \varrho \ddot{u} \cdot \, d\Omega + \int_\Omega \mathcal{P}(u) : \nabla v \, d\Omega = \int_\Omega \varrho g \cdot v \, d\Omega + \int_{\Gamma_N} t \cdot v \, d\Gamma_N \qquad (1.24)$$

for all $v \in C^0([0,T]; H^1(\Omega))$ vanishing on Γ_D, where $A : B$ denotes $\mathrm{tr}(A^T B)$.

Hyperelastic Material   By definition a material is hyperelastic, if there exists a stored energy function $W : \Omega \times \mathbb{R}^{3\times3} \to \mathbb{R}$ which is differentiable in the second argument such that

$$\mathcal{P}(X) = \frac{\partial W}{\partial F}(X, F).$$

Obviously, the stored energy function depends on the material. For a *St. Venant-Kirchhoff material*, which is an isotropic and homogeneous material the stored energy function is given by

$$W_{\mathrm{VK}}(E) = \frac{\lambda}{2}(\mathrm{trace}(E))^2 + \mu\,\mathrm{trace}(E^2)$$

where $\lambda, \mu \in \mathbb{R}$ are the Lamé constants [Cia88].
Then the potential energy of a deformed body is given by

$$\mathcal{U}^{\mathrm{CM}}(u) = \int_\Omega W(X, \mathrm{id} + \nabla u)\,d\Omega + \int_\Omega b \cdot u\,d\Omega + \int_{\Gamma_N} t \cdot u\,d\Gamma_N.$$

The kinetic energy of the moving deformed body has a form similar to (1.6), more precisely

$$\mathcal{T}^{\mathrm{CM}}(\dot{u}) = \int_\Omega \frac{\varrho}{2}|\dot{u}|^2\,d\Omega.$$

Thus, the Hamiltonian and Lagrangian for the continuum setting are

$$\mathcal{H}^{\mathrm{CM}} = \mathcal{T}^{\mathrm{CM}} + \mathcal{U}^{\mathrm{CM}} \quad \text{and} \quad \mathcal{L}^{\mathrm{CM}} = \mathcal{T}^{\mathrm{CM}} - \mathcal{U}^{\mathrm{CM}},$$

respectively.
Having explained the Hamilton and Lagrangian for the atomistic scale and for the continuum scale, we now introduce a link between these two expression, namely the Cauchy-Born rule.

Cauchy-Born rule   In the Cauchy-Born rule [BH54], it is assumed, that the stored energy function W can be computed on the basis of the atomistic potential. Thereby, it is supposed, that all atoms of the volume of a single crystal follow a given (continuum) displacement up to a certain limit. The validity of the Cauchy-Born rule has been examined by [FT02]. It turns out, that the Cauchy-Born rule fails for large deformations and an inhomogeneous atomistic lattice.
The Cauchy-Born rule is useful for deformations ϕ whose modulus does not exceed the plastic limit. Let us discuss this on a unit cell of a hexagonal lattice, which shall be given by Figure 1.7 and the Lennard-Jones potential with $\sigma = \varepsilon = 1$.
As a measure for the validity of the Cauchy-Born rule, let us introduce

$$b = \frac{r_{\mathrm{max}}}{r_0} \quad \text{where } r_{\mathrm{max}} = \max\{r_{\alpha\beta} : \beta = 1, ..., 6\}.$$

By setting the second derivative of the Lennard-Jones potential equal to zero, we obtain the
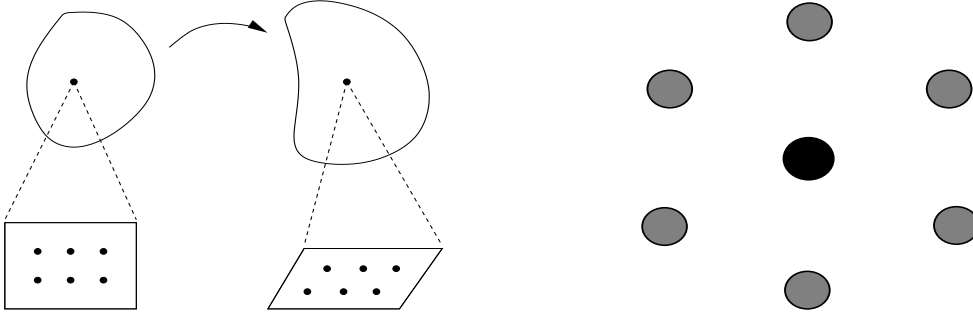
Figure 1.7: *A unit cell of a hexagonal lattice.*

inflection point, at $\left(\frac{26}{7}\right)^{1/6}$. If we assume, that

$$1 < r_{\max} < \left(\frac{26}{7}\right)^{1/6} \iff 1/r_0 < r_{\max}/r_0 < \left(\frac{26}{7}\right)^{1/6}/r_0$$

and insert $r_0 = 2^{1/6}$ to obtain

$$\left(\frac{1}{2}\right)^{1/6} \le b \le \left(\frac{13}{7}\right)^{1/6}.$$

It can be shown that for b in this range, the Cauchy-Born rule serves as an accurate approximation [FT02]. In particular, for $b = 1$ we have that $F = I$.

The Finite Element Method In order to approximate the continuous displacement field u, we now employ a finite element discretization of lower order. Let $\mathcal{T}^h$ denote a mesh with mesh size parameter $h > 0$, such that the family $\{\mathcal{T}^h\}_h$ is shape regular.
Here, we use Lagrangian conforming finite elements of first order (P_1) for the displacements u and denote the set of all nodes of $\mathcal{T}^h$ by $\mathcal{N}_h$. The finite element space $\mathcal{V}_h \subset H^1(\Omega)$ is spanned by the nodal basis

$$\mathcal{V}_h = \mathrm{span}_{p \in \mathcal{N}_h}\{\psi_p^h\}.$$

The Lagrangian basis functions $\psi_p^h \in \mathcal{V}_h$ are uniquely characterized by the Kronecker-delta property

$$\psi_p^h(q) = \delta_{pq}, \qquad p, q \in \mathcal{N}_h, \tag{1.25}$$

where δ_{pq} is the Kronecker-delta. Any function $u_h \in \mathcal{V}_h(\Omega)$ can uniquely be written as

$$u_h = \sum_{p \in \mathcal{N}_h} \bar{u}_p \psi_p^h, \tag{1.26}$$

where $(u_p)_{p \in \mathcal{N}_h} \in \mathbb{R}^{d \cdot |\mathcal{N}_h|}$, $\bar{u}_p \in \mathbb{R}^d$, is the coefficient vector. We can identify each element

of $\mathcal{V}_h$ with its coefficient vector $(u_p)_{p \in \mathcal{N}_h}$. In the forthcoming, we omit the superscript h whenever possible. In space, (1.24) gives a non linear ordinary differential equation in $\mathbb{R}^{d|\mathcal{N}_h|}$ which can be solved by e.g. the Verlet algorithm, discussed before. In other words, we do a spatial discretization followed by a time discretization (method of lines).

Throughout this thesis, we denote nodes by Latin letters, e.g., $p, s, t, \ldots$ and atoms by Greek letters, e.g., $\alpha, \beta, \ldots$.

2 Challenges of Coupling Atomistic and Continuum Models

In the first chapter, we introduced the continuum and the molecular description. When bringing them to practice, either of them exhibits advantages and disadvantages. On the one hand, atomistic simulations are able to describe defects on the small scale, however the required number of atoms - and thus the computational costs - soon become prohibitively large. On the other hand, the simulation methods associated with the continuum mechanics (like FEM) are cheaper with respect to computational costs, but are less accurate. In particular, the abstraction of a continuous body is infeasible under strong local deformations. Multiscale methods strive for combining the advantages of both techniques by employing a continuum description of the whole computational domain and restricting molecular dynamics to regions where a highly resolved simulation is actually needed. The main challenge is to match these two descriptions in a sound way.

As we will see in the following section, speed at which waves propagate is a crucial quantity if a suitable matching along the interface, where the continuum and the atomistic description come into contact, is to be achieved. More precisely, we want that this velocity is conserved when the discretization changes. In order to attain this, we now explore the behavior of waves in continuum as well as atomistic regions. To do so, let us consider a simple case on each scale: a one dimensional mass spring system on the molecular scale and its corresponding continuum counterpart. Even in this simple model reflections occur when an unsuitable coupling of molecular dynamics with continuum mechanics is applied. An analysis of these reflections at the end of this chapter will be exploited during the development of our new coupling strategy.

2.1 The Dispersion Relation

The dispersion relation, which we explain in the following, gives the dependence of the frequency on the wave number [Kit06]. In order to show this relationship, we first briefly introduce the travelling waves in crystals and show then the dispersion relation for the molecular dynamics setting. For sake of simplicity we confine our discussion to the $1d$ case.

Travelling waves in crystals   Recall that $q(X, t)$ denotes the deviation of the atoms from their starting configuration. A harmonic wave in the atomistic model is of the form

$$q(X, t) = \tilde{q} e^{i(kX - \omega t)} \tag{2.1}$$

where $\tilde{q}$ is the amplitude, $kX - \omega t$ is the phase, k the wave vector and ω is the angular frequency. We also define the wave number $\kappa = |k|$ and the wave length $\lambda = 1/\kappa$. In the forthcoming we consider two different kinds of velocities. The *phase velocity* v_{ph} defined as

$$v_{\text{ph}} = \frac{\omega}{\kappa}.$$

Moreover, for the other kind of velocity, we define the wave package as a wave whose amplitude is only in a bounded domain non zero. The velocity of a wave package is the *group velocity*, defined as

$$v_{\text{gr}} = \frac{\partial \omega}{\partial \kappa}.$$

We can decide between longitudinal and transverse vibrations. An example of a $1d$ chain in $2d$ is given by Fig 2.1

Figure 2.1: *An example of longitudinal (left) and transversal (right) waves of a $1d$ chain in $2d$. The arrows show the displacement direction of the particles*

Remark In $3d$ the wave vector k has three components and points into the direction of propagation. The atomistic displacements associated with a wave $q(X, t)$ where X is the equilibrium position of an atom are simultaneously three dimensional vectors. These displacement vectors may be parallel to k (longitudinal), perpendicular to k (transversal) or along a direction, that is not directly related to the direction of k.

To keep things simple, we assume that the time dependent motion of the atoms is a linear superposition of harmonic waves. The gained insights from the linear case then give necessary conditions for non-linear systems such as typical MD simulations. In $1d$ each X can be given by αr_0, where $\alpha \in \mathbb{Z}$ and r_0 is the atomistic spacing. Then, for each α, we have the super position

$$q_\alpha(t) = \sum_k \tilde{q}_k e^{i(k\alpha r_0 - \omega t)}$$

and we can understand the behavior of the solution by examining the harmonic solutions independently, i.e., $q_k = 0$ for all but one k.

Let us consider a mass spring system with lattice spacing r_0, mass m and spring constant K.

Then, the atomistic Hamilton for an harmonic system is given by

$$\mathcal{H}_{\text{MD}} = \frac{1}{2} \sum_{\beta=1}^{|\mathcal{A}|} \frac{p_\beta^2}{m} + \frac{K}{2} \sum_{\beta=2}^{|\mathcal{A}|} (q_\beta - q_{\beta-1})^2. \tag{2.2}$$

Thus, analogously to (1.19), the respective equations of motion of $\mathcal{H}_{\text{MD}}$ can be stated as

$$m \frac{d^2 u_\beta}{dt^2} = K(q_{\beta+1} + q_{\beta-1} - 2q_\beta). \tag{2.3}$$

Then

$$-m\omega^2 \tilde{q}_\kappa e^{i(k\alpha r_0 - \omega t)} = -\tilde{q}_k e^{-i\omega t} K(2e^{ik\alpha r_0} - e^{ik(\alpha-1)r_0} - e^{ik(\alpha+1)r_0})$$

$$m\omega^2 = K(2 - e^{-ikr_0} - e^{ikr_0})$$

$$m\omega^2 = 2K \left(1 - \frac{e^{-ikr_0} + e^{ikr_0}}{2}\right)$$

$$m\omega^2 = 2K(1 - \cos(kr_0)).$$

Furthermore using the relation $\sin^2(x) = 1 - \cos(2x)$ leads us to

$$m\omega^2 = 2K \sin^2 \left(\frac{kr_0}{2}\right),$$

which then gives us

Definition 2.1.1 (Dispersion Relation for the Molecular Case)

$$\omega^2 = \frac{2K}{m} \sin^2 \left(\frac{kr_0}{2}\right). \tag{2.4}$$

Apparently it holds that $\omega(k) = \omega\left(k + \frac{2\pi n}{r_0}\right)$ for any $n \in \mathbb{Z}$. Hence, we only consider the case $k \in (-\pi/r_0, \pi/r_0)$, which is known as the first Brillouin zone. We chose the open interval, as for $k = \pi/r_0$ the group velocity v_{gr} equals zero, meaning that the solution is a standing wave. This physical phenomenon is also known as Bragg-Reflection [Kit06, Bri53]. For symmetry reasons it is sufficient to restrict to $k = \kappa > 0$.

The Dispersion Relation in the Continuum Setting As we have seen, the continuum mechanics as well as the molecular dynamics stem from the same basic physical laws, namely the Hamiltonian or Lagrangian principles. In this section, we consider the dispersion relation for the continuum mechanics. To do so, let us reconsider the molecular dispersion relation given by (2.4) for small wave numbers κ. More precisely let κ^* be such that

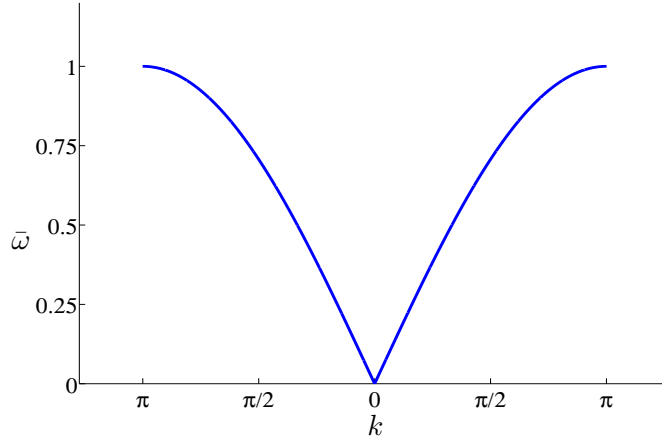$$\sin(\kappa^* r_0) = \kappa^* r_0 + o(\kappa^* r_0), \tag{2.5}$$

Figure 2.2: *The frequency $\bar{\omega} := \frac{m}{2K}\omega$ in dependence of k.*

then for all $0 < \kappa < \kappa^*$ we have

$$\omega_{\kappa \to 0} = \frac{1}{2}r_0\left(\frac{K}{m}\right)^{1/2}\kappa.$$

Moreover the phase velocity $v_{\mathrm{ph}}^{\mathrm{CM}}$ is then given by

$$v_{\mathrm{ph}}^{\mathrm{CM}} = \frac{\omega}{\kappa} = r_0\left(\frac{K}{m}\right)^{1/2}. \tag{2.6}$$

A connection to the macroscopic elastic properties can be given by compressing the one dimensional chain from Section 2.1 giving rise to the strain e, such that the average distance between the atoms becomes $r_c = r_0(1 - e)$, where $e \ll 1$. With respect to (1.18) the energy of the strained chain becomes

$$E_{\mathrm{harm},1d} = NV(\mathbf{r}) + \frac{1}{2}NK(r_0 - r_c)^2.$$

Thus, the strain energy, which can be considered as the extra energy per atom is given by

$$E_{\mathrm{strain},1d} = \frac{1}{2}K(r_0 - r_c)^2 = \frac{1}{2}Kr_0^2 e^2 = \frac{1}{2}\hat{K}e^2$$

where $\hat{K} := Kr_0^2$ is the elastic constant. From the velocity given by (2.6) we have

$$(v_{\mathrm{ph}}^{\mathrm{CM}})^2 = \frac{\omega^2}{\kappa^2} = \frac{Kr_0^2}{m} = \frac{\hat{K}}{m}. \tag{2.7}$$

Summing up, for the long wavelength limit ($\lambda = 1/\kappa$, $\kappa \ll 1$), we obtain

Definition 2.1.2 (Dispersion Relation in the Continuum Case)

$$\omega^2 = \frac{\hat{K}\kappa^2}{2m} = \frac{K\kappa^2 r_0^2}{2m}. \tag{2.8}$$

The meaning of the different dispersion relations (2.4) and (2.8) becomes clear when the phase velocity v_{ph} and the group velocity v_{gr} are considered. It can be easily be seen, that the molecular phase and the group velocity is given by

$$v_{\mathrm{ph}}^{\mathrm{MD}} = \frac{\sqrt{\frac{2K}{m}}\sin(\frac{\kappa r_0}{2})}{\kappa} \qquad \text{and} \qquad v_{\mathrm{gr}}^{\mathrm{MD}} = \sqrt{\frac{K}{2m}}r_0 \cos\left(\frac{\kappa r_0}{2}\right) \tag{2.9}$$

whereas their continuum counterparts are given by

$$v_{\mathrm{ph}}^{\mathrm{CM}} = v_{\mathrm{gr}}^{\mathrm{CM}} = \sqrt{\frac{K}{2m}}r_0.$$

Thus, for small κ we have

$$v_{\mathrm{ph}}^{\mathrm{MD}} \approx v_{\mathrm{ph}}^{\mathrm{CM}} \quad \text{and} \quad v_{\mathrm{gr}}^{\mathrm{MD}} \approx v_{\mathrm{gr}}^{\mathrm{CM}}.$$

In contrast, for large wave numbers close to $\pi/2$ we have $\cos(\frac{\kappa r_0}{2}) \approx 0$, which implies that waves with high frequencies propagate slower than waves with low frequencies, which is not the case in the continuum where the dispersion relation is linear.

Consequences of the different dispersion relation for the discretization So far we have shown, that the continuum and the molecular scale have different dispersion relations, which carries over to the velocities of waves. However, for long wavelengths these differences are insignificant. Next, we examine the numerical dispersion relation, i.e. the case when the continuum is discretized. The finite element model we employ on the macro scale is based on a continuum mechanics approximation of the deformation of our body Ω.

Analogously to the atomistic case we consider a finite element approximation for the continuum Hamiltonian of a harmonic system in $1d$, which is given by

$$\mathcal{H}_{\mathrm{FE}} = \frac{1}{2}\sum_{p\in\mathcal{N}_h}\frac{\varrho h}{2}\dot{u}_p^2 + \frac{Ch}{2}\sum_{p\in\mathcal{N}_h}\left(\frac{u_p - u_{p-1}}{h}\right)^2 \tag{2.10}$$

where we assumed the standard linear "hat" basis with equidistant mesh spacing h. Here ϱ is the mass density, C the elastic modulus. Moreover we choose

$$C = Kr_0 \quad \text{and} \quad \varrho = m/r_0, \tag{2.11}$$

which means that the material of the atomistic as well as of the continuum model have the same parameters. Thus, the respective equations of motion for $\mathcal{H}_{\text{FE}}$ with a spatial discretization can be stated as

$$m\frac{d^2 u_p}{dt^2} = \frac{K r_0^2}{h^2}(u_{p+1} + u_{p-1} - 2u_p). \tag{2.12}$$

Hence, if the mesh size h equals the atomistic spacing r_0 we have that (2.3) and (2.12) coincide.
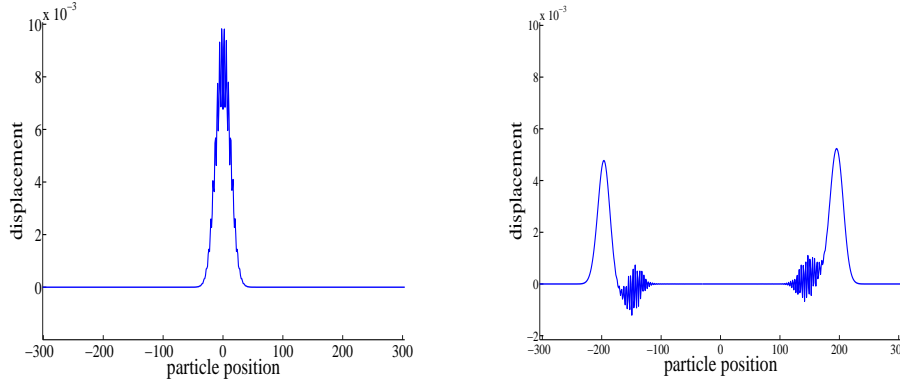

Figure 2.3: *Left: Wave package in* $1d$ *in initial position. Right: propagated initial wave: the waves with lower frequencies move faster*

Let us assume that the solution of (2.12) is given component-wise by

$$u_p(t) = \tilde{u}e^{i(kx_p - \omega t)}, \tag{2.13}$$

where $\tilde{u}$ is the amplitude, ω is the frequency and $k \in (-\pi/h, \pi/h)$ is the wave vector. Again, $\kappa = \pi/h$ would imply that the solution is a standing wave. Analogously to the molecular case, we obtain

Definition 2.1.3 (Numeric Dispersion Relation for the Finite Element Discretization)

$$\omega^2(\kappa) = \frac{2\ell}{m}\sin^2\left(\frac{\kappa h}{2}\right) \qquad \ell := \frac{K r_0^2}{h^2}. \tag{2.14}$$

Comparing (2.4) and (2.14) one can see, that both relations only differ by the factor h/r_0. The phase and the group velocities for the finite element case are given by

$$v_{\text{ph}}^{\text{FE}} = \sqrt{\frac{2K}{m}}\frac{r_0}{h\kappa}\sin\left(\frac{\kappa h}{2}\right) \qquad \text{and} \qquad v_{\text{gr}}^{\text{FE}} = \sqrt{\frac{K}{2m}}r_0\cos\left(\frac{\kappa h}{2}\right), \tag{2.15}$$
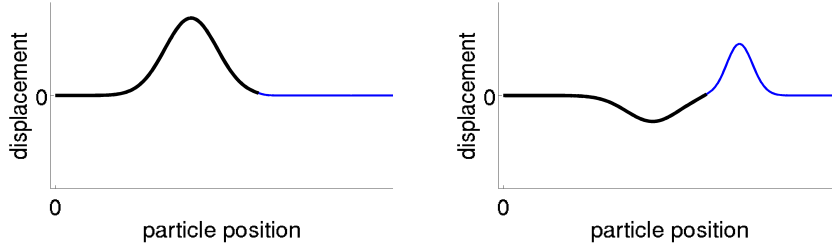
since we assume $k = \kappa > 0$.

Figure 2.4: *Smooth wave entering from a faster wave speed region (bold line) into a slower wave speed region.*
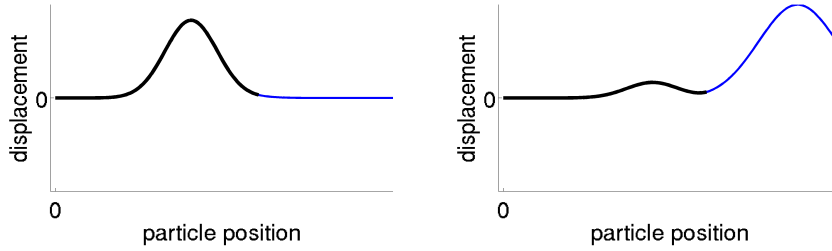
Figure 2.5: *Smooth wave entering from a slower wave speed region (bold line) into a faster wave speed region.*

Moreover, from (2.15) we can see, that for fixed k the speed of a wave decreases as the mesh-size h increases. For very large h no representation of the wave is possible, since we need at least two discretization points per wave length. In Figure 2.4 and Figure 2.5 an example of a wave entering a region of slower (faster) wave propagation speed due to a change of the spatial discretization size is shown. We observe reflections at the interface (cf.(2.15)).

In Figure 2.6 the dependence of the velocity from the space discretization parameter and the wave number is shown. Here the velocity is the normalized phase velocity

$$\bar{v} := v_{ph} \left(r_0 \sqrt{\frac{2K}{m}} \right)^{-1}.$$

One can clearly see, that for $h \ll r_0$ the wave becomes slower.

Consequences of the different dispersion relation for the time discretization   As we have seen by the molecular dispersion relation (2.4) and the numeric dispersion relation (2.14) the difference between the finite element space discretization parameter h and the reference dis-
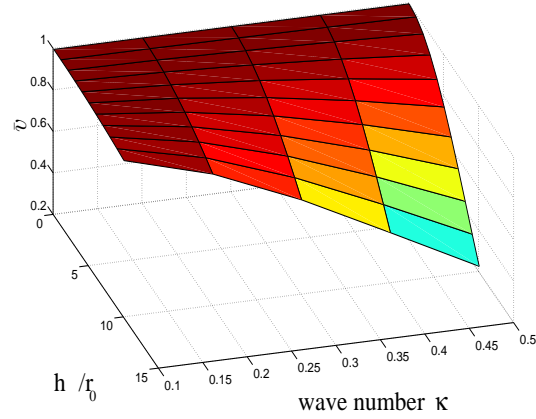
Figure 2.6: *The different dependencies between the space parameters, the normalized velocity and the wave number.*

tance r_0 in the molecular setting causes a difference in the velocities. However, so far we have not yet examined the behavior when a time discretization is employed. To do so, we begin by deriving the dispersion relation with respect to a time discretization. For a given time step Δt we assume that we can approximate

$$\frac{d^2 u}{dt^2} \approx \frac{u(t + \Delta t) - 2u(t) + u(t - \Delta t)}{(\Delta t)^2}.$$

Thus, the equation of motion from (2.12) reads as

$$\frac{m}{(\Delta t)^2}(u_p(t + \Delta t) - 2u_p(t) + u_p(t - \Delta t)) = \frac{K r_0}{h^2}(u_{p-1}(t) - 2u_p(t) + u_{p+1}(t)). \quad (2.16)$$

Let us assume that the harmonic solution for the n-th time step on p is given by

$$u_p^n = e^{i(\omega n \Delta t - p \kappa h)}.$$

Analogously to the derivation of the preceding dispersion relations we obtain

$$\sin^2\left(\frac{\omega \Delta t}{2}\right) = \frac{(\Delta t)^2}{h^2} \hat{C}^2 \sin^2\left(\frac{\kappa h}{2}\right), \quad \hat{C} := \sqrt{\frac{K r_0}{m}}. \quad (2.17)$$

In order to obtain a more handable formulation, we employ the expansion of $\sin$ in ω. Taking the square root of (2.17) gives

$$\sin\left(\frac{\omega\Delta t}{2}\right) = \frac{\Delta t}{h}\hat{C}\sin\left(\frac{\kappa h}{2}\right). \tag{2.18}$$

A linearization then gives

$$\omega = \hat{C}\kappa + o(\kappa^2),$$

without any time or space parameter dependence.

Using a Taylor expansion of second order in (2.18) yields

$$\omega = \hat{C}\kappa + \frac{1}{6}\kappa^3(\hat{C}\Delta t - \hat{C}h) + O(\kappa^5), \tag{2.19}$$

since the $\omega^3 = \hat{C}^3\kappa^3 + O(\kappa^5)$. In order to match the continuum and the molecular dispersion relation we define Δt^{MD} as the atomistic and Δt^{CM} as the continuum time step and obtain from (2.19)

$$\hat{C}^3(\Delta t)^3 - \hat{C}r_0 \overset{!}{=} \hat{C}\Delta t^{\text{CM}} - \hat{C}h.$$

Consequently, for different spatial parameters r_0 and h and a given molecular time discretization parameter Δt^{MD} we can choose a suitable Δt^{CM} such that the dispersion relation on both models is equal. More precisely, we choose

$$\Delta t^{\text{CM}} = \Delta t^{\text{MD}} + \frac{1}{c^2}(r_0 - h). \tag{2.20}$$

Thus a wrong dispersion relation caused by large h can be compensated by choosing larger time steps Δt^{CM}. An obvious consequence is, that any difference in the dispersion relation can be compensated by a suitable large choice of the time step in the finite element discretization. However, it is known by the *Courant-Friedrichs-Lewy stability criteria* [CFL28], that the time step should be chosen to hold

$$\Delta t^{\text{CM}} \leq \frac{h}{v},$$

otherwise the numerical scheme given by (2.16) is unstable [Hir88, Hir90]. Moreover, it also suffer of the inaccuracy which we have elucidated in Chapter 1.

2.2 Determining the Reflection Coefficient

So far we have seen the consequences of different length scales for the molecular as well as for the finite element case.

We now consider the transition of waves from molecular dynamics to a finite element discretization.
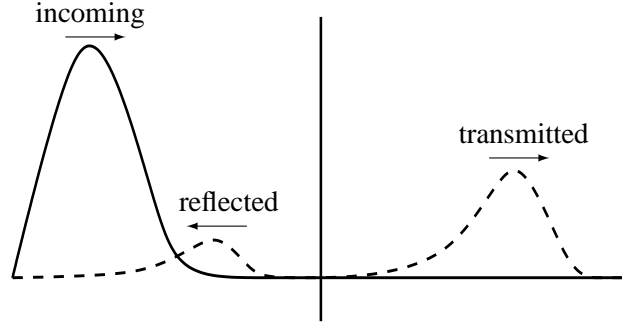

Figure 2.7: *Example of an incoming wave into a medium with a different spatial discretization. As a consequence, we obtain a reflected and a transmitted part of the wave*

Suppose that we have an incoming and a reflected wave in the MD region and a wave transmitted into the finite element region, separated by an interface (thus, in $1d$, a point). In the MD region, we have a resulting wave as superposition of the incoming and reflected waves. Denote by A_I and ω the amplitude and frequency of the incoming wave, and by A_R and A_T the amplitudes of the reflected and transmitted waves, respectively (see Figure 2.7). We demand the solution to be continuous at the interface.[1] Thus, it is required that all waves have the same frequency ω, and it holds that

$$A_T = A_I + A_R. \tag{2.21}$$

Let us recall, that h denotes the mesh size of the FE lattice. The respective energy flows are given by (cf. [Bri53])

$$\Phi_I = \frac{\varrho}{2}\omega^2 A_I^2 v_{\text{gr}}^{\text{MD}}(\omega)$$

$$\Phi_R = \frac{\varrho}{2}\omega^2 A_R^2 v_{\text{gr}}^{\text{MD}}(\omega)$$

$$\Phi_T = \frac{\varrho}{2}\omega^2 A_T^2 v_{\text{gr}}^{\text{FE}}(\omega)\,,$$

where Φ_I, Φ_R, Φ_T are the energy flows of the incoming, reflected, and transmitted waves. The

---

[1]For brevity, we refrain from showing that this is also necessary as a consequence of momentum and energy conservation.

energy conservation imposes that

$$\Phi_I = \Phi_T + \Phi_R.$$

Upon inserting the respective energy flows we obtain

$$A_I^2 v_{\text{gr}}^{\text{MD}}(\omega) = A_T^2 v_{\text{gr}}^{\text{FE}}(\omega) + A_R^2 v_{\text{gr}}^{\text{MD}}(\omega).$$

Solving for the transmission coefficient $T := \frac{A_T}{A_I}$ and for the reflection coefficient $R := \frac{A_R}{A_I}$ yields

$$T^2 = \frac{A_T^2}{A_I^2} = \frac{v_{\text{gr}}^{\text{MD}}(\omega)}{v_{\text{gr}}^{\text{FE}}(\omega)}\left(1 - \frac{A_R^2}{A_I^2}\right) = \frac{v_{\text{gr}}^{\text{MD}}(\omega)}{v_{\text{gr}}^{\text{FE}}(\omega)}\left(1 - R^2\right). \tag{2.22}$$

From (2.21) we obtain the relationship

$$T^2 = (1 + R)^2. \tag{2.23}$$

We set the two representations of T equal (i.e. (2.22) and (2.23) respectively), which implies either $R = -1$ or with the definition

$$f_v := \frac{v_{\text{gr}}^{\text{MD}}(\omega)}{v_{\text{gr}}^{\text{FE}}(\omega)} = \frac{(1 + R)^2}{1 - R^2} = \frac{1 + R}{1 - R}, \tag{2.24}$$

and solve

$$R^2 + \frac{1}{1 + f_v}2R + \frac{1 - f_v}{1 + f_v} = 0$$

$$R_{1/2} = -\frac{1}{1 + f_v} \pm \sqrt{\frac{1}{(1 + f_v)^2} - \frac{1 - f_v}{1 + f_v}}$$

$$R_1 = -1$$

$$R_2 = \frac{f_v - 1}{f_v + 1}$$

since with $R = 1$ neither (2.22) nor (2.23), involving T and R, can be fulfilled. Note that the solution $R = -1$ is trivial, as it describes the case of the reflected wave annihilating the incoming one, resulting in no wave at all. We also see immediately that if $f_v = 1$, i.e., $h = r_0$, the nontrivial solution has zero reflection.

To get a more explicit description of R, we further simplify (2.24). To do so, we solve the dispersion relations (2.4) and (2.14) for κ^{MD} and κ^{FE}, respectively. Abbreviating $c := \sqrt{\frac{2K}{m}}$, we get

$$\kappa^{\text{MD}} = \frac{2}{r_0}\arcsin\left(\frac{\omega}{c}\right) \qquad \text{and} \qquad \kappa^{\text{FE}} = \frac{2}{h}\arcsin\left(\frac{h\omega}{r_0 c}\right). \tag{2.25}$$

We insert into the expressions for $v_{\text{gr}}^{\text{MD}}$ and $v_{\text{gr}}^{\text{FE}}$ given by (2.9) and (2.15), respectively:

$$
\begin{aligned}
f_v &= \frac{v_{\text{gr}}^{\text{MD}}(\omega)}{v_{\text{gr}}^{\text{FE}}(\omega)} \\[2mm]
&= \frac{\cos\left(\arcsin\left(\frac{\omega}{c}\right)\right)}{\cos\left(\arcsin\left(\frac{h\omega}{cr_0}\right)\right)} \\[2mm]
&= \frac{\sqrt{1 - \frac{\omega^2}{c^2}}}{\sqrt{1 - \frac{h^2\omega^2}{c^2 r_0^2}}},
\end{aligned}
$$

where we used that $\cos\arcsin(x) = \sqrt{1 - x^2}$ for all $-1 \leq x \leq 1$.

We conclude that the reflection coefficient is

$$
R = \frac{\sqrt{1 - \frac{\omega^2}{c^2}} - \sqrt{1 - \frac{h^2\omega^2}{r_0^2 c^2}}}{\sqrt{1 - \frac{\omega^2}{c^2}} + \sqrt{1 - \frac{h^2\omega^2}{r_0^2 c^2}}}. \tag{2.26}
$$

To interpret these results in our coupling context, we observe that h shall be significantly larger than r_0 .

For $h \not\approx r_0$ we can see from (2.26) that we cannot hope to achieve $R \ll 1$ independent of ω. If ω tends to the cut-off, i.e. maximum, frequency $\frac{cr_0}{h}$ of the finite element system from below, R approaches 1. Even worse, the maximum frequency of the MD system c (cf. (2.4)) exceeds the maximum frequency of the finite element discretized continuum by a factor of $\frac{h}{r_0}$. For any frequency in between we must observe total reflection: If for a given ω no solution exists in the finite element system, it follows that we have no transmitted wave. In this case energy conservation requires that we have total reflection.

The remaining possibility in this qualitative analysis is that $\frac{h\omega}{r_0 c}$ is small. Since $h > r_0$, this means also that $\frac{\omega}{c}$ is small. Then (2.26) gives that $R \ll 1$ as desired. Moreover, we also have that $v_{\text{ph}}^{\text{MD}} \approx v_{\text{ph}}^{\text{FE}}$ and $v_{\text{gr}}^{\text{MD}} \approx v_{\text{gr}}^{\text{FE}}$ from (2.9) and (2.15). Finally (2.25) shows that $\kappa^{\text{MD}} \approx \kappa^{\text{FE}}$. Altogether we conclude that if

$$
\omega \ll \frac{r_0 c}{h} \tag{2.27}
$$

we have little reflection and incoming and transmitted wave coincide on wavelength, frequency and amplitude, i.e. the solutions in both systems are nearly identical.

Remark The presented results cover only the special case of a uniform, one-dimensional grid together with the linear standard model and a simple harmonic potential. However, it could be easily extended to higher dimensions, and more complex potentials which surely does not improve the situation. One might argue, that a change of the finite element basis or the grid may change the behavior of high frequency waves. Reducing the density of degrees of freedom necessarily reduces the dimension of the finite element space and thus the representable

frequency spectrum. Thus, it is impossible to propagate the full range of wave frequencies that are possibly emitted by the MD domain into the finite element region. Since the frequencies which are higher than the finite element cut-off frequency represent thermical energy from the point of view of the continuum model, they do not contribute significantly to the macroscopic mechanical behavior of the system in regions where this model and its discretization are appropriate. Thus, it is desirable to eliminate high instead of low frequencies.

2.3 Boundary Conditions in the Molecular Setting and Spurious Reflections

Even to increasing computer power a complete resolution of a larger domain is often not possible due to the large number of atoms. In contrast, the continuum mechanics simulations like finite element methods are - compared to atomistic simulations - inaccurate but need less computational power. The overall aim is to exploit the advantage of each simulation, by using a coarse description on the whole domain and a atomistic simulation in small subregions, where a high resolution is needed. For most coupling methods it is necessary to impose boundary conditions on the molecular domain.
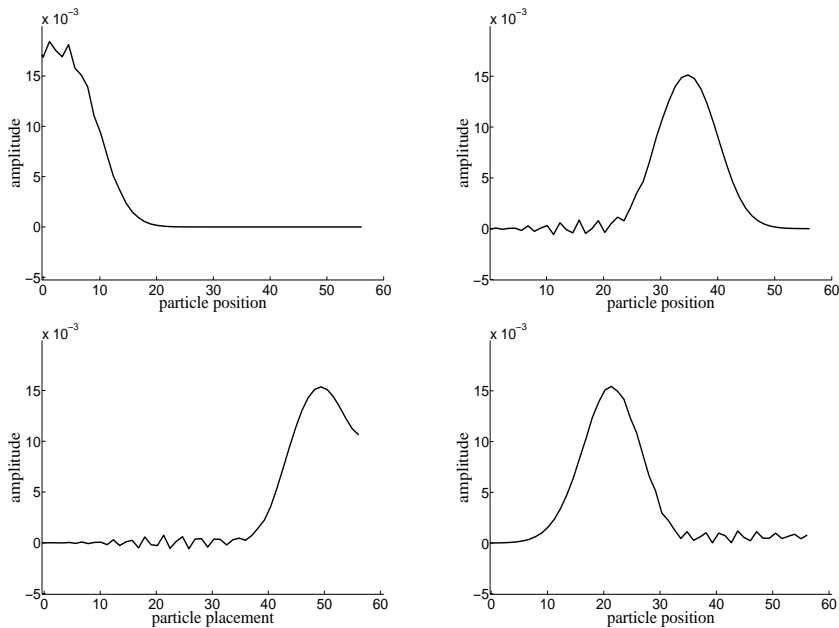

Figure 2.8: *An example on a wave being completely reflected on the right boundary*

In the first chapter we have explained that the particles exert forces due to interaction with other particles. An equilibrium state is reached, when on each particle the forces are in equilibrium (see Figure 2.9) . Let us reconsider the atomistic $1d$ chain with cut off radius $7r_0$. Figure 2.9

shows a cut out from $\alpha = [-7, 7]$ of an infinite linear chain. The force of particle $\alpha = 0$ is given by

$$F_0 = \sum_{\beta=-7}^{7} F_{\alpha\beta}.$$

$$F_{-\alpha\beta} = F_{\alpha\beta}$$
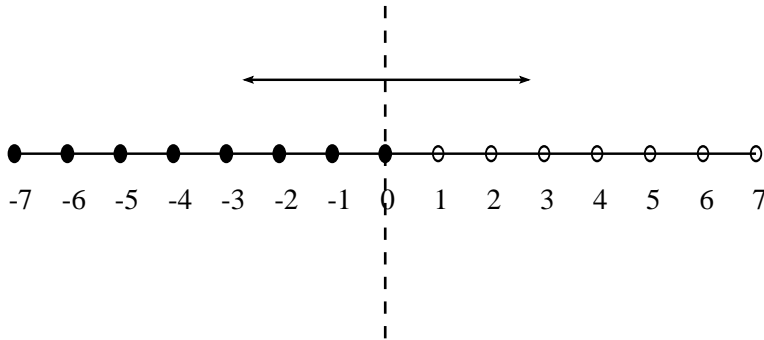
Figure 2.9: *A cut out of a finite* $1d$ *lattice*

It can easily seen that on both sides the force contributions to atom $\alpha = 0$ are in equilibrium. The situation is different in a $1d$ chain where all atoms $\alpha > 0$ are eliminated. The consequence is a miss balance in the forces. In Figure 2.10 this situation is depicted: the particle $\alpha = 0$ cannot exert the forces obtained from its left hand neighbors to its right hand neighbors. As a consequence the force is reflected back into the left hand side (cf. Figure 2.8) of the domain. In order to retain the equilibrium in the system, external forces have to be added, accounting for the forces which the missing atoms would have produced.
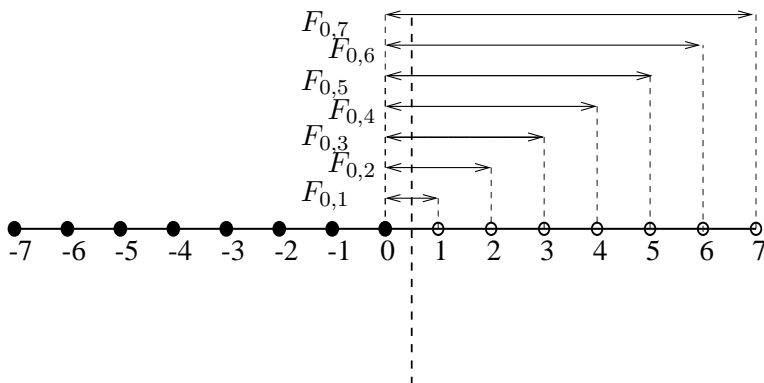
Figure 2.10: *A finite* $1d$ *lattice clipped off between atoms* $\alpha = 0$ *and* $\alpha = 1$

2.4 The Numerical Treatment of Boundary Conditions

In the molecular dynamics, the equations of motion are posed on a spatially unbounded domain. However, from the implementational point of view a truncation of the unbounded physical domain to a bounded computational domain is necessary. This fact makes it necessary to impose artificial boundary conditions which do not essentially alter the original problem.

This problem is well known in the context of wave propagation arising in acoustics, elasto-dynamics and electro magnetics. In the 70's the first approaches for non reflection boundary conditions where introduced. Now basically two approaches in literature can be found. The first class are the kernel based methods, originated form the landmark paper of Adelman and Doll [AD74]. The second class consist of the absorbing boundary conditions or sponge layer methods, where the perfectly matched boundary layer (PML) [Ber94] is a prominent example.

Both methods are originally formulated in the context of continuous waves and thus cannot be applied directly to the heterogeneous structure of the molecular dynamics. In other words, in contrast to the continuous setting, the molecular dynamics are discrete and the phonon spectum spreads over all wave numbers.

In the forthcoming, we give an overview of both approaches in the context of molecular dynamics.

Sponge Layer Methods   The basic idea of sponge layer methods is to surround the domain of interest by some artificial absorbing layers in which waves are trapped and attenuated. In the early 80's the first approaches in the context of wave equations can be found, see [Mur81]. For an overview we refer to [MH06, Tsy98]. The PML method [Ber94] is based on the concept of an analytic continuation of a real function into the complex plane. This PML concept has been extensively studied and analyzed. In the PML, the border region can be matched perfectly for all angles of incidence and all frequencies on the continuum level. However, under discretization this is no longer true [CT01]. For this approach the Fourier transformation is needed, which we define as

$$\mathcal{F}_{t \to \omega}\{u\}(\omega) := \hat{u} = \int_{\mathbb{R}} u(x)e^{-i\omega t}dt.$$

Moreover, we use the following relationship

$$\frac{\partial^n u}{\partial t^n} \stackrel{\mathcal{F}}{\mapsto} i^n \omega^n \hat{u}.$$

In [TL05, LLAT06] the PML method has been transferred to atomistic domains. On the basis of the definition of the matrix K in (1.17) we know, that the equations of motion of particle α

in direction d_1 are given by

$$m_\alpha \ddot{q}_k = f_{\alpha,d_1} = -\sum_{\beta,d_2} \frac{\partial^2 V}{\partial X_{\alpha,d_1} \partial X_{\beta,d_2}} q_{\beta,d_2} \, . \tag{2.28}$$

By applying a Fourier transform in time on (2.28) we obtain

$$m_\alpha \omega^2 \hat{q}_{d_1} = f_{\alpha,d_1} = -\sum_{\beta,d_2} \frac{\partial^2 V}{\partial X_{\alpha,d_1} \partial X_{\beta,d_2}} \cdot \hat{q}_{\beta,d_2} \tag{2.29}$$

As we have seen, the solution of (2.28) is harmonic. Moreover, it is real analytic. Thus, there
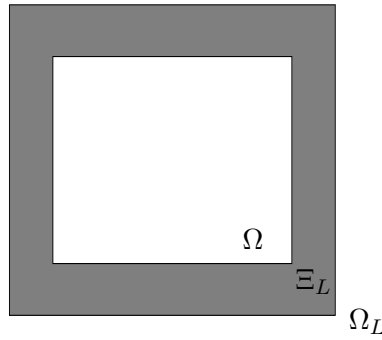
Figure 2.11: *A 2d example of the domain Ω and its layer Ξ*

exists an extension to

$$\Omega_L := \{x \in \mathbb{R}^d \,|\, \mathrm{dist}(\Omega, x) \leq L, \, L > 0\} \supset \Omega,$$

see Figure 2.11, such that (2.29) can be rewritten on Ω_L as

$$m_\alpha \omega^2 \hat{q}_{d_1} = f_{\alpha,d_1} = -\sum_{\beta,d_2} \frac{\partial^2 V}{\partial \widetilde{X}_{\alpha,d_1} \partial \widetilde{X}_{\beta,d_2}} \hat{q}_{\beta,d_2} \tag{2.30}$$

In order to impose the damping on the PML region $\Xi_L = \Omega_L \backslash \Omega$ we introduce a path in Ω_L such that the solution of (2.28) is unaltered in Ω and is damped along this path in Ξ_L. Such a path can be given by

$$z : \widetilde{X} \mapsto \begin{cases} X & \text{if} \quad X \in \Omega \\ X + \frac{i}{\omega} \int_0^X \gamma(X') \, dX' & \text{if} \quad X \in \Xi_L \end{cases}$$

Thus, for a wave along the path we obtain

$$e^{i(\kappa z - \omega t)} = e^{i(\kappa X - \omega t)} \cdot e^{-\frac{\kappa}{\omega} \int_0^X \gamma(X') \, dX'}. \tag{2.31}$$

Since we want no damping in Ω but only in Ξ_L we claim $\gamma \equiv 0$ on Ω and $\gamma > 0$ on Ξ_L. Furthermore, the damping part depends on the frequency ω, which ensures that all wavelengths decay at the same rate.

If we choose $\gamma(X') = (X')^2$, then $\mathsf{d} : \Omega_L \to \mathbb{R}$ the relationship between $\partial \widetilde{X}_{\alpha,d_1}$ and $\partial X_{\alpha,d_1}$ is given by

$$\partial \widetilde{X}_{\alpha,d_1} = (1 + \frac{\mathsf{d}}{i\omega})\partial X_{\alpha,d_1}. \tag{2.32}$$

inserting this into (2.30) we obtain

$$m_\alpha \omega^2 \hat{q}_{d_1} = -\sum_{\beta,d_2} \frac{\partial^2 V}{(1 + \frac{\mathsf{d}}{i\omega})^2 \partial X_{\alpha,d_1} \partial X_{\beta,d_2}} \hat{q}_{\beta,d_2}, \tag{2.33}$$

which is equivalent to

$$m_\alpha \omega^2 \hat{q}_{d_1} \left(1 - i\frac{\mathsf{d}}{\omega}\right)^2 = -\sum_{\beta,d_2} \frac{\partial^2 V}{\partial X_{\alpha,d_1} \partial X_{\beta,d_2}} \hat{q}_{\beta,d_2}$$

$$m_\alpha \omega^2 \hat{q}_{d_1} - 2\mathsf{d}i\omega m_\alpha \hat{q}_{d_1} - \mathsf{d}^2 m_\alpha \hat{q}_{d_1} = -\sum_{\beta,d_2} \frac{\partial^2 V}{\partial X_{\alpha,d_1} \partial X_{\beta,d_2}} \hat{q}_{\beta,d_2}$$

Applying the inverse Fourier transformation we obtain

$$m_\alpha \ddot{q}_{d_1} - 2\mathsf{d}m_\alpha \dot{q}_{d_1} - \mathsf{d}^2 m_\alpha q_{d_1} = -\sum_{\beta,d_2} \frac{\partial^2 V}{\partial X_{\alpha,d_1} \partial X_{\beta,d_2}} q_{\beta,d_2}. \tag{2.34}$$

In (2.34) it can clearly seen, that in addition to the acceleration a friction term (depending on $\dot{q}$) and a stiffness term (depending on q) is introduced. Such frictional terms (i.e. depending of $\dot{q}$) have been used ever since for temperature control in the MD simulation of NVT ensembles [GKZC04, Nos84].

Note, that the coordinate transformation (2.32) depends on the frequency ω, which ensures that all wavelength decay approximately at the same rate (neglecting effects due to the nonlinear dispersion relation).

The Kernel Based Methods In the kernel based methods exact boundary conditions are derived analytically for crystalline solids with linear interaction and an external system at rest. The first approach of Adelmann and Doll [AD74] has been discussed by the authors of [CDBY00] where the first atom outside of the domain is expressed as a convolution of the time history at the interfacial atom. This method in the context of time history kernels has been extended to more general structures [KWL05, LKP06]. However, these methods are non local in space and time since they involve all boundary atoms and the previous history of these boundary atoms. Here, we follow [LE06] for the derivation of exact boundary conditions.

Let us switch from atom α to the triple index (d_1, d_2, d_3) for the different components in the selected basis vectors of the lattice. Then, the Newton equations of motion from (1.17), reads as

$$m u_{d_1,d_2,d_3} = \sum_{d_1',d_2',d_3'} K_{d_1-d_1',d_2-d_2',d_3-d_3'} u_{d_1',d_2',d_3'}. \tag{2.35}$$

Furthermore, we define the basis of the lattice by (b_1, b_2, b_3). Without loss of generality we assume, that the basis vector b_1 coincides with the normal vector to the interface. Then, by applying the Fourier transform in direction b_2 and b_3 we obtain

$$m \widehat{\ddot{u}}_{d_1}(f_2, f_3, t) = \sum_{d_1'} \widehat{K}_{d_1-d_1'}(f_2, f_3) \widehat{u}_{d_1'}(f_2, f_3)$$

where $\widehat{u}$ denotes the discrete Fourier transformation of u. Under the assumption that the initial values can be neglected, which is reasonable for low temperatures, applying the Laplace transform, which is given by (see [Doe74])

$$\mathcal{L}(u)(s) = U(s) = \int_0^\infty e^{-st} u(t) \, dt \,,$$

yields

$$s^2 m \widehat{U}_{d_1} = \sum_{d_1'} \widehat{K}_{d_1-d_1'} \widehat{U}_{d_1'}. \tag{2.36}$$

In [LE05] it is exposed, that for crystalline structures only eigenvalues of the kind

$$\{\lambda_k, \, |\lambda_k| > 1, k = 1, ..., N^{\text{int}}\}$$

have to be considered, where N^{int} is the number of interaction partners of each atom. Let now, ε_β be an arbitrary eigenvector for $\sum_\alpha A_\alpha \lambda_\beta^\alpha$. Then, we can rewrite the right hand side of (2.36) by

$$U_{d_1} = \sum_k c_{k,d_1} \lambda_k^{d_1} \varepsilon_k.$$

Thus for given displacements $U_{-N^{\text{int}}-1}, ..., U_0$ we obtain

$$\sum_k c_{k,d_1} \lambda_k^{d_1} \varepsilon_k = \sum_k c_{k,d_1}(U_{-N^{\text{int}}+1}, ..., U_0) \lambda_k^{d_1} \varepsilon_k =: \sum_{i=-N^{\text{int}}+1}^{0} \theta_{i,d_1} U_i \,.$$

Summing up, for e.g. $d_1 = 1$ we have

$$U_1 = \sum_k c_{k,1} \lambda_k^1 \varepsilon_k = \sum_{i=-N^{\text{int}}+1}^{0} \theta_{i,1} U_i$$

By applying the inverse Fourier transform and the inverse Laplace transform, we obtain

$$u_{1,d_2,d_3}(t) = \sum_i \sum_{d_2',d_3'} \int_0^t \Theta_{i,d_2-d_2',d_3-d_3'}(t-z) u_{i,d_2',d_3'}(z) \, dz$$

where

$$\Theta_{i,d_2-d_2',d_3-d_3'} = \mathcal{F}^{-1}\mathcal{L}^{-1}(\theta_{i,1}(f_2,f_3,s))$$

is the time history kernel. For a further discussion and variants we refer to [KWL05, LKP06, LE05].

Remark A comparative study of the PML method and the time history kernel as boundary conditions of crystalline solids can be found in [YL06]. For an excellent study of the reflection rates of both methods, we refer to [Kra09]

3 A New Classification of Multiscale Methods

Various phenomena on a macroscopic level originate from the interplay of several atomic scale mechanisms. Moreover, it has been understood, that molecular phenomena involve processes over a wide range of length scales. It seems favorable to use a full atomistic large scale simulation since they provide the most rich and detailed information. Additionally, this approach is conceptually simple, since only an increase of the system size, without imposing any artificial boundary conditions, is required. Despite the success of large atomistic computer simulations, real industrial problems (cf. Figure 3.1) have a vast demand on computer power such that a pure MD simulation is in general not possible.

Multiscale methods, the coupling between molecular dynamics and continuum mechanics serves as a tool to overcome this difficulty.

The development of different multiscale methods in different fields started about twenty years ago and has been accelerated in the last few years. Along with this expansion several survey articles have been published in order to classify the multiscale methods by different aspects [CM03, PL04, BCC$^+$04, ELVE04].

The different multiscale methods vary not only in scope and the underlying assumptions but also in their approach to broader questions such as a hierarchical and concurrent multiscale approach. In the first class, the computations are performed on each scale separately. Often, the scale coupling is done by transferring problem parameters, i.e. the results obtained on one scale determine the parameters for the computational model on another scale [EE03, AG05]. Thus for instance a continuum model can be derived from the atomic information [XCP02]. Another approach is pursued in the concurrent coupling techniques. Here, the behavior at each length scale depends strongly on the others and an appropriate model is solved on each scale simultaneously, while a smooth coupling between the scales is introduced. Here, we focus on concurrent coupling techniques.

3.1 Demands on Multiscale Methods and Domain Decompositions

In the following, we show, that Domain Decomposition (DD) methods serve as a good motivation for a classification of multiscale methods. To do so, we briefly explain some basic concepts from DD methods.

The term DD [Sch70, LM72] is often used to describe a data distribution, in which the local
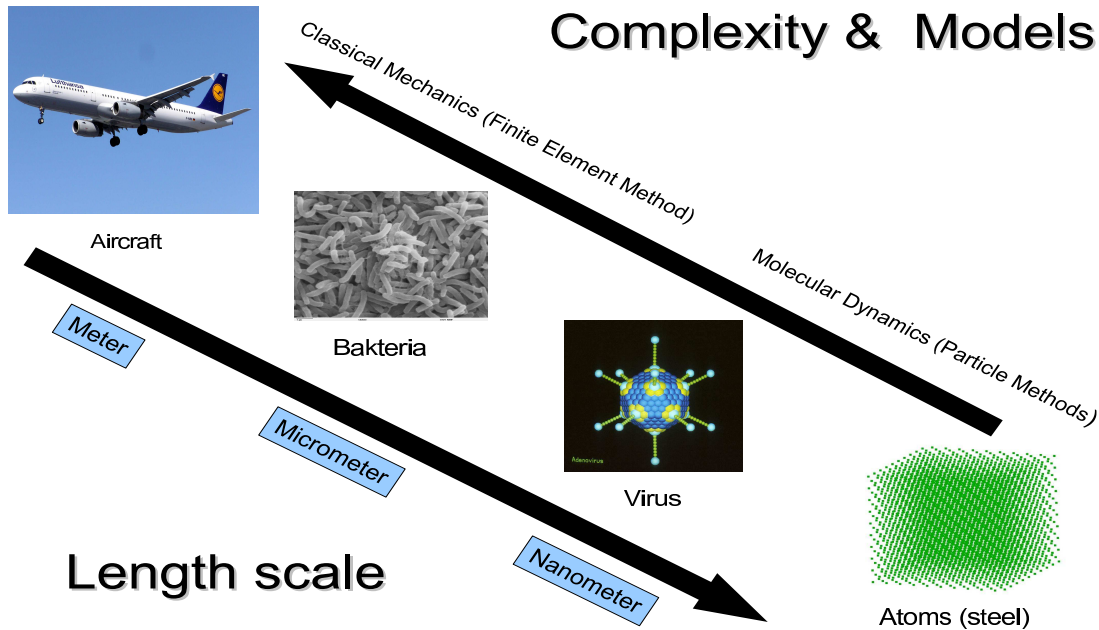
Figure 3.1: *Different Scales in Industrial Problems*

data of each process corresponds topologically to a subdomain $\Omega_S \subset \Omega$ of the whole computational domain Ω.

In the following we use a different approach by defining DD as certain numerical methods, that split the computational domain into two or more sub domains. Although DD methods have been developed for the purpose of achieving concurrency, they can be used in sequential as well as concurrent computations.

In their origin DD techniques have been developed as a powerful iterative method for solving systems of algebraic equations stemming from the discretization of partial differential equations (PDE), i.e. from a continuum description, see [QV99, TW05] for an overview. Therein DD is considered as a decomposition of the finite element space into a sum of subspaces. Then these subproblems are solved by a direct or iterative method. In a next step, projection operators are developed for the information transfer between the subspaces. As a matter of fact, the quality of the approximation on each subdomain depends on the corresponding properties of the approximation subspace. Vice versa, the DD method allows to take benefit of the presence of the subdomains in order to choose the discretization method, which is best adapted to the local behavior of the solution of the PDE which has to be approximated. Thus the shape of the subdomains and their magnitude of overlap (interface) can be chosen problem dependent. Summing up, the choice of overlapping or non-overlapping domains and the choice of the transfer operators deeply influence the performance of the DD method. In particular, the choice of an overlapping or non-overlapping method directly influences the choice of the transfer operator.

From the DD we can draw conclusions for the multiscale Coupling. More precisely, all multiscale methods can be interpreted as DD methods except for the fact, that in DD methods two or more continuum models are matched, whereas multiscale methods consider the coupling of molecular and continuum models.

In the new framework, which we introduce in the following, even a coupling of two different molecular models can be considered.

However, let us now confine to the continuum / molecular coupling. Then, the following three points have to be clarified:

- Definition of the domain

- Design of the coupling region

- Design of suitable transfer operators

Let us elucidate this DD motivated classification:

Definition of the Domain   Depending on the type of problem and on the considered domain, the regions with highly local interest have to be defined. For example cracks and similar defects can involve a global simulation by finite elements and highly localized regions with strong deformations (e.g. crack tips) which are resolved by a molecular dynamics simulation. More precisely, the domain $\Omega \subset \mathbb{R}^d$ is decomposed by

$$\Omega = \Omega^{\mathrm{MD}} \cup \Omega^{\mathrm{CM}}$$

where in Ω^{MD} a fine resolution down to the atomistic scale is employed and in Ω^{CM} a coarser representation by finite elements is applied. As afore mentioned, since the simulation on Ω^{MD} is a higher computational burden, the size of Ω^{MD} plays an important role for the overall performance of any multiscale scheme. In the existing literature mainly two approaches can be found for decomposing the domain into Ω^{MD} and Ω^{CM}. As a particular advantage of DD methods the size and shape of the subdomains and thus the interface or handshake region $\Xi = \Omega^{\mathrm{MD}} \cap \Omega^{\mathrm{CM}}$ can be chosen arbitrarily. For the different types of interfaces we can distinguish between three cases, these are the

- *Interface*: The two scales are separated by an interface, which is often a manifold of dimension $d - 1$ ($\Gamma = \overline{\Omega}^{\mathrm{MD}} \cap \overline{\Omega}^{\mathrm{CM}}$).

- *Handshake Region*: The atomistic and the continuum part are matched in an overlap region $\Xi = \Omega^{\mathrm{MD}} \cap \Omega^{\mathrm{CM}}$, $\Xi \subset \mathbb{R}^d$ and $\mathrm{meas}_d(\Xi) > 0$.

- *Completely Overlapping Methods*: The continuum mechanic description is on the whole domain Ω and the molecular part is a portion of it. In other words, the atomistic simulation is everywhere accompanied by the continuum simulation ($\Omega^{\mathrm{MD}} \cap \Omega^{\mathrm{CM}} = \Omega^{\mathrm{MD}}$).
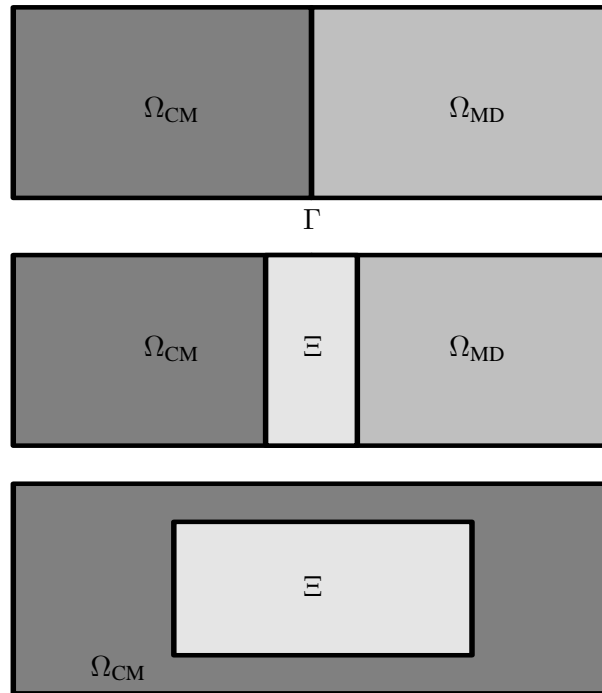
Figure 3.2: *Types of DDs: Upper: non-overlapping. Middle: overlapping/ partial overlapping. Down: overlapping / complete overlapping.*

An illustration of the three approaches is given in Figure 3.2.

The design of the coupling regions has consequences for the coupling between the molecular dynamics and the continuum mechanics. In non-overlapping methods, the separation of the fine and the coarse scale is defined by the interface. In other words, the interface is the border between coarse and fine such that a coexistence in some coupling region can be excluded.

Design of the Coupling region   In the coupling region the two description of the matter have to be matched. However, in general, the molecular dynamics is based on a description in some Euclidean space, whereas the continuum mechanics is often given in a weak sense, i.e. in a function space. Thus, it is a priori not clear, whether the coupling space is a subset of the Euclidean space or of a functions space.

Space and Transfer operator   Here, two entirely different models (finite elements and molecular dynamics) are coupled. However, the relationship between their parameters is usually not direct and thus, care must be taken for the construction of suitable transfer operators

in order to relate them. In other words, any operator has to deal with the incapability of the finite element discretization to resolve displacements down to the atomistic scale (cf. Chapter 2). Moreover the choice of the underlying space for a seamless coupling has to be chosen carefully.
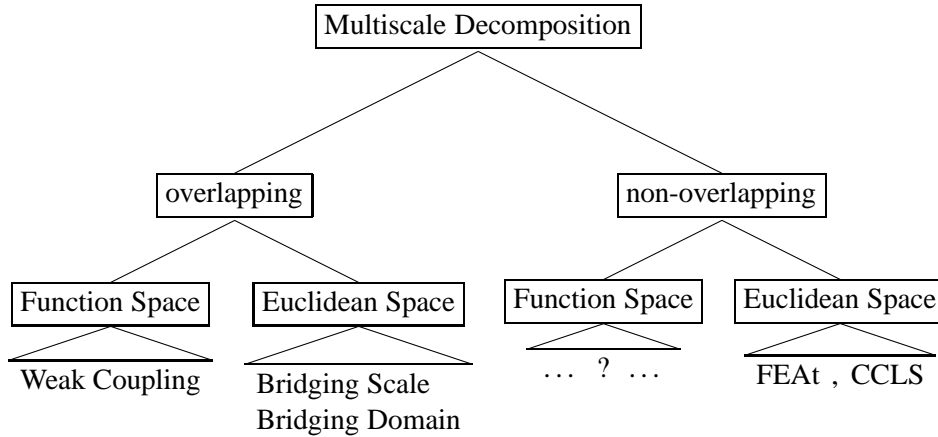

Figure 3.3: *The existing multiscale methods can be divided into overlapping and non-overlapping methods. The interface* Γ *or the handshake region* Ξ *can be chosen as an Euclidean space or function space. As a matter of fact, none of the existing methods uses a function space oriented approach.*

3.2 Overlapping Methods

Mullins and Dokanish   In 1982 Mullins and Dokanish [MD82, Mul84] started the first approach in coupling atoms with finite elements in the context of a quasi static calculation of a crack propagation in a circular domain. The basic idea is that the stresses are evaluated from the inter-atomic potential under the imposing strains stemming from the finite element nodal displacements. In a next step, these stresses are translated into nodal forces.

Bridging Scale   The authors of [WL03] developed the Bridging Scale (BS) method for coupling atomistic and continuum. Inspired by the work of [HFMQ98] the authors of [WL03] introduced the Bridging Scale method, where the molecular dynamics domain is a subset of the continuum domain (complete overlapping). Thus in the overlapping region the total displacement consists of coarse scale and fine scale displacements. A multiscale decomposition relying on a projection operator ranging from the total displacement field into the coarse part, is then applied in order to separate the two coexisting scales.
In Chapter 5 we explain this method in the context of our function space oriented multiscale approach. Therein, we discover the method of [WL03] as a special case of our concept.

Quasicontinuum Method   In the quasicontinuum (QC) method [MT02, MT04] the basic idea is to systematically coarsening out the atomic description by introducing kinematic constraints. In contrast to the convenient atomic description, the energy of a solid is computed as a function of a subset of the atoms, namely the representative atoms. Modelled after the construction of the displacement field in the finite element method, the position of the "non-representative" atoms are obtained by piecewise linear interpolation.

Originally, this method was developed in order to analyze the static atomic configurations in equilibrium. However, in the last years the QC method has been developed to handle even finite temperature and dynamic problems. The overall aim of the static QC method is to minimize the total energy by finding the corresponding atomic displacements. As a typical complete overlapping method, the QC scheme is only used in "critical sections" since the total number of degrees of freedom is $3|\mathcal{A}|$. The total energy E can be written as the sum over the energy for all atoms in the body by

$$E = \sum_{\alpha \in \mathcal{A}} E_\alpha$$

where E_α is obtained in different ways depending on the approach which is used. An example, is the Embedded Atoms Method, where E_α is determined as an electron-density dependent embedding plus the sum of a pair potential. A selection of atoms is represented by finite element nodes (representative atoms). The remaining non-representative atoms are constrained by the nodes by interpolation. The deformation gradient of linear interpolation functions can be transferred to the non-representative atoms by the Cauchy Born rule.

Coarse Grained Molecular Dynamics   The Coarse Grained Molecular Dynamics (CGMD) [RB98, RB05] reduces the atomic degrees of freedom by replacing the atomics lattice with nodes which represent either a single atom or a weighted average collection of the atoms. The energy functional on the coarse scale is defined as the atomic energy constrained to the nodes plus a thermal energy term for the degrees of freedom have been coarsed out. This substitution is justified by the equipartition theorem, which states that in thermal equilibrium the energy is shared equally. Thus, a relationship between the degrees of freedom and the thermal field is given.

The Bridging Domain Method   The Bridging Domain (BD) method has been developed by [BX03, XB04]. It is based on a Handshake region (partly overlapping), where the continuum and the atomistic description coexist. In this region both scales are combined by a weightening function for the energy. They are glued together by constraining the degrees of freedom in the bridging zone. Further work on the Bridging Domain method in a continuum to continuum coupling context [GB07], from the theoretical point of view [BPO$^+$07] as well as from the $3d$ performance aspect [ACR06] can be found in literature.

3.3 Interface Methods / Non-Overlapping Methods

Flexible Border Method   Motivated by crack propagation in a crystal in the Flexible Border Method [Sin71, SGHH78], an atomistic simulation in the next neighborhood of the crack tip is used and the remainder of the crystal is considered as an elastic continuum.

In the early applications of these models, the boundary between the atomistic and continuum was kept fixed, which led to undesirable effects like reflections. In order to avoid this, flexible boundary conditions [Sin71, SGHH78] have been proposed. Therein, the continuum elastic solution in the outer region is obtained by using the tractions from the inner atomistic region as a boundary condition. The continuum displacements from the outer region, in turn, provide the boundary conditions for the inner region. In e.g. [TZCT92] an extension of this method is described by using Greens function approach for the propagation of the perturbation from the atomistic region into the surrounding. However, these methods can hardly be transferred to $3d$ and non-linear stress strain relations are not possible.

FEAt   Nine years after the first approach of Mullins and Dokainish [MD82, Mul84] Kohlhoff et al. [KGF91] developed the FEAt method, where an atomistic model is surrounded by a finite element mesh with a small overlap region enforcing boundary condition on the atomistic as well as on the continuum domain. In particular, the authors of [KGF91] tried to overcome the capturing problem described in [MD82, Mul84] by a refinement of the FE mesh down to the atomic scale with nodal positions dictated by the crystal lattice structure.

Concurrent Coupling of Length Scale   The Concurrent Coupling of Length Scales Method (CCLS) was developed in 1998 [FBNE98, BABK99]. Even though, that the CCLS is an interface method it can be considered as a dynamic version of the QC method.

In the CCLS method, the domain is divided into a molecular dynamics and a continuum mechanics region. The choice of a continuum or a molecular description of a region depends on the required accuracy of the solution. Then an overall Hamiltonian is given by

$$\mathcal{H}(q, \dot{q}, u, \dot{u}) = \mathcal{H}^{\mathrm{MD}}(q, \dot{q}) + \mathcal{H}^{\mathrm{MD/CM}}(q, \dot{q}, u, \dot{u}) + \mathcal{H}^{\mathrm{CM}}(u, \dot{u})$$

where $\mathcal{H}^{\mathrm{MD}}(q, \dot{q})$ is the atmomistic Hamiltonian and $\mathcal{H}^{\mathrm{CM}}(u, \dot{u})$ is the continuum mechanical Hamiltonian [FBNE98]. The intermediate Hamilton $\mathcal{H}^{\mathrm{MD/CM}}(q, \dot{q}, u, \dot{u})$ accounts for the forces due to the interaction over the interface where the CM and the MD forces contribute both with half of their weight.

However the displacements q and the velocities $\dot{q}$ of the molecular Hamilton $\mathcal{H}^{\mathrm{MD}}$ are elements of the Euclidean space, whereas the displacement u and the velocity $\dot{u}$ of the continuum Hamilton are elements of a function space. Therefore, it is not possible to simply merge the different descriptions. Thus the continuum Hamilton is discretized by finite elements, such that $\mathcal{H}^{\mathrm{CM}}$ can be interpreted pointwise.

More precisely, at the interface every nodal displacement can be considered as a displacement

of an atom from its equilibrium position and vice versa. Analogously the velocities on the molecular and the continuum scale are equal. Further closely related work by the same group can also be found under the synonym Macroscopic, Atomistic, Ab-initio Dynamics (MAAD) [FBNE98].

4 The Function Space Oriented Multiscale Decomposition

In the foregoing chapter, we classified and introduced different existing approaches for multiscale coupling, i.e. the coupling between molecular dynamics and continuum mechanics concurrent.

In this section we derive a new approach for the coupling between molecular dynamics (fine scale) and continuum mechanics (coarse scale). Our approach is based on ideas from non-conforming domain decomposition methods, namely mortar methods. The key ideas of mortar methods is to provide a stable coupling between different discretizations or meshes by means of using a weak continuity condition on the respective interfaces. Starting from linear problems [BMP94], mortar methods have been extensively studied in the context of elliptic partial differential equations, see, e.g. [Bel99] and the references cited therein.

In the context of multiscale simulations, however, the coupling is often realized by means of the interpolation operator, since the atoms are in general interpreted as points in $\mathbb{R}^d$, see, e.g. [WL01, LKP06]. This chapter is structured as follows. In the first section we show how the molecular dynamics can be interpreted in a function space setting. Thereby we use the Partition of Unity Method (PUM) [BM97, Sch03] and show some basic results concerning the approximation properties. In the following section, the transfer operator, which interacts between the coarse and the fine scale is introduced in a function space setting. Without the background of molecular dynamics and continuum mechanics, we consider for the fine scale the meshfree method (PUM) and for the coarse scale the finite element method. Then, under some simplifying assumptions, like that there exists a quadratic energy on each scale, we interpret the multiscale coupling problem for the static case as a saddle point problem and show its stability.

4.1 Design of a Function Space Oriented "Coupling Space"

Let us assume, for sake of simplicity, that $\Omega = \Omega^{\mathrm{MD}} = \Omega^{\mathrm{CM}}$. Then we consider, that the configuration given by the equations of motion (1.2) can also be interpreted as a scattered data set

$$\chi_{|\mathcal{A}|}(\Omega) := \{(X_\alpha, q_\alpha) \,|\, \alpha \in \mathcal{A},\, x_\alpha \in \Omega\,,\, q_\alpha \in \mathbb{R}^d\} \subset (\mathbb{R}^d \times \mathbb{R}^d)^{|\mathcal{A}|}\,. \tag{4.1}$$

This motivates to construct an operator ι on the basis of the Moving Least Squares (MLS) approach which originated in scattered data approximation, in order to map the atoms into a function space.

The MLS method was introduced in the landmark paper by Lancaster and Salkauskas [LS81] in the context of smoothing and interpolating data. In contrast to the standard least square method in the Backhus-Gilbert sense, the moving least square method does not attempt to minimize the error point wise. The connection between these methods is pointed out in [BS89].

In the MLS method one wishes to find the best approximation from a certain approximation space to the data at a some point x with respect to a wighted ℓ_2 inner product. It is important to note, that in this context the resulting shape functions are not interpolating, more precisely they have no Kronecker delta property (1.25). However there are also interpolating versions of the MLS e.g. [LS81, She68].

For the deduction of the MLS function we can use different starting points. In the original paper the MLS shape functions are deducted by minimizing a wighted least-squares functional, however a deduction by Taylor-Series expansion of direct imposition of the consistency conditions is also possible. In [OIea96] Oñate et al. pointed out that the starting point of all least squares methods is to minimize the square distance of the error at any point with respect to a weight.

In the engineering literature the approximation space is usually the space of polynomials. This is due to the fact, that the Gram matrix can be interpreted as a moment matrix for the weights. There are also other techniques, which produce a partition of unity like for example the Reproducing Kernel Particle Methods (RKPM) for example [CPW97, LJL$^+$95, LJZ95]. More precisely an equivalence between the MLS and the RKPM can be shown. Each of the approaches described above to construct a partition of Unity can be seen as a generalization of the Shepard functions [She68], which are introduced in the following.

Our aim is to find a function $w : \overline{\Omega} \to \mathbb{R}$, such that

$$w(X_\alpha) \approx q_\alpha \text{ for all } \alpha = 1, ..., |\mathcal{A}|. \tag{4.2}$$

The starting point for our PUM is to build an approximation space V_δ. To do so, a patch $\omega_\alpha \in \mathbb{R}^d$ is attached to each point, such that the union of these patches form an open cover $C_\omega := \{\omega_\alpha\}_{\alpha \in \mathcal{A}}$ of the domain. To this end, we define for each atom α a patch ω_α associated with $X_\alpha \in \Omega$ as

$$\omega_\alpha = \{x \in \mathbb{R}^d \ : \ \|X_\alpha - x\| < h_\alpha\}. \tag{4.3}$$

The most basic property, which these patches have to fulfill, is that they cover the complete domain Ω:

$$\bigcup_{\alpha \in \mathcal{A}} \omega_\alpha \supset \Omega. \tag{4.4}$$

For an example of a 2D sketch see Figures of 4.1. On the basis of such a suitable cover C_ω we can define a partition of unity via data fitting techniques.
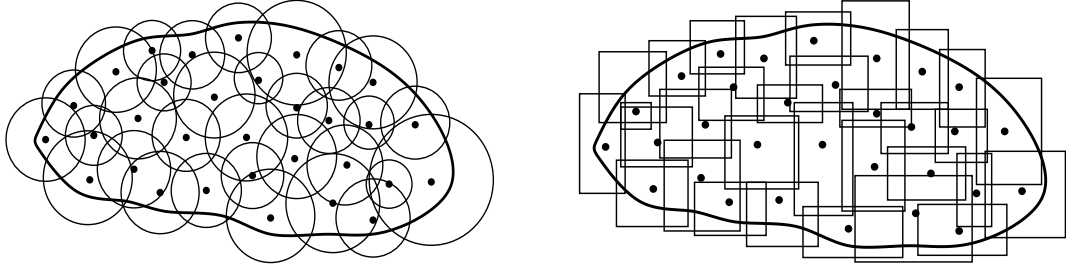
Figure 4.1: *Left: A domain with circular patches. Right: A domain with rectangular patches*

In order to construct a moving least squares (MLS) fit, we consider the approximation space being the space $\mathbb{P}_m$ of polynomials with the basis $\{P_i\}_{i=1}^n$ of degree $n := \binom{m+d}{d}$ in d variables and a set of non-negative weight functions

$$W_\alpha : \mathbb{R}^d \to \mathbb{R}_0^+ \text{ with } \mathrm{supp}(W_\alpha) = \bar{\omega}_\alpha,$$

and the dilatation parameter h_α of $W_\alpha(x) = W\left(\frac{x-X_\alpha}{h_\alpha}\right)$.

Now, we minimize for each fixed x the quadratic functional

$$J(\tau)(x) = \sum_{\alpha=1}^{|\mathcal{A}|} W_\alpha(x)(q_\alpha - \tau(X_\alpha))^2 \tag{4.5}$$

over all $\tau \in \mathbb{P}_m$.

In order to minimize (4.5), we set the derivative of (4.5) equal to zero and obtain the system of equations

$$\sum_{\alpha=1}^{|\mathcal{A}|} W_\alpha(x)q_\alpha P_j(X_\alpha) = \sum_{\alpha=1}^{|\mathcal{A}|} W_\alpha(x) \sum_{i=1}^n P_i(X_\alpha)P_j(X_\alpha)c(x) \qquad j=1,...,n. \tag{4.6}$$

With the definitions

$$P(x) := [P_1(x)\ P_2(x)\ \cdots\ P_n(x)]^T$$
$$W(x) := [W_1(x)\ W_2(x)\ \cdots\ W_{|\mathcal{A}|}(x)]^T$$
$$B := (B_{\alpha j})_{\substack{\alpha=1,\ldots,|\mathcal{A}| \\ j=1,\ldots,n}},\ B_{\alpha j} = W_\alpha(x)P_j(x)$$
$$f := [q_1\ q_2\ \cdots\ q_{|\mathcal{A}|}]^T$$
$$A(x) := (A_{ij})_{i,j=1,\ldots,n},\ A_{ij} = \sum_{\alpha=1}^{|\mathcal{A}|} P_i(X_\alpha)W_\alpha(x)P_j(X_\alpha)$$
$$c(x) := [c_1(x)\ c_2(x)\ ...\ c_n(x)]^T,$$

equation (4.6) can be written as

$$A(x)c(x) = B(x)f. \tag{4.7}$$

The above matrix $A(x)$ is also known as Gram's matrix. The minimizer $u(x)$ of (4.5) is given by the linear combination

$$w(x) = \sum_{\alpha=1}^{|\mathcal{A}|} q_\alpha \varphi_\alpha(x), \tag{4.8}$$

where the shape functions φ_α are

$$\varphi_\alpha(x) = P^T(X_\alpha)[A(x)]^{-1}W_\alpha(x)P(X_\alpha). \tag{4.9}$$

Properties of the Gram-Matrix   Note that (4.9) involves the inverse of the Gram matrix $A(x)$ for each point of evaluation. Thus, we must be concerned with the regularity of $A(x)$ for all $x \in \Omega$. Here, we attain the positive definiteness of $A(x)$ for all $x \in \Omega$ from the $\mathbb{P}_m$-unisolvence of the sets $\chi_{|\mathcal{A}|}(\Omega) \cap \omega_\alpha$ for all α. We say, that $\chi_{|\mathcal{A}|}(\Omega) \cap \omega_\alpha$ is $\mathbb{P}_m$ unisolvent if the only polynomial of total degree at most m interpolating zero data on $\chi_{|\mathcal{A}|}(\Omega) \cap \omega_\alpha$ is the zero polynomial. However, the regularity also depends on the particle distribution. This is elucidated in Section 4.1.2 .

Weight Functions and Scaling   The size of the support of the weight functions W_α, i.e. of the shape functions φ_α can be determined by

$$\omega_\alpha = \{y \in \mathbb{R}^d \mid \|X_\alpha - y\| < h_\alpha\}$$

where the dilatation parameter h_α can in principle be chosen individually for each data site X_α. However, this choice is closely related to the accuracy and stability of the approximation. Recall that the $\mathbb{P}_m$-unisolvence of $\chi_{|\mathcal{A}|}(\Omega) \cap \omega_\alpha$ for all α must be ensured. Note also that the smoothness of the approximation depends on the smoothness of the weight function, i.e. if $W_\alpha \in C^r(\Omega)$ then $\varphi_\alpha \in C^r(\Omega)$.

Reproduction Properties   From (4.8) with $q_\alpha = q(X_\alpha)$ for $q \in \mathbb{P}_m$ and (4.9) it is clear that $\mathbb{P}_m \subset \text{span}\langle\varphi_\alpha\rangle$, thus reproduction of polynomials of order m in MLS is guaranteed.

Partition of Unity and Shepard's Approach   We denote $\{\varphi_\alpha\}$ as a partition of unity of order r if the reproducing property

$$\sum_{\alpha=1}^{|\mathcal{A}|} \varphi_\alpha(x)b(x_\alpha) = b(x)$$

and the derivative reproducing conditions

$$\sum_{\alpha=1}^{|\mathcal{A}|} D^s\varphi_\alpha(x)b(x_\alpha) = D^s b(x), \quad |s| \leq r$$

hold for all $b \in \mathbb{P}_m$. In the case of $m = 0$, the approximation space is given by $\mathbb{P}_m = \{1\}$ and the Gram matrix reduces to

$$A(x) = \sum_{\alpha=1}^{|\mathcal{A}|} W_\alpha(x).$$

Thus the shape functions are given by

$$\varphi_\beta(x) = \frac{W_\beta(x)}{\sum_{\alpha=1}^{|\mathcal{A}|} W_\alpha(x)} = W(x) \cdot (A(x))^{-1}$$

which is also known as Shepard's method. One can thus easily verify, that

$$0 < \varphi_\beta(x) \leq 1 \ \text{ and } \ \sum_{\beta=1}^{|\mathcal{A}|} \varphi_\beta(x) = 1 \ \forall x \in \Omega.$$

The Shepard partition of unity is an efficient method for the approximation of scattered data, since the Gram matrix reduces to a scalar, and thus an explicit form of φ_α is given. As a drawback, the type of information captured in a function space is confined to displacements and/or velocities. For gradient based information a higher order MLS method has to be applied, which requires the implicit representation (4.9).

Thus, the shape functions φ_α are defined as

$$\varphi_\alpha(x) = \frac{W_\alpha(x)}{\sum_\beta W_\beta(x)}, \tag{4.10}$$

with weight functions W_α. Shepard [She68] originally proposed the use of

$$W_\alpha(x) = \|x - X_\alpha\|^{-t} \quad , \quad t > 0, \quad x \in \Omega. \tag{4.11}$$

It can easily be seen that the weight functions defined in (4.11) have a global support and therefore the functions φ_α have also a global support. Consequently, the evaluation of one shape function involves all weight functions W_β. Hence a localized version of Shepard's method should be employed to ensure the compact support of φ_α, i.e. we assume $\mathrm{supp}(W_\alpha) = \bar{\omega}_\alpha$ so that

$$\varphi_\alpha(x) = \frac{W_\alpha(x)}{\displaystyle\sum_{\omega_\beta \in \{\omega_\gamma \,:\, \omega_\gamma \cap \omega_\alpha \neq \emptyset\}} W_\beta(x)}\,, \quad x \in \omega_\alpha\,.$$

Thus a displacement $w \in L^2(\Omega)$ can be given by

$$w := \iota(X, q) = \sum_{\alpha=1}^{|\mathcal{A}|} q_\alpha \varphi_\alpha(x). \tag{4.12}$$

Besides the support of the W_α, the smoothness of the weight functions directly influences the smoothness of the shape functions. Here, we use splines as weight functions [Sch03]. For more details concerning the approximation properties of the PUM we refer to [BM97].
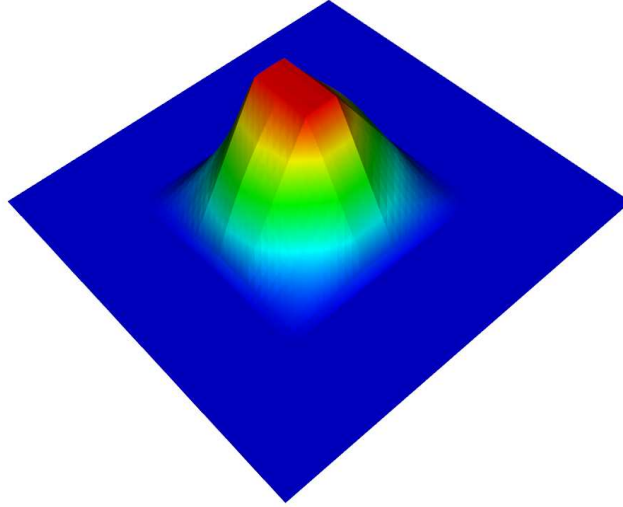

Figure 4.2: *Example of a partition of unity basis function with triangulated evaluation points.*

Our construction is essentially L^2 based and so Shepard's method should be sufficient to obtain at least first order in L^2. If we also need to bound the error in H^1 then MLS of first order should be employed.

Numerical Experiment To confirm this assertion, we consider the idealized but representative reference scattered data approximation problem (4.2) via the minimization of (4.5) for the data $f_\alpha = u(x_\alpha)$ where $u(x) = x^2$. We compare the results obtained via the MLS approach for the point set $[-3, 3]$ with $\delta = 1$ using the approximation spaces $\mathbb{P}_m$ with $m = 0, 1$. Here, we anticipate to find an asymptotic convergence behavior of $O(\delta)$ in the L^2-norm for $m = 0$ and $O(\delta^2)$ for $m = 1$. Here δ is related to the maximal atomic distance.

Furthermore, the approximation error will stagnate with respect to the H^1-norm for the Shepard functions with $m = 0$ whereas the MLS shape functions with $m = 1$ will provide an $O(\delta)$ convergence also in H^1. This expected convergence behavior can be clearly observed from Figure 4.4.
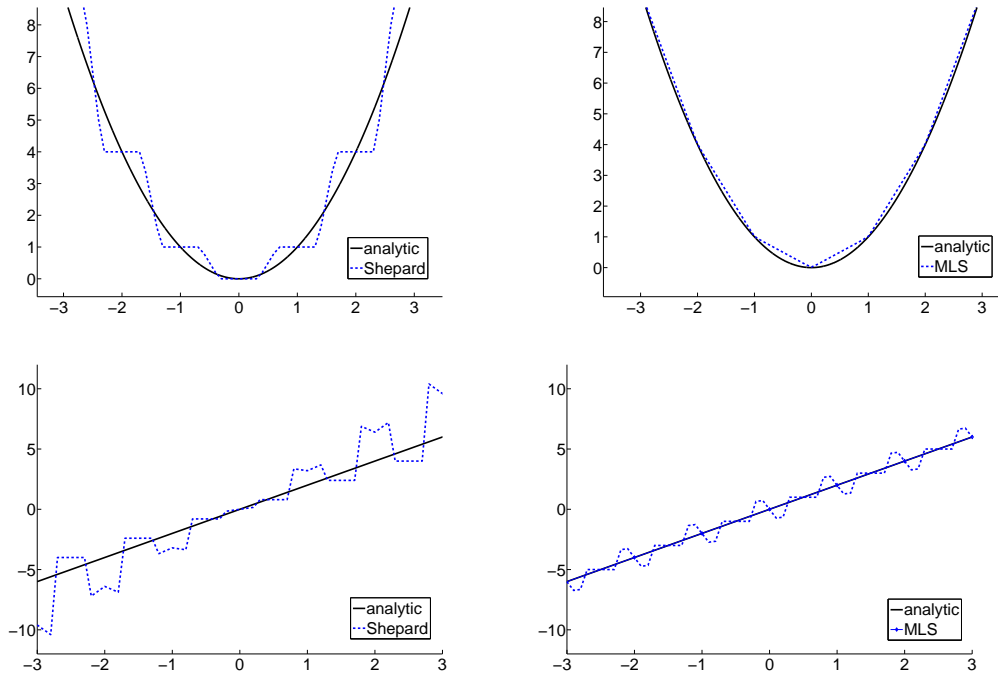
Figure 4.3: Approximation (top row) by Shepard's Method (left) and MLS (right) and the respective derivatives (bottom row).

Thus, the construction of a weak coupling operator aimed at transferring function values may be based on the Shepard functions (if the error bound of $O(\delta)$ is acceptable), compare Figure 4.3. However, if the transfer of gradient information is required the use of higher order moving least squares functions is necessary.
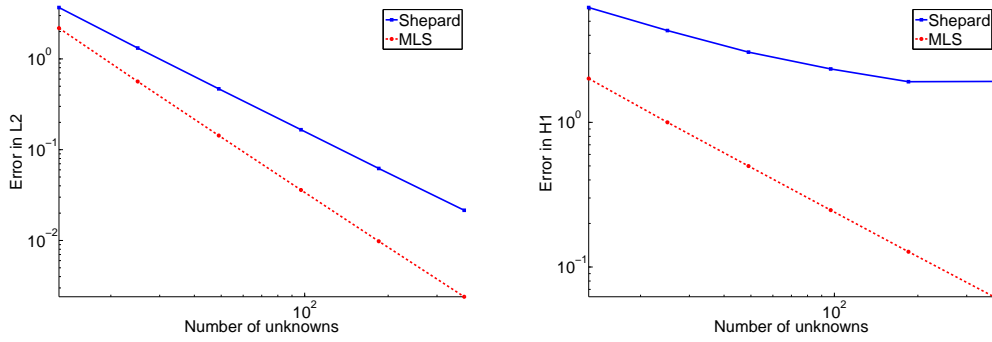
Figure 4.4: Error in the L^2-norm (left) and H^1-norm (right) of Shepard's method (solid) and the MLS (dashed).

4.1.1 Approximation Properties

In the foregoing section we explained the technical details for the construction of the Shepard functions, which form a partition of unity.

Here, we are interested in the approximation properties of the space spanned by these Shepard functions. We show, that with the aid of the partition of Unity a global conforming space can be constructed. More precisely it can be shown [BM97] that under mild assumptions the global space inherits the approximation properties of the local approximation spaces. In the following exposition we follow [BM97].

We start with the following definition:

Definition 4.1.1 *Let $\Omega \subset \mathbb{R}^d$ be an open set and $\{\omega_\alpha\}_\alpha$ an open overlapping of Ω satisfying the following pointwise overlapping condition*

$$\exists M \in \mathbb{N} \ \forall x \in \Omega \ |\{\alpha | x \in \omega_\alpha\}| \leq M \ . \tag{4.13}$$

Moreover, let $\{\varphi_\alpha\}$ be a collection of Lipschitz functions subordinate to the cover $\{\omega_\alpha\}$ satisfying

- *supp $\varphi_\alpha \subset \bar{\omega}_\alpha$*

- *$\sum_\alpha \varphi_\alpha \equiv 1$ on Ω*

- *$\|\varphi_\alpha\|_{L^\infty(\Omega)} \leq C_\infty$*

- *$\|\nabla \varphi_\alpha\|_{L^\infty(\Omega)} \leq \frac{C_G}{\text{diam} \, \omega_\alpha}$,*

where C_∞ and C_G are two constants. Then we call $\{\varphi_\alpha\}_\alpha$ a partition of unity subordinate to the cover $\{\omega_\alpha\}$.

Definition 4.1.2 *Let $\{\omega_\alpha\}$ be an open cover of $\Omega \subset \mathbb{R}^d$ and let $\{\varphi_\alpha\}$ be a partition of unity subordinate to $\{\omega_\alpha\}_\alpha$. Let $\mathcal{V}_\alpha \subset H^1(\omega_\alpha \cap \Omega)$ be given. Then we call*

$$\mathcal{V}_\delta = \sum_\alpha \varphi_\alpha \mathcal{V}_\alpha = \{\sum_\alpha \varphi_\alpha v_\alpha \,|\, v_\alpha \in \mathcal{V}_\alpha\} \subset H^1(\Omega)$$

a PUM-space. We recall, δ is proportional to the particle distance. The PUM space is said to be of degree $m \in \mathbb{N}$ if $\mathcal{V}_\delta \subset C^m(\Omega)$. The spaces $\mathcal{V}_\alpha$ are referred to as the local approximation spaces.

Having this, we give the following theorem which enables us to construct a global approximation space $\mathcal{V}_\delta$ from the local approximation spaces $\mathcal{V}_\alpha$.

Theorem 4.1.3 *Let $\Omega \subset \mathbb{R}^d$ be a Lipschitz domain. Let $\{\omega_\alpha\}, \{\varphi_\alpha\}$ and $\{\mathcal{V}_\alpha\}$ be given by Definitions 4.1.1, 4.1.2. Let $u \in H^1(\Omega)$ be the function to be approximated. Assume that the local approximation spaces $\mathcal{V}_\alpha$ have the following approximation properties: On each patch $\omega_\alpha \cap \Omega$, u can be approximated by a function $v_\alpha \in \mathcal{V}_\alpha$ such that*

(i)
$$\|u - v_\alpha\|_{L^2(\omega_\alpha \cap \Omega)} =: \varepsilon_1(\alpha)$$

(ii)
$$\|\nabla(u - v_\alpha)\|_{L^2(\omega_\alpha \cap \Omega)} =: \varepsilon_2(\alpha).$$

Then the function
$$u_\delta = \sum_\alpha \varphi_\alpha v_\alpha \in \mathcal{V}_\delta \subset H^1(\Omega)$$

fulfills for $u \in H^1(\Omega)$

$$\|u - u_\delta\|_{L^2(\Omega)} \leq \sqrt{M} C_\infty \left(\sum_\alpha \varepsilon_1^2(\alpha) \right)^{1/2} \tag{4.14}$$

$$\|\nabla(u - u_\delta)\|_{L^2(\Omega)} \leq \sqrt{2M} \left(\sum_\alpha \left(\frac{C_G}{\mathrm{diam}(\omega_\alpha)} \right)^2 \varepsilon_1(\alpha) + C_\infty^2 \varepsilon_2^2(\alpha) \right)^{1/2}. \tag{4.15}$$

For the proof we refer to [BM97].

Remark The assumption, that the patches ω_α are a Lipschitz domain is required to ensure that $\mathcal{V}_\delta \subset H^1(\Omega)$. Note, that the constant M in (4.13) controls the number of overlaps of the patches. However, the size of the overlap is also crucial since for $M = 1$ we have $\varphi_\alpha = \chi_{\bar{\omega}_\alpha}$, where $\chi_{\bar{\omega}_\alpha}$ is the characteristic function. Thus, small overlaps cause large gradients.
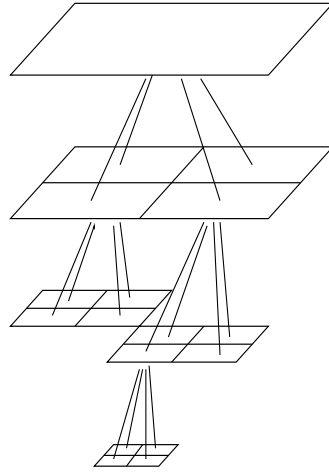
Figure 4.5: *An example of an octree.*

4.1.2 Particle Distribution and Crystalline Structures

As we have seen, the construction of ι starts with an arbitrary scattered data set. Here, we consider crystals and thus an almost regular particle distribution can be expected. We now seek for an efficient construction of a Partition of Unity for the molecules in their reference configuration. This can be best reached by a d-binary tree cover [GKZC04].

Starting point of the tree is the construction of the root node. This is done, by assigning an axes parallel cube Q with $\Omega \subset Q$ to the root. Then we partition the domain in each coordinate direction into two equal parts. Thus, in $2d$ after the first iteration we would have four subdomains. Then, in a next step, every sub domain is again separated into smaller sub domain by the same rule. This recursion is terminated, when there is either no particle or only one particle in the sub domain. These subs domains are then called leaves. Thus each leaf corresponds to a particle (cf. Figure 4.5).

For the patches we proceed as follows: We use d-rectangular shaped patches, whose boundaries are axes parallel. Then, we arrange them, such that for each node p of the tree, which is not a leaf, the corresponding patch is defined such that:

$$\omega_p \supseteq \omega_\alpha \qquad \text{for all sons } \alpha. \tag{4.16}$$

The demand (4.16) on the patches is crucial for the cut detection with finite elements, which is explained in the next chapter. More precisely, due to (4.16) we can exploit the property that for each node p in the tree and $t \in \mathcal{T}^h$ we have

$$t \cap \omega_p = \emptyset \Rightarrow t \cap \omega_\alpha = \emptyset \qquad \text{for all sons } \alpha \text{ of } p.$$

Later on we see that this property dramatically increases speed in a cut detection.

4.2 The Scale Transfer

Our aim is to construct a coarse scale approximation $\bar{w} \in \mathcal{V}_h$ of the total displacement function given by (4.12). The coarse scale representation $\bar{w} \in \mathcal{V}_h$ of the molecular displacement function w is defined by means of the L^2-projection $\pi_h \colon L^2(\Omega) \longrightarrow \mathcal{V}_h$, i.e.

$$\pi_h(w) \in \mathcal{V}_h \ : \ (\pi_h(w), \mu)_{L^2(\Omega)} = (w, \mu)_{L^2(\Omega)} \qquad \forall \mu \in \mathcal{M}_h \,, \qquad (4.17)$$

where, the multiplier space $\mathcal{M}_h$ is defined by

$$\mathcal{M}_h = \mathrm{span}\{\mu_s \,|\, s \in \mathcal{N}_h\} \,. \qquad (4.18)$$

Here, the basis functions $\mu_s, \ s \in \mathcal{N}^h$ are assumed to have the local support $\mathrm{supp}\mu_s \subseteq \mathrm{supp}\lambda_s|_{\overline{\Omega}}$. As is the case in the mortar setting, there are several possible choices for the basis functions μ_s of $\mathcal{M}_h$. We follow the standard approach, see, e.g. [BMP94, Bel99] by setting

$$\mu_s = \psi_s|_{\overline{\Omega}}, \quad s \in \mathcal{N}_h \,. \qquad (4.19)$$

Remark Of course, for the construction of the L^2 projection the domain and in particular the boundary of the domain is crucial. Since here, the main concern is the general construction of the transfer operator from the coarse to the fine scale, we neglect the domain aspect and elaborate it in Chapter 5 and 6.

4.3 A Simplified Model Problem and the Saddle Point Formulation

In this section we elaborate the technical details for coupling of the two scales. As we have seen, the transfer operator π_h couples the coarse and the fine scale in an L^2 framework.
Here, we consider this coupling in a more abstract sense and consider the coarse/- fine coupling problem as a coupling between two different discretization methods. More precisely, we examine the stability of the L^2 projection between the mesh free partition of unity method and the mesh based finite element method.
In the literature several approaches for coupling mesh free and mesh based methods have been proposed. Most of these methods are motivated by the problem of imposing boundary conditions in a mesh free method. Indeed, in contrast to the shape functions used in the finite element method, most of the mesh free methods do not satisfy the Kronecker delta property, i.e. $\varphi_p(q) = \delta_{pq}$. One method to overcome this difficulty is to couple them with finite element close to the domain boundary.

An early approach is the coupling by a ramp function [BOK95]. Later on the coupling by the Enrichment Technique [FMH02] and the coupling by the Bridging Scale [WL01] were introduced. In a comparison of the Bridging Scale and the Enrichment Technique ([HFML04])

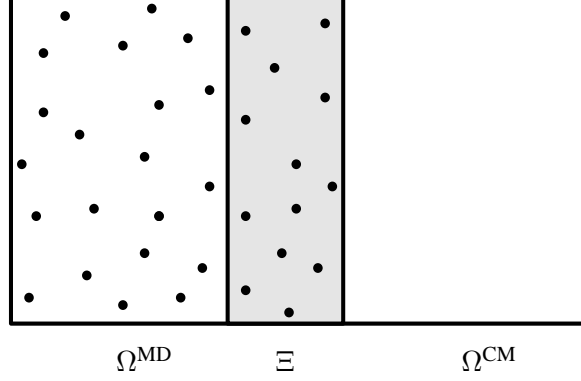it is pointed out that the Bridging Scale method is not advisable for this meshfree and mesh based coupling.

Figure 4.6: *An example of the intersection of a continuum and a molecular domain*

Here we are interested in examining the stability of this method. Based on the domain $\Omega \subset \mathbb{R}^d$ we define

$$\Omega = \Omega^{\text{MD}} \cup \Omega^{\text{CM}} \qquad \Xi = \Omega^{\text{MD}} \cap \Omega^{\text{CM}},$$

where $\text{meas}_d(\Xi) > 0$. In contrast to [HFML04] we consider the coupling of a meshfree and meshbased method as a constrained minimization problem. We assume, that we have a static problem, moreover the energy on the continuum scale and on the molecular scale are given by the bilinear forms

$$a_{\text{CM}}(\cdot, \cdot) : H^1(\Omega^{\text{CM}}) \times H^1(\Omega^{\text{CM}}) \to \mathbb{R} \qquad (4.20)$$

$$a_{\text{MD}}(\cdot, \cdot) : H^1(\Omega^{\text{MD}}) \times H^1(\Omega^{\text{MD}}) \to \mathbb{R} \qquad (4.21)$$

respectively and the external forces are given by the linear forms $f_{\text{CM}}(\cdot) : H^1(\Omega^{\text{CM}}) \to \mathbb{R}$ and $f_{\text{MD}}(\cdot) : H^1(\Omega^{\text{MD}}) \to \mathbb{R}$. We furthermore define the Lagrange multiplier space by $M := (H^1(\Xi))'$, where we denote by $(H^1(\Xi))'$ the dual of $H^1(\Xi)$. Let us therefore denote by $\mathbf{H}_{\text{CM,MD}}$ the product space of $H^1(\Omega^{\text{CM}})$ and $H^1(\Omega^{\text{MD}})$, i.e.

$$\mathbf{H}_{\text{CM,MD}} := H^1(\Omega^{\text{CM}}) \times H^1(\Omega^{\text{MD}}),$$

which is a Sobolev space with the product norm [Ada75]

$$|||v||| := (\|v_{\text{CM}}\|^2_{H^1(\Omega^{\text{CM}})} + \|v_{\text{MD}}\|^2_{H^1(\Omega^{\text{MD}})})^{1/2}. \qquad (4.22)$$

Furthermore we define

$$\mathbb{H}_{\text{CM,MD}} := H_{\text{CM,MD}} \backslash \{0\} \,.$$

Then we define on this tensor space the bilinear from

$$a(\cdot, \cdot) := a_{\text{CM}}(\cdot, \cdot) + a_{\text{MD}}(\cdot, \cdot)$$

and

$$f(\cdot) = f_{\text{CM}}(\cdot) + f_{\text{MD}}(\cdot)$$

Then we can give the saddle point formulation:

Saddle Point Problem 4.3.1 *Find* $(u, \lambda) \in \mathbf{H}_{CM,MD} \times M$

$$a(u, v) + b(\lambda, \begin{bmatrix} u_{CM} \\ u_{MD} \end{bmatrix}) = f(u) \qquad \forall v \in \mathbf{H}_{CM,MD} \qquad (4.23)$$

$$b(\mu, \begin{bmatrix} u_{CM} \\ u_{MD} \end{bmatrix}) = 0 \qquad \forall v \in \mathbf{H}_{CM,MD} \qquad (4.24)$$

where

$$b(\lambda, \begin{bmatrix} u_{\text{CM}} \\ u_{\text{MD}} \end{bmatrix}) := (u_{\text{CM}} - u_{\text{MD}}, \lambda)_{L^2(\Xi)}.$$

From the saddle point theory it is well known that the choice of the space M of the Lagrange multipliers is essential for the well posedness of the saddle point formulation. More precisely the spaces have to satisfy the inf-sup condition [Bab73, Bre74, BF91], which is given by

$$\exists \beta : \forall \lambda \in M, \ \sup_{u \in \mathbb{H}_{\text{CM,MD}}} \frac{b(\lambda, u)}{|||u|||} \geq \beta \|\lambda\|_{(H^1(\Xi))'}. \qquad (4.25)$$

Other choices of the multiplier space can result in non optimal estimates for the discretized problem. Here, we show that our choice $M = (H^1(\Xi))'$ fulfills these demands. To do so let us recall the following facts.

For the relation between an element and its dual, we need

Theorem 4.3.2 (Riesz Representation Theorem) *Let* $\mathcal{V}$ *be a Hilbert space and let* $\mathcal{V}'$ *be its dual. Let furthermore* $l \in \mathcal{V}'$. *Then there exists a unique* $u \in \mathcal{V}$ *for which*

$$l(v) = (v, u) \qquad \forall v \in \mathcal{V}.$$

In addition we have

$$\|l\|_{\mathcal{V}'} = \|u\|_{\mathcal{V}}.$$

Definition 4.3.3 (Gelfand Triple) *Let* $\mathcal{V} \subset U$ *be Hilbert spaces and let us assume, that the embedding* $\mathcal{V} \hookrightarrow U$ *is continuous and dense. Furthermore we identify* U' *with its Riesz repre-*

sentation of U. Then we have the Gelfand triple

$$\mathcal{V} \subset U \subset \mathcal{V}'.$$

Having introduced these tools we can now give

Theorem 4.3.4 *Let us assume that there exists a bounded extension operator onto $H^1(\Omega^{CM})$ (cf. [Ste70][Thm 5, p. 181]) such that for $u \in H^1(\Xi)$ we have*

$$u_{CM} = \mathcal{E}(u) \in H^1(\Omega^{CM}) \tag{4.26}$$

with

$$C\|\mathcal{E}(u)\|_{H^1(\Omega^{CM})} \leq \|u\|_{H^1(\Xi)}. \tag{4.27}$$

then the inf-sup condition

$$\exists \beta : \forall \lambda \in M, \ \sup_{u \in \mathbb{H}_{CM,MD}} \frac{b(\lambda, u)}{|||u|||} \geq \beta \|\lambda\|_{(H^1(\Xi))'} \tag{4.28}$$

holds.

Proof. Since

$$\sup_{u \in \mathbb{H}_{CM,MD}} \frac{b(\lambda, u)}{|||u|||} \geq \sup_{u_{CM} \in H^1(\Omega^{CM})\setminus\{0\}} \frac{(\lambda, u_{CM})_{L^2(\Xi)}}{\|u_{CM}\|_{H^1(\Omega^{CM})}}.$$

it is adequate to show

$$\exists \beta : \forall \lambda \in M, \ \sup_{u_{CM} \in H^1(\Omega^{CM})\setminus\{0\}} \frac{(\lambda, u_{CM})_{L^2(\Xi)}}{\|u_{CM}\|_{H^1(\Omega^{CM})}} \geq \beta \|\lambda\|_{(H^1(\Xi))'}, \tag{4.29}$$

then (4.28) follows.

Due to the Gelfand triple 4.3.3 we can write formally [Wlo82]

$$(\lambda, u)_{L^2(\Xi)} = \langle \lambda, u \rangle_{(H^1(\Xi))' \times H^1(\Xi)},$$

where $\langle \cdot, \cdot \rangle$ is the duality between $(H^1(\Xi))' \times H^1(\Xi)$. Then, by applying the Riesz Representation Theorem 4.3.2 there exists $u_\lambda \in H^1(\Xi)$ such that

$$\langle \lambda, u \rangle_{(H^1(\Xi))' \times H^1(\Xi)} = (u_\lambda, u)_{H^1(\Xi)}, \qquad \forall u \in H^1(\Xi),$$

i.e. u_λ is the representing element of λ. Thus we write

$$(\lambda, u_{CM})_{L^2(\Xi)} = (u_\lambda, u)_{H^1(\Xi)}. \tag{4.30}$$

Inserting (4.30) into (4.29) yields

$$\sup_{u_{\mathrm{CM}}\in H^1(\Omega^{\mathrm{CM}})\setminus\{0\}} \frac{(\lambda, u_{\mathrm{CM}})_{L^2(\Xi)}}{\|u_{\mathrm{CM}}\|_{H^1(\Omega^{\mathrm{CM}})}} = \sup_{u_{\mathrm{CM}}\in H^1(\Omega^{\mathrm{CM}})\setminus\{0\}} \frac{(u_\lambda, u_{\mathrm{CM}})_{H^1(\Xi)}}{\|u_{\mathrm{CM}}\|_{H^1(\Omega^{\mathrm{CM}})}}$$

By choosing $u_{\mathrm{CM}} = \mathcal{E}(u_\lambda)$ we obtain

$$\sup_{u_{\mathrm{CM}}\in H^1(\Omega^{\mathrm{CM}})\setminus\{0\}} \frac{(u_\lambda, u_{\mathrm{CM}})_{H^1(\Xi)}}{\|u_{\mathrm{CM}}\|_{H^1(\Omega^{\mathrm{CM}})}} \geq \frac{(u_\lambda, u_\lambda)_{H^1(\Xi)}}{\|\mathcal{E}(u_\lambda)\|_{H^1(\Omega^{\mathrm{CM}})}} \tag{4.31}$$

$$\geq \frac{1}{C} \frac{\|u_\lambda\|^2_{H^1(\Xi)}}{\|u_\lambda\|_{H^1(\Xi)}} \tag{4.32}$$

$$\geq \frac{1}{C} \frac{\|u_\lambda\|_{H^1(\Xi)}\|\lambda\|_{(H^1(\Xi))'}}{\|u_\lambda\|_{H^1(\Xi)}} \tag{4.33}$$

$$\geq \beta\|\lambda\|_{(H^1(\Xi))'}. \tag{4.34}$$

Thus we have

$$\sup_{u\in\mathbb{H}_{\mathrm{CM,MD}}} \frac{b(\lambda, u)}{|||u|||} \geq \beta\|\lambda\|_{(H^1(\Xi))'},$$

with $\beta = 1/C$. $\qquad\qquad\square$

In a next step we want to ensure the stability of the discrete counterpart of the saddle point problem. More precisely, we want to show, that for

Saddle Point Problem 4.3.5 *Find* $(u_{h,\delta}, \lambda_h) \in \mathcal{V}_{h,\delta} \times \mathcal{M}_h$

$$a(u_{h,\delta}, v_{h,\delta}) + b\left(\lambda_h, \begin{bmatrix} u_h \\ u_\delta \end{bmatrix}\right) = f(u_{h,\delta}) \qquad\qquad \forall v_{h,\delta} \in \mathcal{V}_{h,\delta} \tag{4.35}$$

$$b\left(\mu_h, \begin{bmatrix} u_h \\ u_\delta \end{bmatrix}\right) = 0 \qquad\qquad \forall \mu_h \in \mathcal{M}_h \tag{4.36}$$

the discrete inf-sup condition holds, i.e.

$$\sup_{u_{h,\delta}\in\mathcal{V}_{h,\delta}\setminus\{0\}} \frac{b\left(\lambda_h, \begin{bmatrix} u_h \\ u_\delta \end{bmatrix}\right)}{|||u_{h,\delta}|||} \geq \beta\|\lambda_h\|_{\mathcal{M}_h}, \tag{4.37}$$

where β is independent of h and δ and

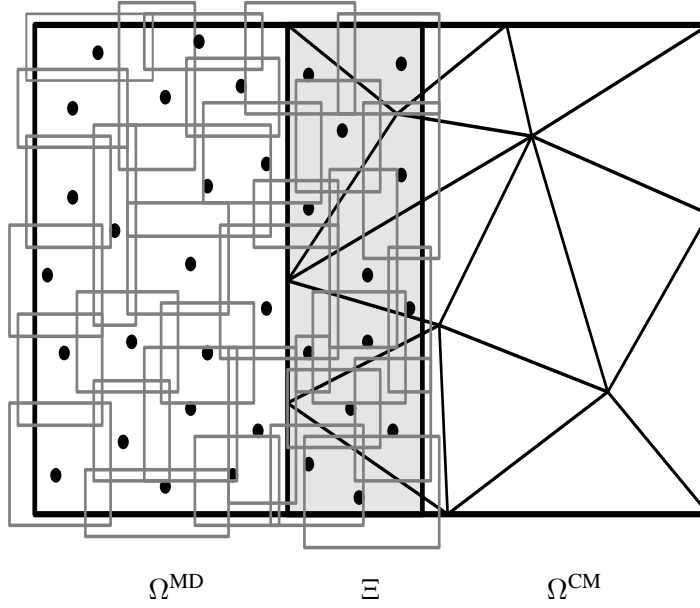$$\mathcal{V}_{h,\delta} := \mathcal{V}_h \times \mathcal{V}_\delta$$

Figure 4.7: *The domain Ω where Ω^{MD} is described by a meshfree method and Ω^{CM} is described by the FE method.*

is equipped with the norm $||| \cdot |||$. The multiplier space $\mathcal{M}_h$ is equipped with the norm $\| \cdot \|_{(H^1(\Xi))'}$.

In order to show the discrete inf-sup condition, we employ the continuous inf-sup condition and apply the Fortin trick [For77, BF91]:

Lemma 4.3.6 (Fortin Trick) *Let the bilinear form $b : \mathbf{H}_{CM,MD} \times M \to \mathbb{R}$ fulfill the continuous inf-sup condition (4.28). Furthermore, assume, that there exists to the subspaces $\mathcal{V}_{h,\delta}$ and $\mathcal{M}_h$ a bounded linear operator $\hat{\pi} : \mathbf{H}_{CM,MD} \to \mathcal{V}_{h,\delta}$ such that*

$$b(v - \hat{\pi}v, \mu_h) = 0 \qquad \forall \mu_h \in \mathcal{M}_h.$$

If $|||\hat{\pi}||| \leq c$ with a constant $c > 0$ independent of h, then $\mathcal{V}_{h,\delta}$ and $\mathcal{M}_h$ fulfill the discrete inf-sup condition (4.37)

We define for $u = (u^{CM}, u^{MD})^T$

$$\hat{\pi}(u) = \left(\begin{array}{c} \pi_h(u^{CM} - u^{MD}) \\ 0 \end{array} \right).$$

Here $\pi_h : L^2(\Xi) \to \mathcal{V}_h$ is defined for suitable $\mathcal{M}_h$ by

$$(\pi_h w, \mu_h)_{L^2(\Xi)} = (w, \mu_h)_{L^2(\Xi)} \qquad \forall \mu \in \mathcal{M}_h.$$

Thus we have, that

$$b(\mu_h, u - \hat{\pi} u) = b\left(\mu_h, \begin{bmatrix} u^{\mathrm{CM}} \\ u^{\mathrm{MD}} \end{bmatrix} - \hat{\pi} u\right) = (\mu_h, u_{\mathrm{CM}} - u_{\mathrm{MD}} - \pi_h(u^{\mathrm{CM}} - u^{\mathrm{MD}}))_{L^2(\Xi)} = 0.$$

We can show, that

$$|||\hat{\pi}||| \leq c \qquad c \neq c(h).$$

To do so, we consider

$$\begin{aligned}
|||\hat{\pi}||| &= \sup_{v \in \mathbb{H}_{\mathrm{CM,MD}}} \frac{|||\hat{\pi} v|||}{|||v|||} \\
&= \sup_{v \in \mathbb{H}_{\mathrm{CM,MD}}} \frac{\|\pi_h(v^{\mathrm{CM}} - v^{\mathrm{MD}})\|_{H^1(\Xi)}}{(\|v^{\mathrm{CM}}\|^2_{H^1(\Omega^{\mathrm{CM}})} + \|v^{\mathrm{MD}}\|_{H^1(\Omega^{\mathrm{MD}})})^{1/2}} \\
&\leq \sup_{v \in \mathbb{H}_{\mathrm{CM,MD}}} \frac{\|\pi_h v^{\mathrm{CM}}\|_{H^1(\Omega^{\mathrm{CM}})} + \|\pi_h v^{\mathrm{MD}}\|_{H^1(\Omega^{\mathrm{CM}})}}{(\|v^{\mathrm{CM}}\|^2_{H^1(\Omega^{\mathrm{CM}})} + \|v^{\mathrm{MD}}\|_{H^1(\Omega^{\mathrm{MD}})})^{1/2}} \quad (4.38) \\
&\leq \frac{\|v^{\mathrm{CM}}\|_{H^1(\Omega^{\mathrm{CM}})} + \|v^{\mathrm{MD}}\|_{H^1(\Omega^{\mathrm{MD}})}}{(\|v^{\mathrm{CM}}\|^2_{H^1(\Omega^{\mathrm{CM}})} + \|v^{\mathrm{MD}}\|_{H^1(\Omega^{\mathrm{MD}})})^{1/2}} \leq 2. \quad (4.39)
\end{aligned}$$

Since $a + b \leq 2(a^2 + b^2)$, $a, b > 0$ by Young's inequality. For the step from (4.38) to (4.39) we exploited the $H^1(\Xi)$ stability of π_h. In [BX91] the H^1 stability of the projection π_h has been shown, if the multiplier space is chosen as $\mathcal{M}_h = \mathcal{V}_h$.

To show the H^1 stability for a wider class of multiplier spaces we follow [KLPV01]. This class of multiplier spaces is characterized by the following assumptions:

M1 The discrete multiplier space $\mathcal{M}_h$ contains constant functions.

M2 We have that $\dim(\mathcal{V}_h) = \dim(\mathcal{M}_h)$.

M3 There exists a constant C independent of h, such that

$$\|u_h\|_{L^2(\Xi)} \leq C \sup_{\lambda_h \in \mathcal{M}_h} \frac{(u_h, \lambda_h)_{L^2(\Xi)}}{\|\lambda_h\|_{L^2(\Xi)}} \qquad \forall u_h \in \mathcal{V}_h$$

Lemma 4.3.7 *Let the triangulation $\mathcal{T}^h$ be globally quasi uniform, that is $h_t \geq c\bar{h}$ for all $t \in \mathcal{T}^h$. Moreover let the domain Ξ be polygonal, and M1-M3 hold. Then*

$$\|\pi_h u\|_{H^1(\Xi)} \leq C \|u\|_{H^1(\Xi)}, \qquad u \in H^1(\Xi)$$

where C does not depend on the meshsize.

Proof. By our assumption, that the mesh is quasi uniform, there exists an operator $Q :$ $L^2(\Xi) \to \mathcal{V}_h$ (Clément interpolation), such that [Cle75]

$$\|Qu\|^2_{H^1(\Xi)} + \sum_{t \in \mathcal{T}^h} h_t^{-2} \|(I - Q)u\|^2_{L^2(t)} \leq C \|u\|^2_{H^1(\Xi)}. \tag{4.40}$$

Let us for fixed $u \in H^1(\Xi)$ show, that the operator Q full fills

$$\|(\pi_h - Q)u\|_{H^1(\Xi)} \leq C \|u\|_{H^1(\Xi)}. \tag{4.41}$$

By the inverse inequality, we have

$$\|(\pi_h - Q)u\|^2_{H^1(\Xi)} \leq h^{-2} \|(\pi_h - Q)u\|^2_{L^2(\Xi)}. \tag{4.42}$$

Together with M3 and by exploiting that π_h is a L^2 projection, we obtain

$$\|(\pi - Q)u\|_{L^2(\Xi)} \leq C \sup_{\psi_h \in \mathcal{M}_h} \frac{((\pi_h - Q)u, \psi_h)_{L^2(\Xi)}}{\|\psi_h\|_{L^2(\Xi)}}$$

$$= C \sup_{\psi_h \in \mathcal{M}_h} \frac{((I - Q)u, \psi_h)_{L^2(\Xi)}}{\|\psi_h\|_{L^2(\Xi)}}.$$

We then furthermore have that

$$C \sup_{\psi_h \in \mathcal{M}_h} \frac{((I - Q)u, \psi_h)_{L^2(\Xi)}}{\|\psi_h\|_{L^2(\Xi)}} \leq C \sup_{\psi_h \in \mathcal{M}_h} \frac{\sum_{t \in \mathcal{T}} h_t^{-2} \|(I - Q)u\|_{L^2(t)} h_t^2 \|\psi_h\|_{L^2(t)}}{\|\psi_h\|_{L^2(\Xi)}}$$

$$\leq C \sup_{\psi_h \in \mathcal{M}_h} \frac{\left(\sum_{t \in \mathcal{T}} h_t^{-2} \|(I - Q)u\|^2_{L^2(t)} \right)^{1/2} \left(\sum_{t \in \mathcal{T}} h_t^2 \|\psi_h\|^2_{L^2(t)} \right)^{1/2}}{\|\psi_h\|_{L^2(\Xi)}}$$

$$\leq Ch \|u\|_{H^1(\Xi)}.$$

In the last step we used (4.40), in particular we only need, that
$\sum_{t \in \mathcal{T}} h_t^{-2} \|(I - Q)u\|^2_{L^2(t)} \leq C \|u\|^2_{H^1(\Xi)}$.
Thus we obtain (4.41). By the negative triangle inequality, i.e. $\|x\| - \|y\| \leq \|x - y\|$ and (4.40) we have

$$\|\pi_h u\|^2_{H^1(\Xi)} \leq \|(\pi_h - Q)u\|^2_{H^1(\Xi)} + \|Qu\|^2_{H^1(\Xi)}$$

$$\leq C \|u\|^2_{H^1(\Xi)}$$

$\square$

Finally, we can now prove

Theorem 4.3.8 *Under the above assumptions, we have that for the discrete saddle point problem the inf-sup condition holds.*

Proof.

Analogously to the Fortin operator [For77], we have

$$\beta \|\lambda_h\|_{(H^1(\Xi))'} \leq \sup_{u \in \mathbb{H}_{\text{CM,MD}}} \frac{b(\lambda_h, u)}{|||u|||} \tag{4.43}$$

$$= \sup_{u \in \mathbb{H}_{\text{CM,MD}}} \frac{b(\lambda, \hat{\pi}u)}{|||u|||} \tag{4.44}$$

$$\leq c \sup_{u \in \mathbb{H}_{\text{CM,MD}}} \frac{(\lambda_h, \pi_h(u^{\text{CM}} - u^{\text{MD}}))_{L^2(\Xi)}}{|||\hat{\pi}u|||} \tag{4.45}$$

$$= c \sup_{u_{\delta,h} \in \mathcal{V}_{h,\delta}} \frac{b(\lambda_h, u_{\delta,h})}{|||u_{\delta,h}|||} \tag{4.46}$$

$$\square$$

Summing up, we have developed a new transfer operator based on a weak coupling approach. The key idea is to construct the transfer operator on the basis of weighted local averaging instead of using point wise taken values, which is done - to our knowledge - in all existing methods. For the construction of the local weight functions we assign a partition of unity to the molecular degrees of freedom. This allows for decomposing the micro scale displacements into a low frequency and a high frequency part by means of a weighted L^2 projection. Thus, the entire formulation is in the setting of a function space. Moreover, we have shown for the static case, that our weak coupling operator for the coupling of a meshfree and a mesh based method is H^1 stable.

5 The Weak Multiscale Method for the Completely Overlapping Case

In the foregoing chapter we introduced the function space oriented approach, which allows us to interpret the atoms in a function space and and L^2 projection to separate the displacement into a coarse and fine scale displacement. Thereby, we assumed, that the coarse scale and the fine scale domain coincide. However for most applications it is plausible, that $\Omega^{\mathrm{MD}} \subset \Omega^{\mathrm{CM}}$ where $\mathrm{diam}(\Omega^{\mathrm{MD}}) \ll \mathrm{diam}(\Omega^{\mathrm{CM}})$. Here, we consider this case, more precisely we assume that the whole domain Ω is discretzed by finite elements, i.e. $\Omega^{\mathrm{CM}} = \Omega$ and only in a small subset $\Omega^{\mathrm{MD}} \subset \Omega$ the molecular dynamics is employed. Thus the handshake region is $\Xi = \Omega^{\mathrm{MD}}$.

Note, that in Ξ the molecular description and the continuum description coexists. Thus the displacement on Ξ can be decomposed into a coarse and a fine scale.

5.1 Multiscale Decomposition

In Chapter 2 it has been understood, that a molecular displacement can be interpreted as a superposition of waves. Furthermore on the finite element side, for a given mesh size, there exists a maximum frequency, which can be represented. In other words, for a given finite element mesh size h only waves with a wavenumber

$$\kappa_{\mathrm{max}} = \kappa_{\mathrm{max}}(h) \leq \frac{\pi}{h} \tag{5.1}$$

can be represented. Otherwise effects like aliasing might occur. As a consequence of the dispersion relation, then the maximum frequency for the representation of waves is bounded, too.

This observation is the starting point for a multiscale decomposition, which decomposes the total displacement field into coarse and fine scale.

More precisely, the total atomistic displacement field is decomposed by

$$q = \bar{q} + q', \tag{5.2}$$

where $\bar{q}$ is the coarse part and q' is the fine scale part. Here, the difficulty that the atomistic displacements are given as point-values in the "discrete" space $\mathbb{R}^{d|\mathcal{A}|}$, whereas the macro-scale displacements are usually assumed to be some functions in, e.g., a Sobolev space. As a

consequence, at a first glance a direct sum decomposition of the underlying function space as in [HFMQ98] is not possible.

In the bridging scale method [WL03], the Euclidean space is chosen as underlying space of the decomposition (5.2) Then the authors of [WL03] define the coarse scale displacement $\bar{q}$ as the mass weighted least squares fit of q. To do so, they write

$$d := \operatorname{argmin}_{v \in \mathcal{V}_h} \sum_{\alpha \in \mathcal{A}} m_\alpha |q - Nv|^2, \tag{5.3}$$

where N is the interpolation from the finite element nodes to the atomistic scale, i.e. $N_{\alpha,p} = \psi_p(X_\alpha)$. Here ψ_p is the finite element basis function (see (1.26)). With $M_\mathcal{A}$ defined in (1.3) we rewrite (5.3) to obtain

$$d = (N^T M_\mathcal{A} N)^{-1} N^T M_\mathcal{A} q.$$

Then a linear mapping P can be defined by

$$Pq = \bar{q} = Nd = N(N^T M_\mathcal{A} N)^{-1} M_\mathcal{A} q.$$

Summing up, the decomposition (5.2) is given by

$$q = Pq + Qq = Nd + Qq,$$

with $Q = I - P$.

5.2 Multiscale Decomposition in Function Space

In contrast to this, we consider a scale decomposition in a function space. We therefore employ the approach introduced in Chapter 4 by interpreting the discrete displacements $q_\alpha \in \mathbb{R}^d$ as elements of the function space $\mathcal{V}_\delta$. Let us recall, that this is done by means of the linear operator which maps the discrete displacements of the atoms $q_\alpha, \alpha \in \mathcal{A}$ into a function space, i.e.

$$\iota : (\mathbb{R}^d \times \mathbb{R}^d)^{|\mathcal{A}|} \to \mathcal{V} \subset L^2(\Omega). \tag{5.4}$$

This embedding can be chosen in a problem-dependent fashion and the properties of the resulting multiscale decomposition depend strongly on the choice of a basis $\{\varphi_\alpha\}$ for $\mathcal{V}$. Recall, that the total displacement in function space from (4.12) was given by $w = \iota(X, q) = \iota(q) \in \mathcal{V}$ and thus the displacement is

$$w = \overline{w} + w', \tag{5.5}$$

where $\overline{w}$ is the coarse part and w' is the fine scale part.

Remark The origin of this scale decomposition can be found in the contributions to the variational multiscale decomposition in the context of conforming finite element spaces
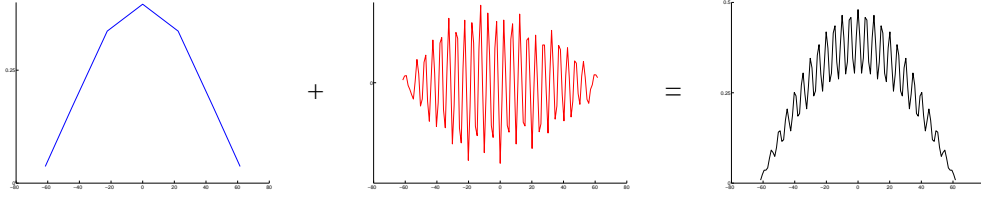
Figure 5.1: *Scale decomposition of the total displacement field ν*

[HFMQ98].

5.2.1 The Weak Approach for a Multiscale Decompostion in Function Space

Let us reconsider a body $\Omega \subset \mathbb{R}^d$, $d = 1, 2, 3$, which, under the influence of external and internal forces, undergoing some deformation. Here, we give a multiscale approach for the description of the body's deformation.

In the style of Chapter 1 we briefly review the discrete models on the continuum and atomistic scale. Let us start with the micro scale. For reasons of computational efficiency, the MD-simulation is only applied locally to a portion $\Xi \subset \Omega$ of our body. This domain of interest Ξ might be the neighborhood around a crack tip or at the vicinity of a contact boundary, where local effects are expected to take place which cannot be represented on the coarser scale.

The material behavior on the micro scale is now modelled by means of an isolated system of atoms or molecules of a crystalline solid. The atomic displacements $q = (q_\alpha)_{\alpha \in \mathcal{A}_\Xi}$ are assumed to obey Newton's law of motion $M_{\mathcal{A}_\Xi} \ddot{q} = F$, where $\mathcal{A}_\Xi := \{\alpha \in \mathcal{A} : X_\alpha \in \Xi\}$. However, for sakes of simplicity, we simply set $\mathcal{A} = \mathcal{A}_\Xi$.

In the remaining part $\Omega \backslash \Xi$ only the coarse scale model is employed. There FE model employed on the macro scale is based on a continuum mechanics approximation of the deformation of our body Ω. Following the basic approach of continuum mechanics, on the macro scale the body in its reference configuration is identified with the smooth and bounded domain $\Omega \subset \mathbb{R}^d$. In order to approximate the continuous displacement field, we employ a finite element discretization of lower order as described in Chapter 1, more precisely given in (1.26).

Here, we do not incorporate any Dirichlet boundary conditions into the ansatz–space $\mathcal{V}_h(\Omega)$, since the finite element space $\mathcal{V}_h$ will only serve as the coarse scale space for the representation of the total displacement field.

On the basis of the weak coupling concept we now can give the Bridging Scale method in a function space based setting. In a next step we define the subset $\Xi \subset \Omega$ where the coarse as well as the fine scale simulation is present. To do so, we define $\mathcal{T}_\Xi^h \subset \mathcal{T}^h$ as the set of
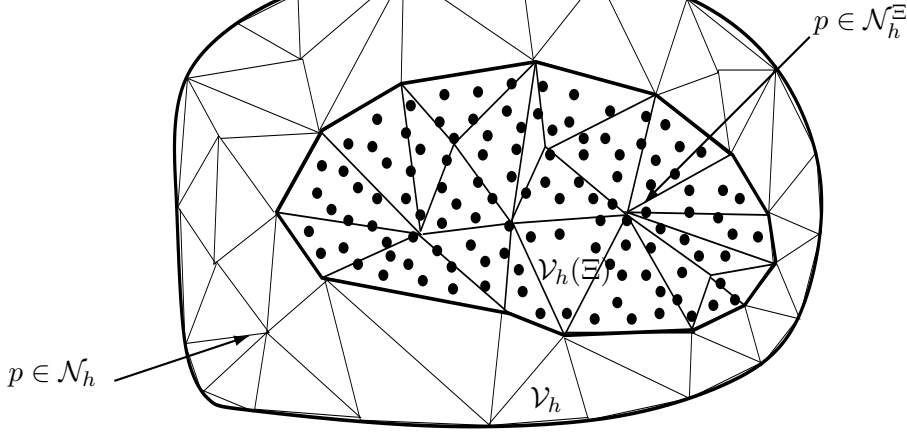
Figure 5.2: *Example of a domain* Ω *with the complete overlapping.*

simplexes having a nonempty intersection with the particles, i.e.

$$\mathcal{T}_\Xi^h = \{t \in \mathcal{T}^h, \bar{t} \cap \chi \neq \emptyset\},$$

and its set of nodes by $\mathcal{N}_h^\Xi$. Here, $\chi = \chi_{|\mathcal{A}|}$ is the set of particles defined in (4.1).

Thus we have

$$\Xi = \bigcup_{t \in \mathcal{T}_\Xi^h} \bar{t} \text{ and } \mathcal{V}_h(\Xi) = \mathcal{V}_h\big|_\Xi$$

Let us remark that the size and shape of the domain Ξ is not predetermined and can be chosen arbitrary. As a consequence the choice of the size of the handshake region Ξ is a design decision. In practice this is a balancing of affordable computer power and required accuracy.

Like in the Bridging Scale Method, the coupling between the coarse and the fine scale is often realized by means of the interpolation operator. This seems natural since in general the atoms are interpreted as points in $\mathbb{R}^d$.

Using the techniques described in the previous chapter, however, we are free to interpret atoms either as elements in $\mathbb{R}^d$ or as functions in L^2. This allows for a function space based coupling, leading to our weak multiscale operator.

In order to perform the decomposition given in (5.5) we define the coarse scale representation $\bar{w} \in \mathcal{V}_h$ of the molecular displacement function w by means of the L^2-projection $\pi_h \colon L^2(\Xi) \longrightarrow \mathcal{V}_h(\Xi)$, i.e.

$$\pi_h(w) \in \mathcal{V}_h(\Xi) \; : \; (\pi_h(w), \mu)_{L^2(\Xi)} = (w, \mu)_{L^2(\Xi)} \qquad \forall \mu \in \mathcal{M}_h, \tag{5.6}$$

where, the multiplier space $\mathcal{M}_h$ is defined by

$$\mathcal{M}_h = \mathrm{span}\{\mu_s \,|\, s \in \mathcal{N}_h^\Xi\}\,.$$

Here, the basis functions μ_s, $s \in \mathcal{N}_h^\Xi$ are assumed to have the local support $\mathrm{supp}\mu_s \subseteq \mathrm{supp}\psi_s|_{\overline{\Xi}}$. As is the case in the mortar setting, there are several possible choices for the basis functions μ_s of $\mathcal{M}_h$. We follow the standard approach, see, e.g. [BMP94, Bel99] by setting

$$\mu_s = \psi_s|_{\overline{\Xi}}, \quad s \in \mathcal{N}_h^\Xi\,. \tag{5.7}$$

Our coarse scale representation is now defined by extending $\pi_h(w) \in \mathcal{V}_h(\Xi)$ to $\bar{w}$, i.e. $\bar{w} = \mathcal{E}(\pi_h(w))$, where $\mathcal{E}: \mathcal{V}_h(\Xi) \to \mathcal{V}_h$ is an extension operator. Thus we can rewrite (5.5) by

$$w = w' + \bar{w} = (w - \mathcal{E}(\pi_h(w))) + \mathcal{E}(\pi_h(w))\,. \tag{5.8}$$

For the extension operator $\mathcal{E}$, different choices are possible cf. [QV99]. Here we chose the discrete extension

$$\mathcal{E}(v) = \sum_{p \in \mathcal{N}_h} v_p \psi_p \ \text{with} \ \begin{cases} v_p = w_p &, \quad p \in \mathcal{N}_h^\Xi, \\ v_p = 0 &, \quad \text{otherwise}\,. \end{cases}$$

In the spirit of mortar methods, we call the finite-element space $\mathcal{V}_h$ the slave space and the approximation space spanned by the Shepard functions the master space.

By construction, our coupling operator π_h allows for the decomposition of the L^2-kinetic energy $\tilde{\mathcal{T}}$ into a coarse scale and a fine scale part in an L^2 sense, analogue to [WL03]. In the case $\mathcal{M}_h = \mathcal{V}_h(\Xi)$ which is known as the standard multiplier space in the mortar setting, we moreover have

$$\begin{aligned}
\tilde{\mathcal{T}} &= \frac{1}{2}(\dot{w}, \dot{w})_{L^2(\Xi)} \\
&= \frac{1}{2}(\dot{w}, \dot{\bar{w}})_{L^2(\Xi)} + \frac{1}{2}(\dot{w}, \dot{w}')_{L^2(\Xi)} \\
&= \frac{1}{2}(\dot{\bar{w}}, \dot{\bar{w}})_{L^2(\Xi)} + \frac{1}{2}(\dot{w}', \dot{\bar{w}})_{L^2(\Xi)} + \frac{1}{2}(\dot{w}, (I - \pi_h)\dot{w})_{L^2(\Xi)} \\
&= \frac{1}{2}(\dot{\bar{w}}, \dot{\bar{w}})_{L^2(\Xi)} + \frac{1}{2}(\dot{w}, (I - \pi_h)\dot{w})_{L^2(\Xi)}
\end{aligned}$$

since the mixed term $\frac{1}{2}(\dot{w}', \dot{\bar{w}})_{L^2(\Xi)}$ vanishes due to the fact that $\mathrm{range}(I - \pi_h)\perp\mathcal{M}_h$.

Relation to the Bridging Scale Method In order to show, that the BS method is a special case of our framework from Chapter 4, we consider the case that the domain Ξ is decomposed

into non overlapping patches ω_α such that

$$\Xi = \bigcup_{\alpha \in \mathcal{A}} \omega_\alpha.$$

On these patches we define basis functions $(\tilde{\varphi}_\alpha)_{\alpha \in \mathcal{A}}$ by

$$\tilde{\varphi}_\alpha(x) = \begin{cases} 1 & \text{if} \quad x \in \omega_\alpha \\ 0 & \text{if} \quad x \notin \omega_\alpha \end{cases}$$

and thus we can replace the underlying Euclidean space from the decomposition (5.2) by

$$H_{\text{BS}} := \sum_{\alpha \in \mathcal{A}} \text{span}(\varphi_\alpha) \subset L^2(\Xi).$$

The atomistic density $\rho_\mathcal{A}$ can then be given by $\rho_\mathcal{A} = \sum_{\alpha \in \mathcal{A}} \frac{m_\alpha}{\text{meas}(\omega_\alpha)} \varphi_\alpha$.

In a next step, the projection operator in the original context of the bridging scale method is replaced by an L^2 projection on the weighted L^2 scalar product $(\cdot, \cdot)_{\rho_\mathcal{A}} = (\cdot, \rho_\mathcal{A} \cdot)_{L^2(\Xi)}$ from H_{BS} to $\mathcal{V}_h$. More precisely for $q \in H_{\text{BS}}$ the finite element representation of $d \in \mathcal{V}_h$ is given by

$$(d, \mu)_{\rho_\mathcal{A}} = (q, \mu)_{\rho_\mathcal{A}} \qquad \text{for all } \mu \in \mathcal{V}_h(\Xi). \tag{5.9}$$

Here, the coarse scale part of the total displacement field is given by $\bar{q} = Nd$, where N is defined by $N\psi_p = \sum_{\alpha \in \mathcal{A}} \psi_p(X_\alpha)\tilde{\varphi}_\alpha$. Thus the operator form of (5.9) is given by

$$\bar{q} = NM^{-1}\widetilde{N}^T q \tag{5.10}$$

with the finite element mass matrix $M = (m_{pq})_{pq \in \mathcal{N}_h^\Xi}, m_{pq} = \int_\Xi \rho_\mathcal{A} \psi_p \psi_q$ and

$$(\widetilde{N})_{\alpha p} = \int_\Xi \rho_\mathcal{A} \varphi_\alpha \psi_p \approx \text{meas}(\omega_\alpha)\rho(X_\alpha)\psi_p(X_\alpha) = m_\alpha \psi_p(x_\alpha) = (M_\mathcal{A}N)_{\alpha p}.$$

Here the usage of the midpoint rule quadrature is justified if $\text{diam}\,(\omega_\alpha) \ll \text{diam}\,(t)$, $t \in \mathcal{T}_\Xi^h$.

What we have done so far is to replace the discrete space in the Bridging Scale method by a function space $H_{\text{BS}} \subset L^2(\Xi)$. The function space approach assumes a continuous extension of the molecular displacement field. Then, in a next step, we used an approximation of this extended molecular displacement field for the construction of a projection, which then involves the evaluation at all spatial points $X_\alpha \in \Xi$.

However the construction of piecewise constant basis functions $(\tilde{\varphi}_\alpha)_{\alpha \in \mathcal{A}_\Xi}$ has a less approximation order than our function space oriented approach.

5.2.2 Discrete Representation of the Weak Approach

Let us now describe, how to obtain the discrete representation of our transfer operator. Inserting $w = \sum_{\alpha \in \mathcal{A}} q_\alpha \varphi_\alpha$ and $\pi_h(w) = \sum_{p \in \mathcal{N}_h} \pi_p \psi_p$ into (5.6), we obtain

$$M\pi = Rq \tag{5.11}$$

with $M = (m_{ts})_{t,s \in \mathcal{N}_h}$ and $R = (r_{s\alpha})_{s \in \mathcal{N}_h, \alpha \in \mathcal{A}}$ and

$$r_{s\alpha} = \int_\Omega \mu_s \varphi_\alpha \quad \text{and} \quad m_{ts} = \int_\Omega \psi_t \mu_s \,. \tag{5.12}$$

here, we have set $q = (q_\alpha)_{\alpha \in \mathcal{A}}$ and $\pi = (\pi_p)_{p \in \mathcal{N}_h}$. This gives rise to our weak coupling operator in its algebraic representation

$$W = M^{-1}R, \tag{5.13}$$

which transfers the low-frequency information from the fine to the coarse scale.

In order to compute the algebraic representation of π_h in (5.6), we need to assemble two (generalized) mass matrices. For the matrix M, we need to evaluate integrals of the form $\int_\Omega \mu_p \psi_q \, dx$, where μ_p are the basis functions spanning the multiplier space $\mathcal{M}_h$, and ψ_q are the basis functions of $\mathcal{V}_h$. Here, p, q are assumed to be in some index set $\mathcal{N}_h$ with $d|\mathcal{N}_h| = \dim(\mathcal{V}_h)$. The computation of the resulting mass matrix can be done in a similar fashion as the assembly of the standard mass matrix.

For assembling the matrix R, we need to evaluate integrals of the form

$$\int_{\omega_\alpha \cap \text{supp}(\mu_p)} \mu_p \varphi_\alpha \, dx. \tag{5.14}$$

In order to compute these integrals, the cut between the support of μ_p and the patch ω_α has to be computed. On the resulting polytope, then the quadrature has to be carried out. Since, following our approach, the cut polytopes can be controlled in their size but not in their shape, the quadrature is a challenging task. In order to deal with this problem we have developed and implemented the library CUTLIB [DK08], which allows for cut detection and quadrature on the resulting cut-polytopes. We explain this in the next paragraph.

Assembling the rectangular Matrix R   The assembling of the transfer operator in dimensions $d \geq 2$ is a subtle task. Due to the large number of atoms in Ω we are in need for an efficient, yet robust, algorithm for the construction of the algebraic representation of π. Since the assembling of the rectangular matrix R requires the computation of all intersections $\omega_\alpha \cap t$, $t \in \mathcal{T}^h$, $\mathcal{T}^h$ being the set of all elements in the finite element mesh, we haven chosen rectangular/cuboid patches ω_α (see [Sch03]).

In the engineering literature, often radial patches are used in connection with a fixed background mesh for the quadrature. This allows for the use of radial basis functions φ_α which is mathematically very appealing. However, exact integration with a background mesh and standard quadrature formulas (such as Gauss quadrature) is almost impossible. Rectangular patches allow for exact quadrature, which is needed for the stability of $M^{-1}R$. Furthermore, the computation of the cuts $\omega_\alpha \cap t$ can be handled by using ideas from computational geometry as described below. For representing the projection π we need to assemble the matrices M and R. The assembling of M and R is similar, even though for special choices of $\mathcal{M}_h$ the computation of M is simpler (e.g., if $\mathcal{M}_h = \mathcal{V}_h$).

For the efficient implementation of the assembling we need to perform the following tasks with (quasi-)optimal complexity:

1. Given a finite element mesh-element $t \in \mathcal{T}^h$ find all atoms α such that $\omega_\alpha \cap t \neq \emptyset$.

2. Compute the polytope $\omega_\alpha \cap t$.

3. Decompose $\omega_\alpha \cap t$ into simpler polytopes on which quadrature formulas for the exact integration can be applied.

The use of an quadtree (octree) or kd-trees structure yields quasi-optimal complexity for queries as in Step 1. For the cut-computations in Step 2 we apply the quickhull algorithm [BDH96] along with a simplex method. For each cut $\omega_\alpha \cap t$ we need to compute an interior point. This is realized by describing each cut $\omega_\alpha \cap t$ as the intersection of finitely many half planes $\{x \in \mathbb{R}^d \mid -n_j^T x + g_j \geq 0, j = 1, \ldots, n\}$. For $d = 3$, after the introduction of the two additional variables x_4, x_5, an interior point $(p_1, p_2, p_3)^T = \left(\frac{x_1}{x_4}, \frac{x_2}{x_4}, \frac{x_3}{x_4}\right)^T$ can be obtained from the linear constrained maximization problem:

Maximize x_5 among all tuples $(x_1, x_2, x_3, x_4, x_5)$ such that

$$-n_j^T (x_1, x_2, x_3)^T + g_j \cdot x_4 - x_5 \geq 0, \ j = 1, .., n$$

and $x_5 > 0, x_4 \geq \varepsilon$ with small $\varepsilon > 0$.

Given such an interior point, the intersection algorithm from [PS85] is applied, which gives a description of $\omega_\alpha \cap t$ by means of half planes.

In case of sufficiently smooth basis functions, i.e. $\varphi_\alpha \in C^1(\bar{\omega}_\alpha)$, Step 3 could be carried out by computing a Delaunay triangulation of the polytope $\omega_\alpha \cap t$ and applying a quadrature formula of sufficient high order on each triangle/tetrahedron. However, in our application $\varphi_\alpha \in C^1(\bar{\omega}_\alpha)$ generally is not fulfilled, for the following two reasons:

- The functions W_α are constructed from one-dimensional splines by a tensor-approach. For linear splines, a jump in the derivatives along the connections between the center of mass of ω_α and the midpoints of the edges/sides occurs.

- The derivative of φ_α can be discontinuous along $\omega_\alpha \cap \partial\omega_\beta$, $\alpha \neq \beta$ and $\omega_\alpha \cap \omega_\beta \neq \emptyset$.

As a consequence, for the assembling of R the set

$$D_{\alpha,t} = \{x \in t \,:\, \nabla \varphi_\alpha \text{ discontinuous in } x\}$$

needs to be resolved for each $t \in \mathcal{T}^h$. This can be done by either choosing a Delaunay triangulation which conforms to the constraint that $D_{\alpha,t}$ is contained in the union of all edges/sides, or by subdividing ω_α prior to the cut detection and applying Step 2 and Step 3 to each sub-rectangle/sub-cuboid separately.

Assembling the Matrix M　Due to the definition of $\mathcal{V}_h$ and for suitably chosen $\mathcal{M}_h$, the matrix M has the character of a finite element mass matrix, is well conditioned and $M^{-1}\mu$ can be computed easily for any $\mu \in \mathcal{M}_h$.
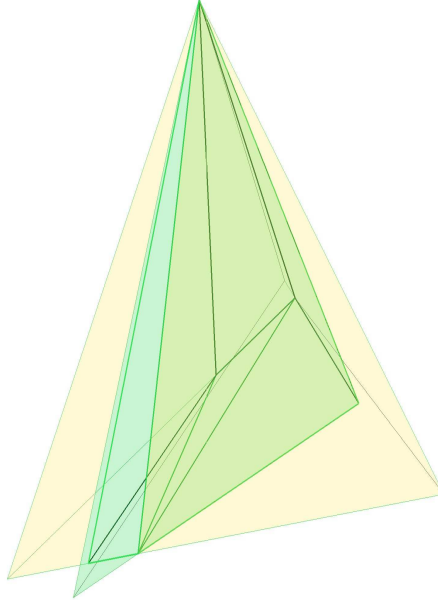

Figure 5.3: Two tetrahedra in $\mathbb{R}^3$ and Delaunay triangulation of the resulting cut polytope

Relation to the Bridging Scale method　In contrast to (5.13), the coarse scale description in the Bridging Scale Method [WL03] is given by

$$\widetilde{W} = M_{\text{con}}^{-1} N^T M_{\mathcal{A}}, \tag{5.15}$$

with $M_{\text{con}} = N^T M_{\mathcal{A}} N$ and $M_{\mathcal{A}}$ given by (1.3). In the Bridging Scale Method, the transition from coarse to fine scale is defined by interpolation and the projection from fine to coarse is defined as the least squares approximation of the atomistic displacements with respect to the

atomistic mass matrix M_A. More precisely, the components of $M_{\text{con}} = \tilde{m}_{p,q \in \mathcal{N}^h}$ are given by

$$\tilde{m}_{pq} = \sum_{\alpha \in \mathcal{A}} m_\alpha \lambda_p(X_\alpha) \lambda_q(X_\alpha) = \sum_{\alpha \in \mathcal{A}} \frac{m_\alpha}{\text{meas}(\omega_\alpha)} \lambda_p(X_\alpha) \lambda_q(X_\alpha) \cdot \text{meas}(\omega_\alpha) \approx \int_\Xi \lambda_p \lambda_q \, dx \, .$$
(5.16)

Thus, assuming that the density $\frac{m_\alpha}{\text{meas}(\omega_\alpha)}$ is one and that the patches $(\omega_\alpha)_{\alpha \in \mathcal{A}_\Xi}$ fulfill $\omega_\alpha \cap \omega_\beta = \emptyset \iff \alpha \neq \beta$, (5.16) can be interpreted as a summed quadrature rule.

By introducing the scalar product $\langle \cdot, \cdot \rangle_{\text{BS}} := \langle M_A \cdot, \cdot \rangle$ on $\mathbb{R}^{|\mathcal{A}|} \times \mathbb{R}^{|\mathcal{A}|}$ the projection from the total displacement field w to the coarse part $\bar{w}$ is given by

$$\langle N\bar{w}, N\mu \rangle_{\text{BS}} = \langle w, N\mu \rangle_{\text{BS}} \qquad \forall \mu \in \mathbb{R}^{|\mathcal{N}_h^\Xi|},$$

i.e. the bridging scale method can be seen to be based on the choice $\mathcal{M}_h = \text{span}\{\lambda_p \,|\, p \in \mathcal{N}_h^\Xi\}$. However, the coupling itself uses the discrete scalar product $\langle \cdot, \cdot \rangle_{\text{BS}}$, which distinguishes it from our approach, where the L^2 scalar product connected to the coarse scale is used. This probably seems to be the more natural approach within the weak formulation of the finite element method.

For investigating the structure of the bridging scale operator $\widetilde{W}$ in more detail, let us consider the case that the masses of the atoms are equal, i.e. $m = m_1 = m_2 = ... = m_{|\mathcal{A}|}$. Then, the atomistic mass matrix M_A reduces to $M_A = m \, \text{Id}$ and the coarse scale mass matrix becomes $M_{\text{con}} = N^T M_A N = m N^T N$. Thus, the operator $\widetilde{W}$ reduces to

$$\widetilde{W} = (N^T N)^{-1} N^T \, ,$$

which are simply the normal equations stemming from

$$\langle N\bar{w} - w, N\mu \rangle = 0 \ \mu \in \mathbb{R}^{|\mathcal{N}_h^\Xi|}.$$

We now want to explore more differences and commonalities between (5.15) and (5.13). For sake of simplicity, we consider the case, that only two particles X_α and X_β are in the support of the two shape functions ψ_1 and ψ_2. Then the matrix N in (5.15) as well as the matrix R in (5.13) become quadratic:

$$N = \begin{pmatrix} \psi_1(X_\alpha) & \psi_1(X_\beta) \\ \psi_2(x_\alpha) & \psi_2(X_\beta) \end{pmatrix} \qquad R = \begin{pmatrix} \int_{\omega_{1\alpha}} \psi_1 \varphi_\alpha & \int_{\omega_{1\beta}} \psi_1 \varphi_\beta \\ \int_{\omega_{2\alpha}} \psi_2 \varphi_\alpha & \int_{\omega_{2\beta}} \psi_2 \varphi_\beta \end{pmatrix},$$

where $\omega_{j\alpha} = \text{supp}(\psi) \cap \omega_\alpha$

In the forthcoming, we consider the condition numbers $\kappa(\widetilde{W})$ and $\kappa(W)$ in dependence of the distance $d_{\alpha\beta} := |X_\alpha - X_\beta|$. The condition number is indicative of the stability or sensitivity of the transfer operators.

In Table 5.1, the condition number in dependence of the distance is shown. It can be seen that
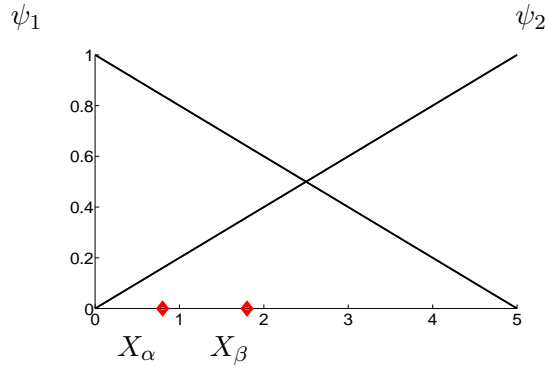
Figure 5.4: *Two particles in the support of one element*

$d_{\alpha\beta}$	1	0.9	0.8	0.7	0.6	0.5	0.4	0.3
$\kappa(\widetilde{W})$	6.1905	6.9812	7.9746	9.2577	10.9756	13.3893	17.0212	23.0900
$\kappa(W)$	3.1027	3.2188	3.3274	3.4186	3.5502	3.6052	3.6559	3.7311

Table 5.1: *Comparison of the condition number of N and W w.r.t. the distance between the two particles α and β*

the condition number $\kappa(\widetilde{W})$ is increasing while $\kappa(W)$ grows very slowly. In fact, the growth of the condition number of the matrix R can be controlled, since the integration domains ω can be chosen individually such that the patches are pairwise different. Obviously, the argumentation above also holds for the case of more than two particles in the support of the element.

In the following, we compare our new weak transfer operator with the transfer operator $\widetilde{W}$. As measures for the comparison we chose the norms $\|\cdot\|_{L^2(\Omega)}$ and $\|\cdot\|_{L^\infty(\Omega)}$.

We adopt the numerical example of [LKP06]:
The interval $[-100r_0, 100r_0]$ is covered by 40 linear finite elements with mesh size $h = 5r_{\text{EQ}}$. To each of the 56 atoms between $-28r_0$ and $28r_0$, a patch of size $0.6r_0$ is attached. For the molecular scale the Lennard-Jones (LJ) potential see (1.13) is used.
Outside the MD/FE region the nodal forces are calculated via the Cauchy-Born rule.
The initial amplitude in the molecular part is given by

$$q_{\text{init}} = q(X, t = 0) = \begin{cases} A\dfrac{e^{-(X/\sigma)^2} - q_c}{1 - q_c}\left(1 + b\cos\left(\frac{2\pi X}{H}\right)\right) & \text{if } |X| \le L_c \\ 0 & \text{if } |X| > L_c \end{cases} \qquad (5.17)$$

Here, A is the amplitude, σ is the width and truncation at L_c of the initial wave. It can be clearly seen, that $1 + b\cos\left(\frac{2\pi X}{H}\right)$ is the fine scale contribution, where the length scale H is small compared to σ. The parameter b determines the magnitude of the fine scale. Finally $q_c = e^{-(L_c/\sigma)^2}$ is the unshifted impulse at $X = L_c$.

Let T_{end} be the total run time of the simulation. We follow [LKP06] by advancing both simulations by a time step $\Delta t \in [0, T]$. Thus in a single time step the coarse scale simulation is advanced once and the fine scale simulation is advanced m times. The fractional time steps in the n-th coarse scale time step is given by $[j] := n + \frac{j}{m}$ and the sub cycle time step is given by $\tau_m = \frac{\tau}{m}$. On the fine scale the velocity Verlet and on the coarse scale the explicit central difference algorithm are used. We furthermore assume that p^n, q^n, s^n are given, then the update is given by:

$$
\begin{aligned}
p^{[j+1]} &= p^{[j]} + q^{[j]}\tau_m + 1/2 s^{[j]}\tau_m^2 & & p \text{ MD displacement} \\
q^{[j+1/2]} &= q^{[j]} + s^{[j]}\tau_m & & q \text{ MD velocity} \\
s^{[j+1]} &= M_A^{-1} f(p^{[j+1]}) & & s \text{ MD acceleration} \\
q^{[j+1]} &= q^{[j+1/2]} + \frac{1}{2}s^{[j+1]}\tau_m. & &
\end{aligned}
$$

After $m = 50$ fine scale steps the molecular dynamics quantities of the coarse time step $n + 1$ are obtained. In order to advance the coarse scale simulation from n to $n + 1$ the internal forces are computed by combining the coarse scale displacement $\bar{w}$ and the fine scale part $Q = (I - NW)$ of the molecular simulation.

$$
\begin{aligned}
d^{n+1} &= d^n + v^n \Delta t + \frac{1}{2}a^n \tau^2 & & d \text{ FE displacement} \\
a^{n+1} &= M^{-1} N^T f(Nd + Qq) & & a \text{ FE acceleration} \\
v^{n+1} &= v^n + \frac{1}{2}(a^n + a^{n+1})\Delta t & & v \text{ FE velocity.}
\end{aligned}
$$

In order to measure the difference between the discrete displacement field stemming from the atomistic scale with the values of the coarse scale, in our approach we choose the the L^2 norm. On Ξ, this error can easily be computed as

$$
\|w - k_i(w)\|_{L^2(\Xi)}^2 = w^T M_{\text{PUM}} w - 2w^T R k_i(w) + k_i(w)^T M k_i(w), \qquad i = 1, 2, \quad (5.18)
$$

where M_{PUM} is the PUM mass matrix whose elements are given by $m_{\alpha\beta}^{\text{PUM}} = \int \varphi_\alpha \varphi_\beta$. Here, k_1 is the least squares projection $\widetilde{W}$ and k_2 is the weak coupling operator W. For the error in the $\|\cdot\|_\infty$ norm, we simply computed

$$
\|w - N(k_i(w))\|_\infty^2, \qquad i = 1, 2, \tag{5.19}
$$

Table 5.2 shows the obtained errors for $i = 1, 2$.

	$\|\cdot\|_{L^2(\Xi)}$		$\|\cdot\|_\infty$	
coarse time step	bridging scale	weak coupling	bridging scale	weak coupling
3	$6.0 \cdot 10^{-3}$	$2.7 \cdot 10^{-4}$	$2.8 \cdot 10^{-2}$	$6.7 \cdot 10^{-3}$
6	$3.0 \cdot 10^{-2}$	$1.1 \cdot 10^{-4}$	$5.3 \cdot 10^{-2}$	$4.8 \cdot 10^{-3}$
9	$6.0 \cdot 10^{-2}$	$5.7 \cdot 10^{-4}$	$7.5 \cdot 10^{-2}$	$4.8 \cdot 10^{-3}$
12	$8.1 \cdot 10^{-2}$	$1.2 \cdot 10^{-3}$	$7.3 \cdot 10^{-2}$	$3.9 \cdot 10^{-3}$
15	$8.3 \cdot 10^{-2}$	$2.3 \cdot 10^{-3}$	$7.4 \cdot 10^{-2}$	$6.1 \cdot 10^{-3}$
18	$7.5 \cdot 10^{-2}$	$2.1 \cdot 10^{-3}$	$7.3 \cdot 10^{-2}$	$5.1 \cdot 10^{-3}$

Table 5.2: *Difference between the discrete displacement field stemming from the atomistic scale with the values of the coarse scale in the $\|\cdot\|_{L^2(\Xi)}$- and $\|\cdot\|_\infty$ norm*

5.3 Frequency Sensitivity of the Coupling Operator

Even though our weak coupling operator is designed for the transfer of displacements, it has notable properties with regard to the transfer of energy. In the forthcoming we show the L^2 projection surpresses the energy stored in high frequency waves and conserves the energy stored in low frequency waves. The precise meaning of "high" and "low" in this context is given by (2.27). Again, for the sake of simplicity we stick to a single dimension, a harmonic potential and the linear standard FE basis for an equidistant mesh.

As starting point for our discussion, let us recall that the solutions of both system (2.2), (2.10) in Chapter 2 were of the form

$$q_\alpha(t) = \sum_k \tilde{q}_k e^{i(kX_\alpha - \omega t)} \quad \text{and} \quad u_p(t) = \sum_k \tilde{u}_k e^{i(kx_p - \omega t)} \tag{5.20}$$

In our simplified setting we consider the projection of an harmonic displacement in the molecular dynamics. We set $q(x) = \cos(kx)$ and analyze the L^2 projected image $\pi^h(q) \in \mathcal{V}_h$. Note that here we neglect the approximation error introduced by the embedding ι. First we compute the coefficients $r_p = \int \theta_p q \, dx$ with

$$\theta_p(x) = \begin{cases} \frac{x - x_{p-1}}{h} & \text{for} \quad x \in [x_{p-1}, x_p] \\ 1 - \frac{x - x_p}{h} & \text{for} \quad x \in (x_p, x_{p+1}] \\ 0 & \text{else,} \end{cases}$$

so that $\pi^h(q) = M^{-1}r$. We find

$$
\begin{aligned}
r_p &= \int_{\operatorname{supp}\theta_p} \theta_p(x) q(x)\, dx \\
&= \int_{x_{p-1}}^{x_p} \frac{x - x_{p-1}}{h} \cos(\kappa x)\, dx + \int_{x_p}^{x_{p+1}} \left(1 - \frac{x - x_p}{h}\right) \cos(kx)\, dx \\
&= \int_0^h \frac{x}{h} \left(\cos(k(x_{p-1} + x)) + \cos(k(x_{p+1} - x))\right) dx \\
&= \left[\frac{x}{h\kappa}\left(\sin(k(x_{p-1} + x)) - \sin(k(x_{p+1} - x)))\right)\right]_0^h \\
&\quad + \left[\frac{1}{hk^2}\left(\cos(k(x_{p-1} + x)) + \cos(k(x_{p+1} - x)))\right)\right]_0^h \\
&= \frac{1}{hk^2}\left(\cos(kx_p) - \cos(kx_{p-1}) + \cos(kx_p) - \cos(kx_{p+1})\right).
\end{aligned}
\tag{5.21}
$$

Since $|\cos'(kx)| \le \kappa$ we have $r_p \in [-2/\kappa, 2/\kappa]$. For a (quasi-)uniform mesh the eigenvalues m_p of the mass matrix $m_p \sim h$ so that the coefficients π_p of $\pi_h(q)$ are bounded by $\mathcal{O}\left(1/(\kappa h)\right)$. Thus we can clearly see, what we have expected.

We now employ the Fourier transform, and use the notation introduced in the context of Kernel based methods in Chapter 2, in order to determine the frequency senistivity of the new coupling operator. In order to describe the spectrum of the functions properly, we introduce the term *bandlimited*, where we define a function u to be *bandlimited* if its Fourier transform $\hat{u}$ vanishes outside some compact interval Σ. Additionally we define a function to be ε-*bandlimited* if its Fourier transform $\hat{u}$ is less than ε outside some compact interval Σ. In Figure 5.5 we can see
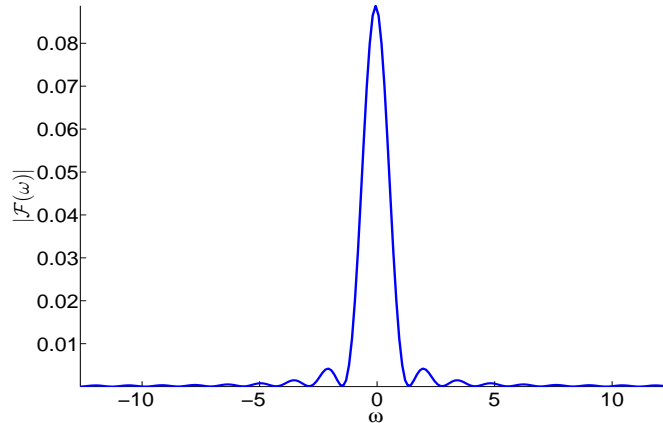

Figure 5.5: *The Fourier transform of the linear finite element basis function*

the Fourier transform of the linear finite element basis function.

Obviously, waves with low wave number are better represented (close to $\kappa = 0$) than high frequencies. This fact is important for the coupling operator, since both, the Bridging scale operator and the weak coupling operator map into the coarse scale " *which can be represented by a set of basis functions, that is, finite element shape functions*"[1]
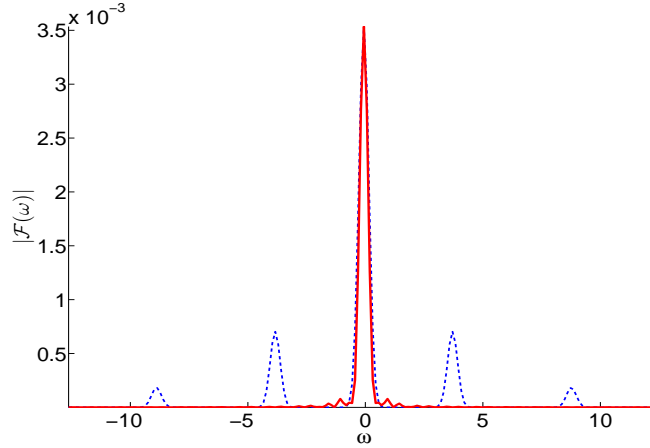

Figure 5.6: *The Fourier transform of the initial wave* u *and its projection*

For the given initial amplitude q the Fourier spectrum is given in Figure 5.6 (blue,dashed). Moreover the Fourier spectrum of the corresponding projected displacement is given (red). As expected, only low frequencies, are transferred and the high frequency, which have no physical meaning on the coarse scale are neglected.

In a next step we examined the error in the frequency domain. As we have already mentioned, the Bridging scale method can be seen as a special case of the weak coupling concept. We showed, that within our weak framework, the Bridging Scale method can be interpreted as piecewise constant approximation. This is the case, when the patch size $|\omega_\alpha|$ of each atom is set to r_0, i.e. exact the distance between the neighboring atoms. In Figure 5.7 we measured the error between the initial amplitude and the image of this initial amplitude under the weak coupling operator

$$\text{err}_{\mathcal{F}} := \|\mathcal{F}(q) - \mathcal{F}(\pi(q))\|_{\ell_2}. \tag{5.22}$$

In Figure 5.7 it can be seen that in this context, the weak coupling approach offers more freedom compared to the Bridging Scale method, since the size of the patch is adjustable.
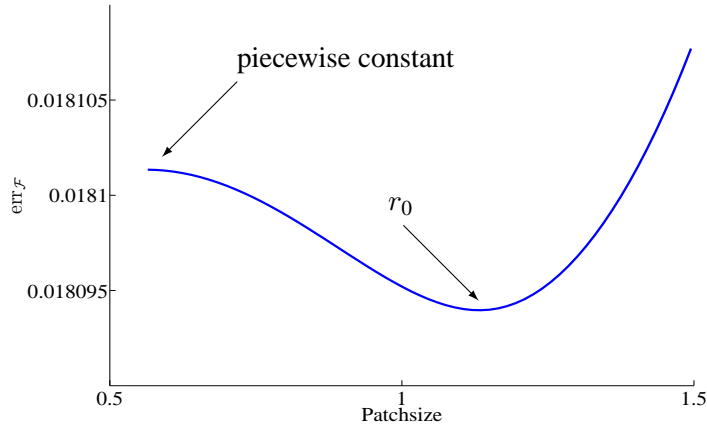
---

[1][LKP06, Chapter 6]

Figure 5.7: *The Error* (5.7) *comparing the weak coupling method with the Bridging Scale method*

5.4 Numerical Examples

In this section the performance of the weak coupling method for the complete overlapping case is presented.

5.4.1 A One Dimensional Example

In our simulation we choose $\Delta t = 0.2$. And use the same staggered time stepping algorithm, as explained in Subsection 5.2.2.
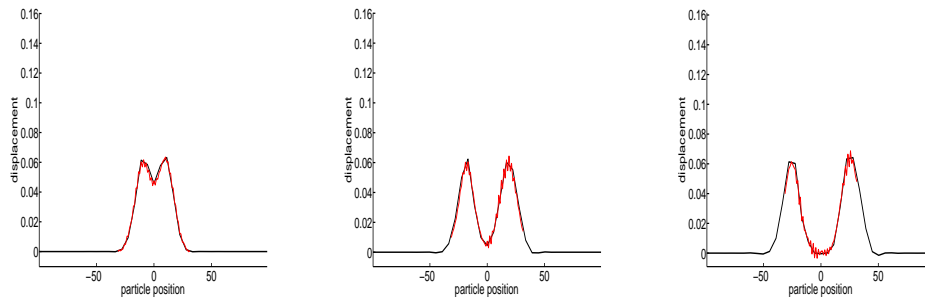

Figure 5.8: *FE-MD simulation for the coarse scale time steps* $n = 3, n = 12$ *and* $n = 18$.

In Figure 5.8, the coupled MD/FE simulation is shown. The square-marked line (red) represents the displacements of the fine scale. The continuous line (blue) maps the displacement of the coarse displacement. For comparison to the multiscale simulation a full atomistic simulation using 420 atoms is shown in Figure 5.9.
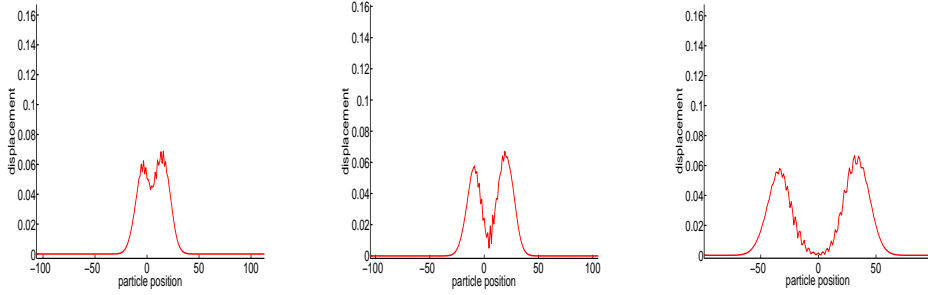
Figure 5.9: *Full MD simulation, for the fine scale time steps:* $m \cdot n = 150, 600$ *and* 900

5.4.2 A Two Dimensional Example

Here we used the Molecular Dynamics Software Package TREMOLO [GKZ07, GH04, GH06] for the atomistic simulation. For the simulation of the continuum mechanics we used the finite element toolbox UG [BBJ$^+$97]. A parallelization of the implementational framework (i.e. the interface between the finite element and the molecular dynamics) can be found in [Kra09] and in the context of MACI (Massively Parallel Atomistic Continuum Interface) of the working group Prof. Dr. Rolf Krause.

In this example, we test the performance of our projection operator π_h for $d = 2$. To do so, we study wave propagation through a small sheet. Considering the domain $\Omega = [0, 80] \times [400, 800] \subset \mathbb{R}^2$ the coupling region chosen is $\Xi = [0, 80] \times [400, 550] \subset \Omega$. An initial displacement in the molecular domain Ξ propagates out of the coupling zone into $\Omega \backslash \Xi$, where only coarse finite elements are used.

The initial displacement in Ξ is a combination of high- and low frequency parts:

$$q(x, y) = \frac{A}{A - q_c} \left(A e^{(-(y-t)/\sigma)2} - q_c \right) \left(1 + b \cos \left(\frac{2\pi}{H} (y - t) \right) \right) e_y \qquad (5.23)$$

with $e_y = (0, 1)^T$, $t = 510$, $\sigma = 15$, $H = \sigma/4$, $A = 0.15$, $b = 0.3$, $r_c = 5 \cdot \sigma$ and $u_c = A e^{(r_c/\sigma)2}$, where we adopted the notation used in [LKP06].

The potential function is the LJ-Potential (1.13) with nearest-neighbor interaction, i.e. $r_{\text{cut}} = 3/2 \cdot r_0$. For the coarse scale we employ the standard linear elastic Saint-Venant material law with elastic modulus $E = 30$ and Poisson ratio $\nu = 0.2589$, discretized on a triangular mesh. The coupling zone contains 11.130 atoms and about 585 triangles. The patch size is $h = 1.7$ for each atom. Since the focus here is put on the properties of the new transfer operator, the MD block was chosen large enough to avoid spurious reflections at the boundary.

For the integration in time, we have used the time-stepping scheme given in Subsection 5.4.1 with the following changes:

- The coarse-scale force is calculated by linear elasticity $F = F(d)$.
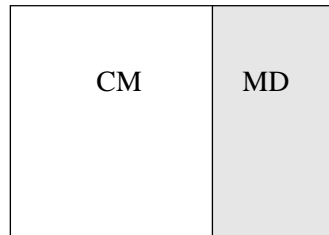
Figure 5.10: *Geometry of the first example in* 2*d.*

- The coupling is done by overwriting the coarse-scale displacement and velocities in each time step in the coupling zone by the values obtained from the L^2 projection of the values on the fine scale.

We choose $\Delta t = 0.1$ and $m = 2$. Figure 5.11 shows the time-evolution of the absolute value of the perturbation as it propagates into the coarse region $\Omega\backslash\Xi$. In the coupling region, only the atomic displacements are shown. It can be seen that by using the L^2 projection an almost seamless transition between the scales can be achieved. In the second example we used the radial symmetric version of (5.23).
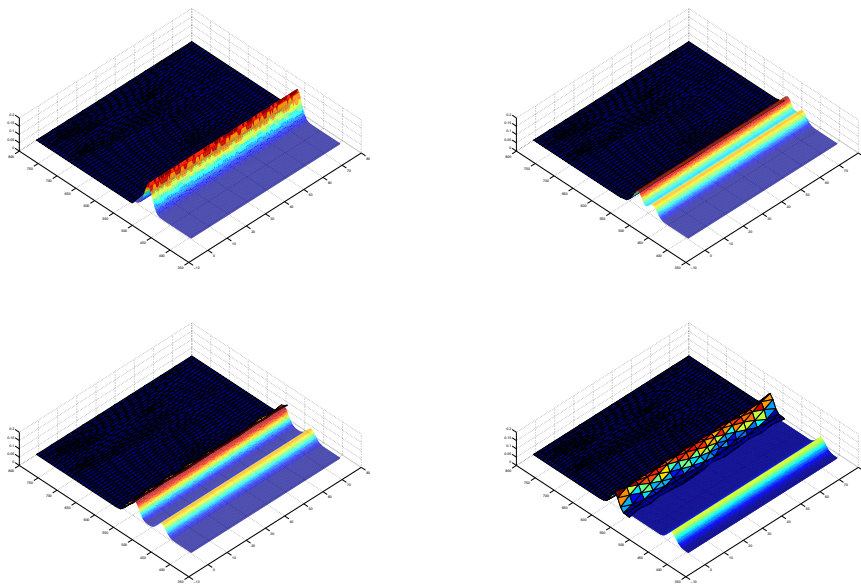

Figure 5.11: *A* 2*d example of a coupled simulation with the weak coupling method: transfer of a wave from micro (MD) to macro (FE), with a comparably large mesh size in the FE region*
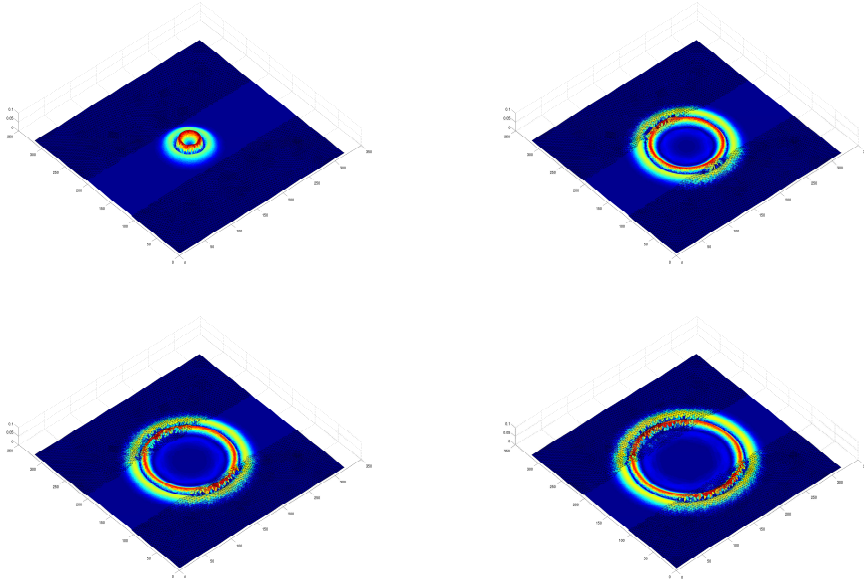
Figure 5.12: *A* 2*d example of a coupled simulation with the weak coupling method: A radial symmetric initial amplitude starting in the bright blue stripe in the middle (MD) entering into the darker coarse scale (CM) region*

6 The Weak Multiscale Method and Coupling with Constraints

In this chapter, we consider a partly overlapping multiscale method. In contrast to the foregoing Chapter, where $\Omega^{\mathrm{MD}} = \Xi$, here, we consider the handshake region as $\Xi = \Omega^{\mathrm{MD}} \cap \Omega^{\mathrm{CM}}$, $\Xi \neq \Omega^{\mathrm{MD}}, \Xi \neq \Omega^{\mathrm{CM}}$. For an illustration consider Figure 6.1.

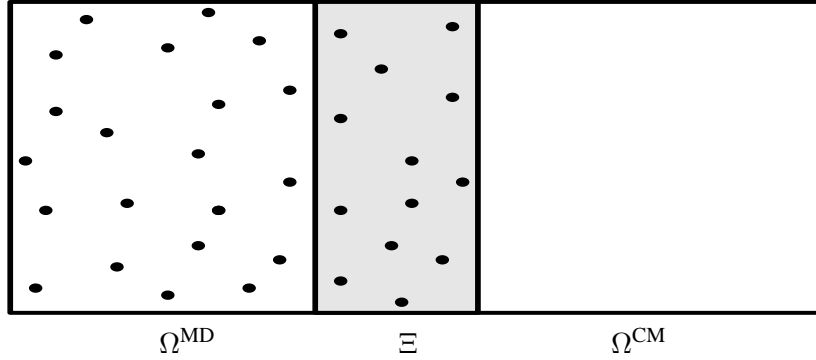$$\Omega^{\mathrm{MD}} \qquad \Xi \qquad \Omega^{\mathrm{CM}}$$

Figure 6.1: *Example of a domain $\Omega \subset \mathbb{R}^2$ with a pure molecular part Ω^{MD}, a pure continuum part Ω^{CM} and a mixed part $\Omega^{MD} \cap \Omega^{CM}$.*

Once again, by q and u we denote the displacement fields in Ω^{MD} and Ω^{CM} respectively.

To couple the MD and continuum system we impose constraints $(q, u) \in \mathcal{C}$ where $\mathcal{C}$ is the configuration manifold (linear subspace). This means that the displacements q and u at each time should lie on the manifold C. The shape and orientation of $\mathcal{C}$ define the way the constraints alter the displacements of the individual, uncoupled systems.

Obviously, the constraints are only active in the handshake region Ξ, where we have the co-existence of the molecular and continuum description. The bridging domain method has been introduced by Xiao and Belytschko [XB04], therein the handshake region, where constraints are imposed is called the bridging domain. In their method they impose point wise constraints, by

$$\mathcal{C} = \left\{ (q, u) \mid q_\alpha = u(X_\alpha) \text{ for each atom } \alpha \in \mathcal{A}_\Xi \right\}. \tag{6.1}$$

Reformulating the constraints in an algebraic form we find

$$\mathcal{C} = \{g = 0\} \text{ with } g(q, u) = q - Nu. \tag{6.2}$$

Let us recall the interpolation operator $N : \mathcal{V}_h(\Xi) \to \mathbb{R}^{d|\mathcal{A}_\Xi|}$ defined by $(Nu)_\alpha = u(X_\alpha)$ of Chapter 5.

The choice of point wise constraints is motivated by the Cauchy-Born rule. The constraints (6.2) are a strong modification of the uncoupled systems since they prohibit the existence of displacement fields q which are not exactly representable on the coarse finite element mesh. As a consequence high-frequent waves are not permitted in the bridging domain and are reflected at the interface $\partial \Xi \cap \Omega^{\mathrm{MD}}$ since energy is conserved.

We can see that the major problem of this approach is the strongness of the constraints which serve two purposes:

- They deliver the information transfer between the scales. In the Bridging domain both systems have the same dynamic yielding a globally consistent displacement field.

- They avoid the reflection of high-frequent waves (roughly speaking, those not representable on the finite element mesh) at the atomistic boundary $\partial \Xi$ by prohibiting the propagation of such waves in the Bridging Domain.

From our point of view, the failure of the coupling method presented above is due to the misuse of the same constraints for both, information transfer and reflection elimination. In Section 6.2 we show how to decouple these tasks by imposing constraints in a "weak" sense. Since small-wavelength waves are not affected by the constraints they can propagate smoothly in the bridging domain where e.g. non-reflecting boundary conditions can be used to eliminate reflections.

In the following we assume the constraint manifold C to be linear. Hence we can find a linear mapping g so that $C = \{g = 0\}$. The map g might be written as

$$g(q, u) = B^{\mathrm{MD}} q - B^{\mathrm{CM}} u.$$

Here, B^{MD} and B^{CM} are linear operators with range in some space $\mathcal{D}$ over Ξ.
In the Bridging Domain method $\mathcal{D}$ is the space of all atomistic displacements and $B^{\mathrm{MD}} = \mathrm{id}$, $B^{\mathrm{CM}} = N$.

6.1 Deriving Constraints in the Lagrangian Setting

In Chapter 1 we showed, that in general the equations of motion on the atomistic as well as on the continuum level can be derived either from the Hamiltonian or the Lagrangian description. In some situations, the derivation from the Lagrangian equations is more natural, since the Hamiltonian approach requires the identification of the canonical conjugated momenta, which are derivatives of the Lagrange function with respect to the velocity.

We assume, that the potential energy $\mathcal{U}$ does not depend on the velocity. Let us recall the Lagrangian equations of motion from (1.11), then the time evolution of such a system is given by

$$\frac{d}{dt}\frac{\partial}{\partial \dot{s}}\mathcal{L} = \frac{\partial}{\partial s}\mathcal{L}\,. \tag{6.3}$$

Since $\mathcal{T}$ does not depend on the displacement, the right hand side of (6.3) is the negative of the gradient of $\mathcal{U}$. However, the canonical conjugated momentum $\frac{\partial}{\partial \dot{s}}\mathcal{L}$ usually differs from the kinetic momentum $m\dot{s}$.

This general formalism applies to the Bridging Domain setting explained before, as follows: Recall from Chapter 1 that

$$\mathcal{L}^{\mathrm{MD}}(q, \dot{q}) = \mathcal{T}^{\mathrm{MD}}(\dot{q}) - \mathcal{U}^{\mathrm{MD}}(q)$$

and

$$\mathcal{L}^{\mathrm{CM}}(u, \dot{u}) = \mathcal{T}^{\mathrm{CM}}(\dot{u}) - \mathcal{U}^{\mathrm{CM}}(u)$$

denote the Lagrange function of the molecular dynamic system and the continuum system. The Lagrangian of the coupled system now is a weighted sum of the individual Lagrange functions plus a contribution due to the constraints.

Since in the overlapping domain the molecular and the continuum description coexist, a weighting function $w : \Omega \rightarrow [0, 1]$ is necessary so that energy is not counted twice in Ξ. We require $w \equiv 1$ in $\Omega^{\mathrm{MD}} \setminus \Xi$ so that the equations of motion is not altered in those subdomains where only one model is valid.
Denoting by $(\cdot, \cdot)_{\mathcal{V}}$ a scalar product on $\mathcal{V}$ the consistent Lagrangian $\mathcal{L}$ reads

$$\mathcal{L}(q, u, \dot{q}, \dot{u}, \lambda) = w \cdot \Big(\mathcal{T}^{\mathrm{MD}}(\dot{q}) - \mathcal{U}^{\mathrm{MD}}(q)\Big) +$$
$$(1 - w) \cdot \Big(\mathcal{T}^{\mathrm{CM}}(\dot{u}) - \mathcal{U}^{\mathrm{CM}}(u)\Big) + (\lambda, g(q, u))_{\mathcal{V}}\,. \tag{6.4}$$

The Lagrange multipliers $\lambda \in \mathcal{V}$ are determined so that the coupled solution (q, u) lies on the configuration manifold $(q, u) \in C$, i.e $g(q, u) = 0$.

Let us remark, that in the above formula the multiplication by w and $(1 - w)$ is an abuse of notation. More precisely,

$$w \cdot \mathcal{T}^{\mathrm{MD}}(\dot{q}) = \frac{1}{2}\sum_{\alpha} m_{\alpha} w(X_{\alpha}) \cdot |\dot{q}_{\alpha}|^2$$

and

$$(1 - w) \cdot \mathcal{T}^{\mathrm{CM}}(\dot{u}) = \frac{1}{2}\int \varrho(1 - w) \cdot |\dot{u}|^2\, dx$$

Inserting the Lagrangian (6.4) into the general Lagrangian equation (6.3) we obtain the coupled

equations of motion

$$\bar{M}\ddot{q} = -\nabla\bar{\mathcal{U}}^{\text{MD}} + \left(\lambda, \nabla_q g(q,u)\right)_{\mathcal{V}} \tag{6.5}$$

$$\bar{\varrho}\ddot{u} = -\nabla\bar{\mathcal{U}}^{\text{CM}} + \left(\lambda, \nabla_u g(q,u)\right)_{\mathcal{V}} \tag{6.6}$$

The equations of motion in Ω^{CM} should be understood in a weak sense.
In (6.5),(6.6) we introduced the notations

$$\bar{M}_\alpha = w(X_\alpha)m_\alpha, \ \bar{\varrho} = (1-w)\varrho$$

as well as

$$\bar{\mathcal{U}}^{\text{MD}} = w \cdot \mathcal{U}^{\text{MD}} \ \text{and} \ \bar{\mathcal{U}}^{\text{CM}} = (1-w) \cdot \mathcal{U}^{\text{CM}}.$$

Comparing (6.5), (6.6) to the equations of motions of the individual uncoupled systems we see that the weighting w alters the forces and does not cancel out. As a result one finds that the waves traveling into the coupling zones are amplified whereas leaving waves are damped. These effects might be troublesome, e.g. because they prohibit the usage of exact non-reflecting boundary conditions. We refer to [ACRZ08] for a discussion of approximations.

Notably we find the canonical conjugated momenta to weighted as well, e.g. $p_\alpha^{\text{MD}} = w(X_\alpha)m_\alpha \cdot \dot{u}_\alpha$. Therefore

$$w \cdot \mathcal{T}^{\text{MD}}(p^{\text{MD}}) = \frac{1}{2}\sum_\alpha \frac{\left|p_\alpha^{\text{MD}}\right|^2}{m_\alpha w(X_\alpha)}$$

In [XB04] the weighted Hamiltonian is always written using the kinetic momenta rather than the canonical conjugated momenta. However, when deriving the Hamiltonian equations it is important to reformulate the Hamiltonian using the conjugated momenta which is only possible through the Lagrange formulation.

6.2 Imposing Constraints in a Weak Sense

In the forthcoming we interpret the constraints, introduced above (6.5) and (6.6) in a weak sense. To do so, we construct a manifold C, which in contrast to (6.2) does not impose constraints pointwise but in a weak sense, i.e.

$$\mathcal{C} = \left\{(q,u) \mid (\lambda, q-u)_{L^2(\Xi)} = 0 \text{ for all } \lambda \in \mathcal{M}_h\right\} \tag{6.7}$$

where $(\cdot,\cdot)_{L^2(\Xi)}$ is the L^2 scalar product over Ξ and $\mathcal{M}_h$ the multiplier space introduced in (4.18).

The choice of the multiplier space ensures, that the high frequent (large wave number) part

of a wave, which can not be represented by the finite element mesh are not constrained. As a consequence these wave with a large wave number can pass unaltered thorough the handshake region Ξ.

The constraints in (6.7) require $q \in L^2(\Xi)$, however the displacement on the molecular scale is given by $(q_\alpha)_{\alpha \in \mathcal{A}}$ which is in the Euclidean space.
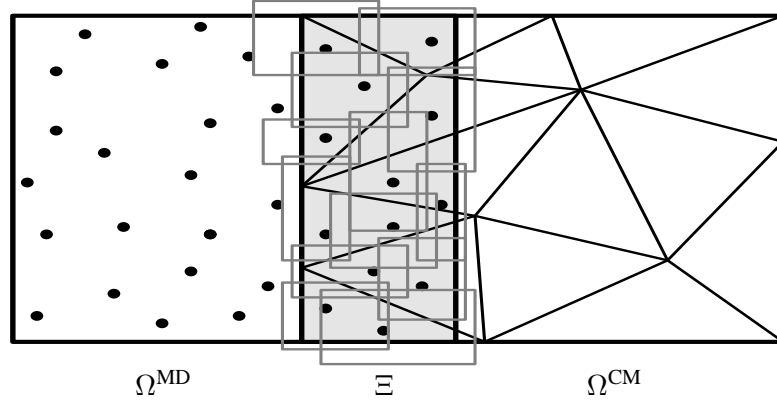

Figure 6.2: A $2d$ example of patches overlapping $\Xi \cup \Omega^{\mathrm{MD}}$

Thus in the fashion of Chapter 4 we define analogue to (4.12)

$$\iota(X, q) = \sum_{\alpha \in \mathcal{A}} q_\alpha \varphi_\alpha \tag{6.8}$$

Let us note that the truncation of the approximation space at the bridging domain boundary leads to a reduced approximation quality near the boundary. However these effects are negligible.

So far we have transferred the molecular displacement into a function space. By means of the scale decomposition of $\iota(q)$ (compare to (5.5)) we can reformulate the definition of $\mathcal{C}$ in (6.7) in a more accessible way. We decompose the total displacement field in the functionspace by

$$\iota(q) = \overline{\iota(q)} + \iota(q)',$$

where $\overline{\iota(q)}$ is a coarse scale part and $\iota(q)'$ is a fine scale part. As a matter of fact not all information of $\iota(q)$ can be represented on the coarse scale.

More precisely, not all wavelengths in the MD solution q can be captured by the finite element space. As stated above constraints should only affect those values, which can be represented

on both scales (i.e. in the function spaces $\mathcal{V}_\delta$ and $\mathcal{V}_h$).

For this purpose let $\mathcal{V}_h(\Xi)$ denote the space of restrictions of functions from $\mathcal{V}_h$ to the Bridging domain Ξ.

Analogue to Chapter 5 the coarse scale representation is now defined by $\overline{\iota(q)} = \pi_h(\iota(q)) \in \mathcal{V}_h(\Xi)$, where π_h is the L^2 projection defined in (5.6), i.e. $\pi_h \colon L^2(\Xi) \longrightarrow \mathcal{V}_h(\Xi)$. Then the displacement stemming from the fine scale can be decomposed by

$$\iota(q) = (\iota(q) - \pi_h(\iota(q))) + \pi_h(\iota(q)). \tag{6.9}$$

Thus we have decomposed the displacement $\iota(q)$ into a part which can be captured by the coarse scale and into a part which can only be represented on the fine scale. Since ι is bijective, this allows us to compute the fine fluctuation field of the MD solution as $\iota^{-1}(\iota(q)') = \iota^{-1}(\iota(q) - \pi_h(\iota(q)))$. With this terminology we may write

$$\mathcal{C} = \left\{ (q, u) \mid u = \overline{\iota(q)} \text{ in } \Xi \right\}. \tag{6.10}$$

Now, (6.10) gives rigorous meaning to the above statements, namely the fact that the high frequency part $\iota(q)' \in \ker \pi_h$ is not affected by the weak constraints.

Once again, inserting $\iota(q) = \sum_{\alpha \in \mathcal{A}_\Xi} q_\alpha \varphi_\alpha$ and $\pi_h(\iota(q)) = \sum_{p \in \mathcal{N}_h^\Xi} \pi_p \lambda_p$ into (5.6), we obtain

$$M\pi = Rq \tag{6.11}$$

with $M = (m_{ts})_{t,s \in \mathcal{N}_h^\Xi}$, $R = (r_{s\alpha})_{s \in \mathcal{N}_h^\Xi, \alpha \in \mathcal{A}_\Xi}$ defined in (5.12) giving rise to the matrix representation

$$W = M^{-1}R \tag{6.12}$$

Hence, we have

$$\mathcal{C} = \left\{ (q, u) \mid u = Wq \right\} = \left\{ (q, u) \mid Mu = Rq \right\} \tag{6.13}$$

so that $B^{\text{CM}} = \text{id}$, $B^{\text{MD}} = W$ or $B^{\text{CM}} = M$, $B^{\text{MD}} = R$. The space $\mathcal{D}$ is the finite element space $\mathcal{V}_h(\Xi)$.

Since the dimension of $\mathcal{D}$ determines the computational burden of the coupling method (it is the size of the multiplier matrix to be inverted in every time step of, e.g., a Shake-Rattle time integrator) the weak constraints are computational more efficient than rigorously applied pointwise constraints of [XB04].

Discretization in time   To solve the coupled equations of motion (6.5),(6.6) we use the well known Shake-Rattle time integration scheme. This is a symplectic, second order time integration scheme for constrained systems which is widely used in molecular dynamics simulations [GKZC04, HLW02].

Let $\{0 < \Delta t < 2\Delta t < \ldots < N\Delta t = T\}$ denote a decomposition of the time interval $[0, T]$. We do not consider multi-rate time integration schemes, i.e., we employ the same step size Δt on both scales.

We denote by $\bar{M}_{\mathrm{MD}}, \bar{F}_{\mathrm{MD}}, \bar{M}_{\mathrm{CM}}, \bar{F}_{\mathrm{CM}}$ the weighted mass matrices and weighted forces on the respective scales. Let us recall that $W = M^{-1}R$ is the algebraic representation of the L^2 projection π_h, see (5.13). Note, that the mass matrix M is truncated mass matrix, since the operator acts only over Ξ Starting from the initial values $q_0, \dot{q}_0, u_0, \dot{u}_0$ the Shake rattle algorithm reads

for $n = 1, \ldots, N - 1$

  Compute velocity trial values $\dot{q}_{n+1/2} = \dot{q}_n + \frac{1}{2}\Delta t \bar{M}_{\mathrm{MD}}^{-1} \bar{F}_{\mathrm{MD}}(q_n, \dot{q}_n)$ and $\dot{u}_{n+1/2} = \dot{u}_n + \frac{1}{2}\Delta t \bar{M}_{\mathrm{CM}}^{-1} \bar{F}_{\mathrm{CM}}(u_n)$.

  Compute displacement trial values $q_{n+1} = q_n + \Delta t \dot{q}_{n+1/2}$ and $u_{n+1} = u_{n+1} + \Delta t \dot{u}_{n+1/2}$.

  Compute the residual $g = Mu_{n+1} - Rq_{n+1}$ and solve the linear system $\Lambda\lambda = g$ with the multiplier matrix $\Lambda = M\bar{M}_{\mathrm{CM}}^{-1}M + R\bar{M}_{\mathrm{MD}}^{-1}R^{\mathsf{T}}$.

  Correct

$$q_{n+1} \leftarrow q_{n+1} + \bar{M}_{\mathrm{MD}}^{-1}R^{\mathsf{T}}\lambda$$
$$\dot{q}_{n+1/2} \leftarrow \dot{q}_{n+1/2} + \Delta t^{-1}\bar{M}_{\mathrm{MD}}^{-1}R^{\mathsf{T}}\lambda$$
$$u_{n+1} \leftarrow u_{n+1} - \bar{M}_{\mathrm{CM}}^{-1}M\lambda$$
$$\dot{u}_{n+1/2} \leftarrow \dot{u}_{n+1/2} - \Delta t^{-1}\bar{M}_{\mathrm{CM}}^{-1}M\lambda$$

  Compute velocity trial values $\dot{q}_{n+1} = \dot{q}_{n+1/2} + \frac{1}{2}\Delta t \bar{M}_{\mathrm{MD}}^{-1}\bar{F}_{\mathrm{MD}}(q_{n+1}, \dot{q}_{n+1/2})$ and $\dot{u}_{n+1} = \dot{u}_{n+1/2} + \frac{1}{2}\Delta t \bar{M}_{\mathrm{CM}}^{-1}\bar{F}_{\mathrm{CM}}(u_{n+1})$.

  Compute the residual $\dot{g} = M\dot{u}_{n+1} - R\dot{q}_{n+1}$ and solve the linear system $\Lambda\lambda = \dot{g}$.

  Correct

$$\dot{q}_{n+1} \leftarrow \dot{q}_{n+1} + \bar{M}_{\mathrm{MD}}^{-1}R^{\mathsf{T}}\lambda$$
$$\dot{u}_{n+1} \leftarrow \dot{u}_{n+1} - \bar{M}_{\mathrm{CM}}^{-1}M\lambda$$

end

Figure 6.3: Shake rattle algorithm

Let us remark that the multiplier matrix Λ is positive definite since

$$x^{\mathsf{T}}\Lambda x = (Mx)^{\mathsf{T}} \bar{M}_{\mathrm{CM}}^{-1} (Mx) + \left(R^{\mathsf{T}}x\right)^{\mathsf{T}} \bar{M}_{\mathrm{MD}}^{-1} \left(R^{\mathsf{T}}x\right) \tag{6.14}$$

Therefore, all steps in the above algorithm are well defined.

6.3 Numerical Examples

Here, in this section, we validate the method explained above. To do so, we used the standard examples in $1d$ and $2d$ explained in the foregoing chapter. These $1d$ and $2d$ examples show well, that atomistic displacements can propagate into the continuum. In the $3d$ example it is shown, that due to the symmetry, also continuum displacements can propagate into the atomistic region.

We already mentioned that the weak constraints allow small wavelength phonons to enter the bridging domain without reflection. In order to cope with reflections at the boundary $\partial\Omega^{\mathrm{MD}}$ additional effort is necessary.
In Chapter 2, we already introduced the PML method which changes the equations of motion by an additional force term
$$F \mapsto F + M \cdot \mathsf{D}\left(2\dot{q} + \mathsf{D}q\right). \tag{6.15}$$

Note that (6.15) contains a frictional term and additionally changes the stiffness of the lattice. Numerical evidence shows that we can omit the last term MD^2q if $\mathsf{D} = (\mathsf{d}(X_\alpha))_{\alpha\in\mathcal{A}}$ is chosen appropriately, (cf. Section 6.3). Thus, in our numerical examples in Section 6.3, we use a "pure" frictional term, i.e.,

$$F \mapsto F + M \cdot \mathsf{D}2\dot{q}. \tag{6.16}$$

Recall that $\mathsf{D} = (\mathsf{d}(X_\alpha))_{\alpha\in\mathcal{A}}$ we see that (2.34) and (6.15) are equivalent.
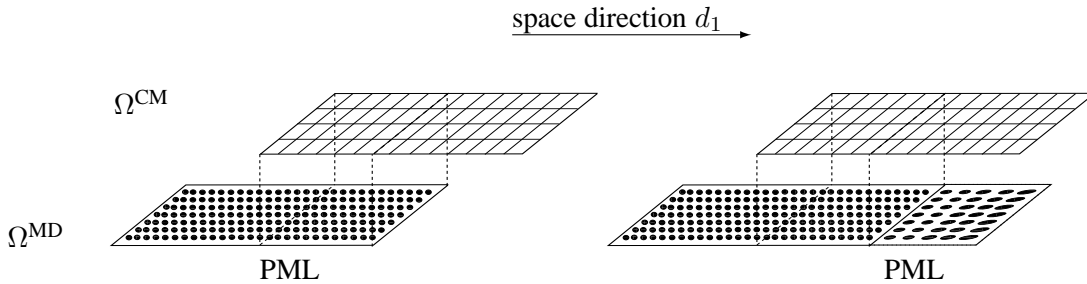

Figure 6.4: An example of a domain $\Omega \subset \mathbb{R}^2$ and its extension Ω_L

Different choices for the damping zone, i.e., the support of d, are possible (see Figure 6.4). The damping zone could be a layer around Ω^{MD}. In this case the full wave spectrum must be removed. If we use Ξ as the damping zone we must take care to damp only the high frequency waves in order to not disturb the information transfer between the scales. Although this approach requires a larger coupling zone Ξ, it is computationally more efficient, since no

additional atoms need to be introduced (see Figure 6.4).

Since (6.15) affects phonons of arbitrary wave numbers, it is not appropriate if the damping zone is equal to Ξ, as mentioned above. Rather we use

$$F \mapsto F + M \cdot D \left(2 Q_h \dot{q} + D Q_h q \right) \tag{6.17}$$

where Q_h is the algebraic representation of $\mathrm{id} - N\pi^h\iota$, N being the interpolation operator (cf. (6.2)). Note that $Q_h q$ is an easily computable approximation to the fine fluctuation $\iota^{-1}(q')$.

The waves with high wave numbers (small wavelengths) are not affected by the constraints and are able to pass through the Bridging domain.

6.3.1 A One Dimensional Example

We consider the propagation of an initial amplitude through a 1 dimensional slab. On the fine scale we use a Lennard-Jones potential with $\sigma = 1$, $\varepsilon = 1$ and nearest neighbour interaction so that a lattice of atoms with distance $r_0 = 2^{1/6}$ is a minimum of the total energy. To derive a continuum model for the coarse scale we use the Cauchy-Born rule [BH54]. This ensures matching elastic coefficients. The FE density $\varrho = 1/r_0$. The initial amplitude in the MD region was

$$q = \frac{A}{A - q_{\mathrm{c}}} \left(A \exp(-(X/\sigma)^2) - q_{\mathrm{c}} \right) \cdot (1 + b \cdot \cos(2\pi X/H)) \tag{6.18}$$

with $A = 0.015$, $\sigma = 30$, $b = 0.1$, $u_{\mathrm{c}} = e^{-5}$ and $H = \sigma/4$. Since the propagation to the left and to the right is completely symmetric we only consider atoms with initial positions $X \geq 0$. We studied two systems with 100 and 50 atoms each. The finite element size was chosen as $5r_0$ and the bridging domain size was 20 and 10 elements. Figure 6.5 shows the coupling geometry of the larger system.

For the PU we use $h_\alpha = 0.75 r_0$. For the numerical integration we use a Shake rattle integrator with $\Delta t = 0.05$. The PML damping function d was chosen as $d(X) = -\log(0.1) \cdot 0.15 \cdot (\mathrm{dist}(X, \Xi)/\mathrm{diam}(\Xi))^2$. We use a linear weighting function.

The pictures show that we achieve a smooth transition of the wave from the fine to the coarse scale. Especially for $\mathrm{diam}\,\Xi = 100 r_0$ we observe no reflections. The energy history (Figure 6.8) supports this observation.

If $\mathrm{diam}\,\Xi = 50 r_0$ we observe small reflections. As Figure 6.7 shows these reflections are caused by insufficient damping. At the boundary of the bridging domain no reflections are visible. Let us note that the strong amplification of high frequent parts at the MD boundary is due to the weighting.

The size of the multiplier matrix in both cases is 20×20 and 10×10 resp. Therefor, even for the large bridging domain the size of the multiplier matrix is smaller than the multiplier matrix in the BD method for typical choices of Ξ (e.g. consisting of more than 5 elements).
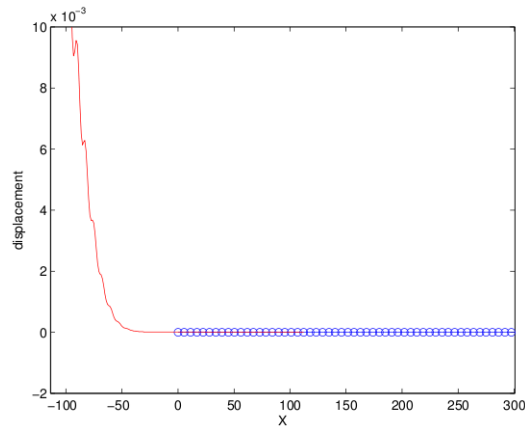
Additionally, Λ has a smaller bandwidth.

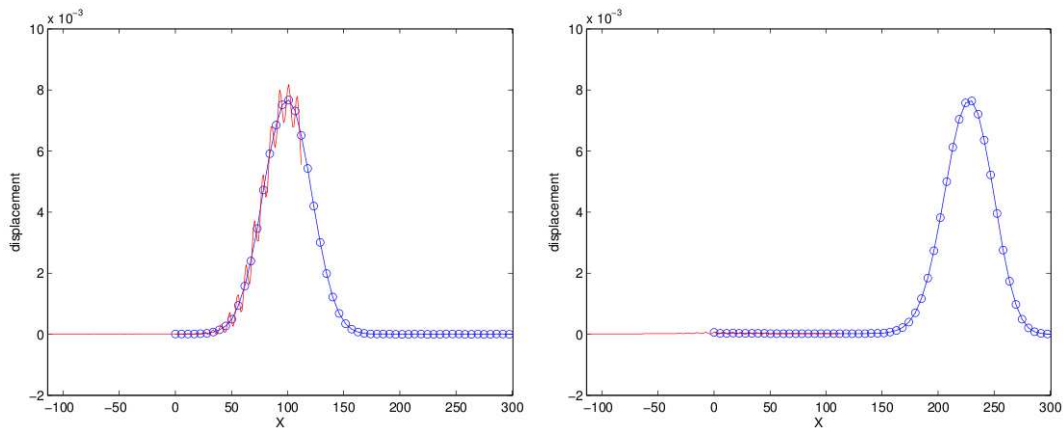Figure 6.5: *Initial amplitude of the* 1*d example.*

Figure 6.6: *Displacement after* 500 *and* 800 *time steps the larger system.*

6.3.2 A Two Dimensional Example

To evaluate our method in higher dimensions we consider the propagation of a radial wave through a 2 dimensional solid. Again, we use a nearest neighbor Lennard-Jones potential with $\sigma = 1, \varepsilon = 1$ as the atomistic interaction potential. The constitutive equation of the continuum is derived by means of the Cauchy-Born rule and $\varrho = 0.92$, the inverse of the volume of the unit cell.

The number of simulated atoms is 60000. For comparison we simulated the 2 dimensional slap with a pure atomistic simulation with 200000 atoms. The finite element mesh contains 8960
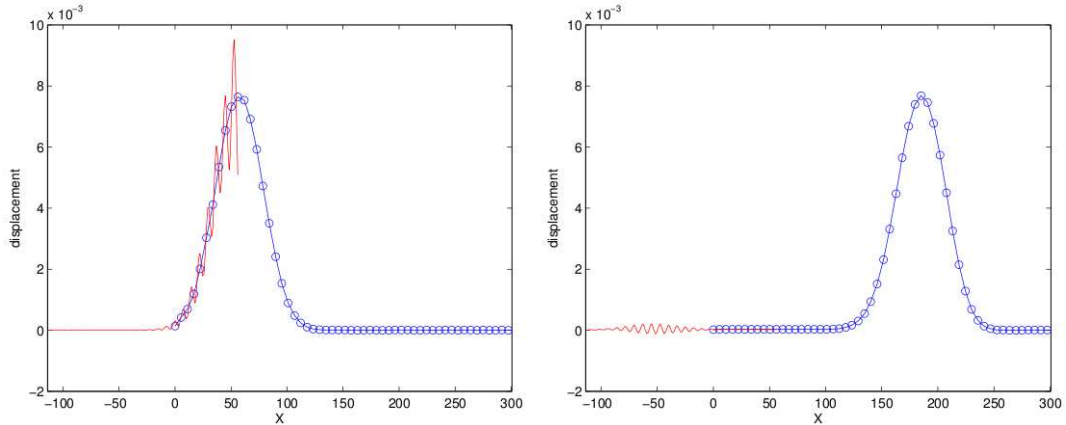
Figure 6.7: Displacement after 400 and 700 time steps for the smaller system.
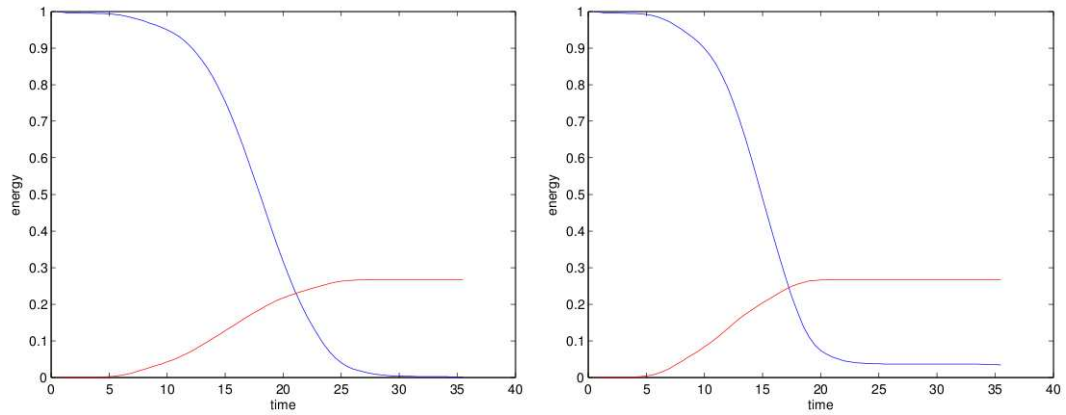

Figure 6.8: Time history of the energy of the $1d$ example.

elements and 9234 nodes. The number of elements in the bridging domain was $2 \cdot 8 \cdot 30 = 480$. Each element contains between 15 and 20 atoms.

The Shake-Rattle time step size is $\Delta t = 0.005$. The patch size $h_\alpha = 0.57 r_0$ and the function d for use in the frictional damping term was chosen as in 1 dimensions except for $R = 0.35$.

Figure 6.9 shows the simulation geometry. Pictures 6.10 and 6.11 show only the relevant portion of the domain.

Again, we observe little or no reflection at the bridging domain boundary. Figure 6.10 shows that the frictional damping efficiently reduces the reflections at the MD border with only small disturbance of the transferable displacements. From Figure 6.10 we infer a (visually) good agreement between the coupled and the pure simulation
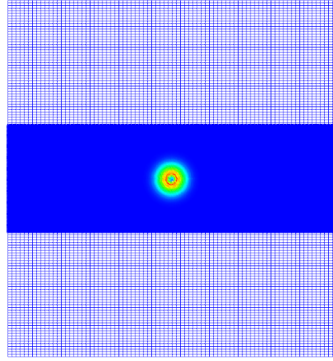
Figure 6.9: 2 dimensional coupling geometry.

6.3.3 Three Dimensional Examples

For the $3d$ examples, we considered the block, where the top and bottom region are discretized by finite elements and the middle part is atomistic.

On the coarse scale we used 2800 elements and on the fine scale 12000 atoms. The material law for the continuum part is given by the Cauchy Born rule, the finite element size is $2.2r_0$ For the atomistic simulation, we employed the Lennard-Jones potential with nearest neighbor interaction, i.e. $r_{\text{cut}} = 1.5r_0$. We computed 10000 time steps the the Shake Rattle algorithm as time integrator and took $\Delta t = 0.005$. The size of the overlap region (handshake region) is four finite elements. In the fist example, we applied a the top $(0., 0., +1.)^T$ and at the bottom $(0., 0., -1.)^T$ as forces. In Figure 6.12 the dynamics of this block at different times is shown, when external forces at the top and at the bottom are applied.

In the second example we applied at the top a force $(-0.2, 0, 0)^T$ and on the continuum part on the bottom we applied $(0.2, 0, 0)^T$.
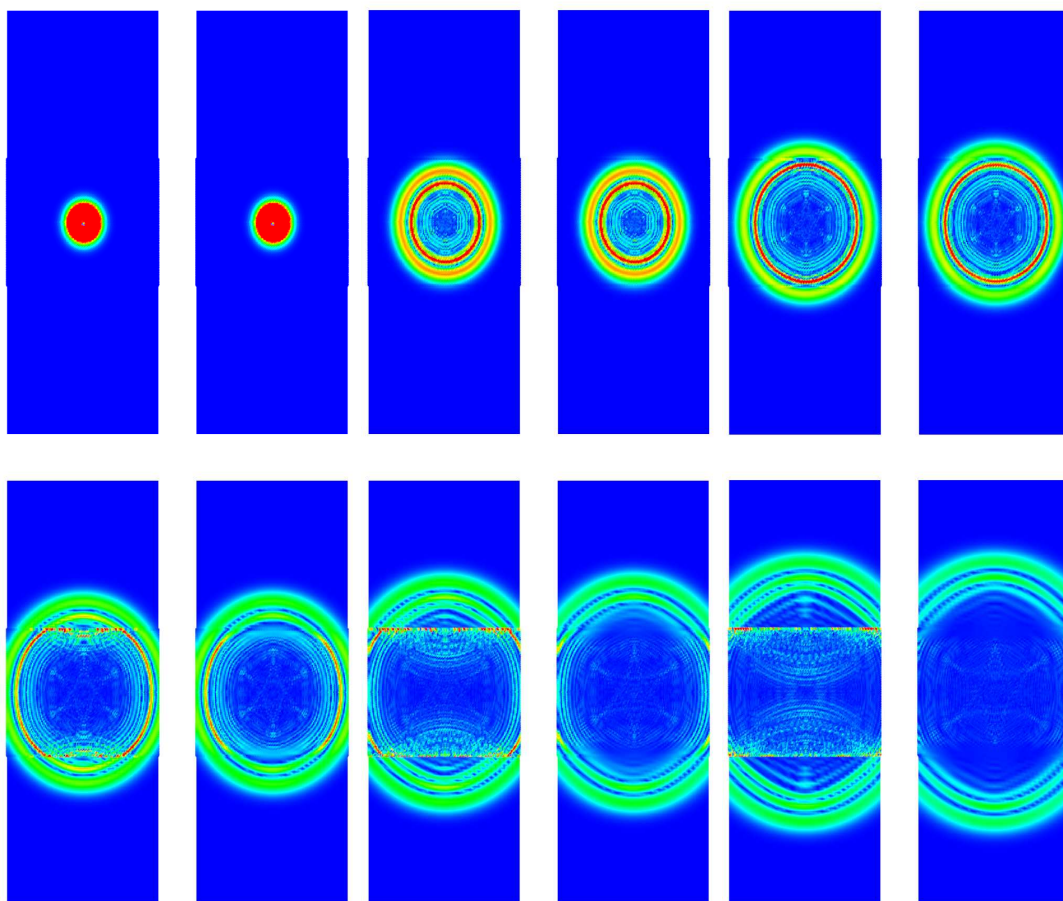
Figure 6.10: *Comparing the weak coupling method with constraints. Left: without damping. Right: with damping*
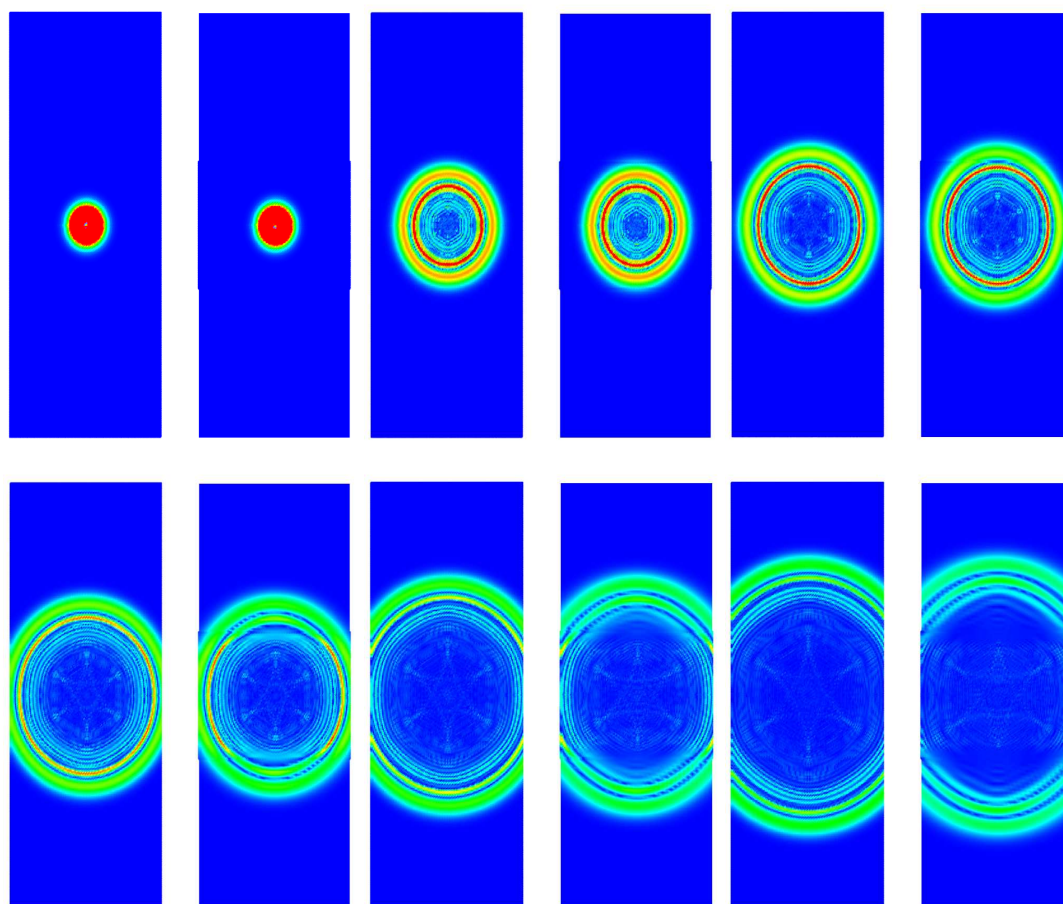
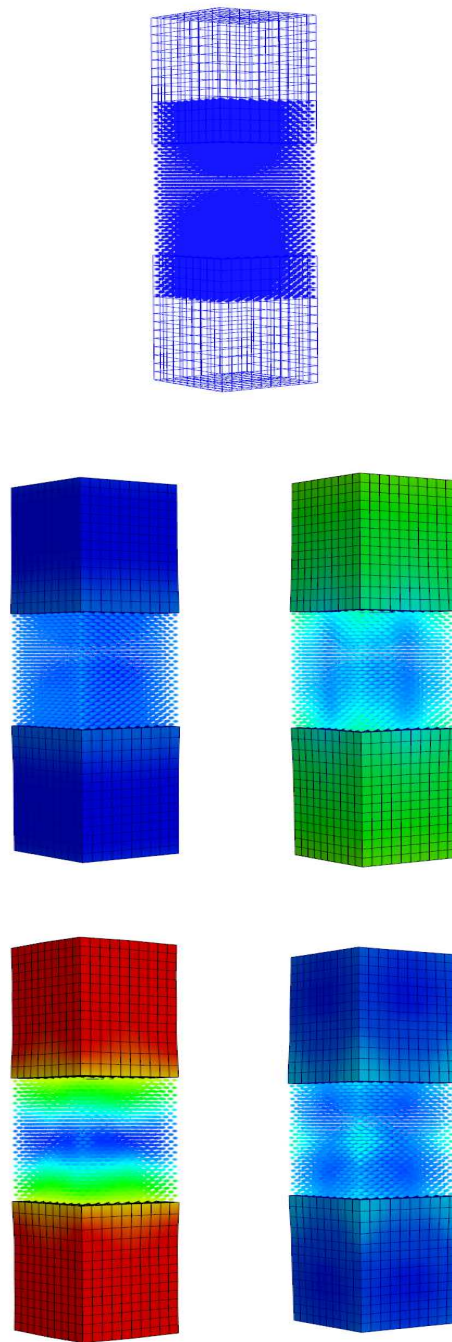Figure 6.11: *Comparing the weak coupling method with constraints. Left: pure MD. Right: coupling with damping.*

Figure 6.12: *A 3d example of the weak coupling method with constraints: External vertical forces are applied.*
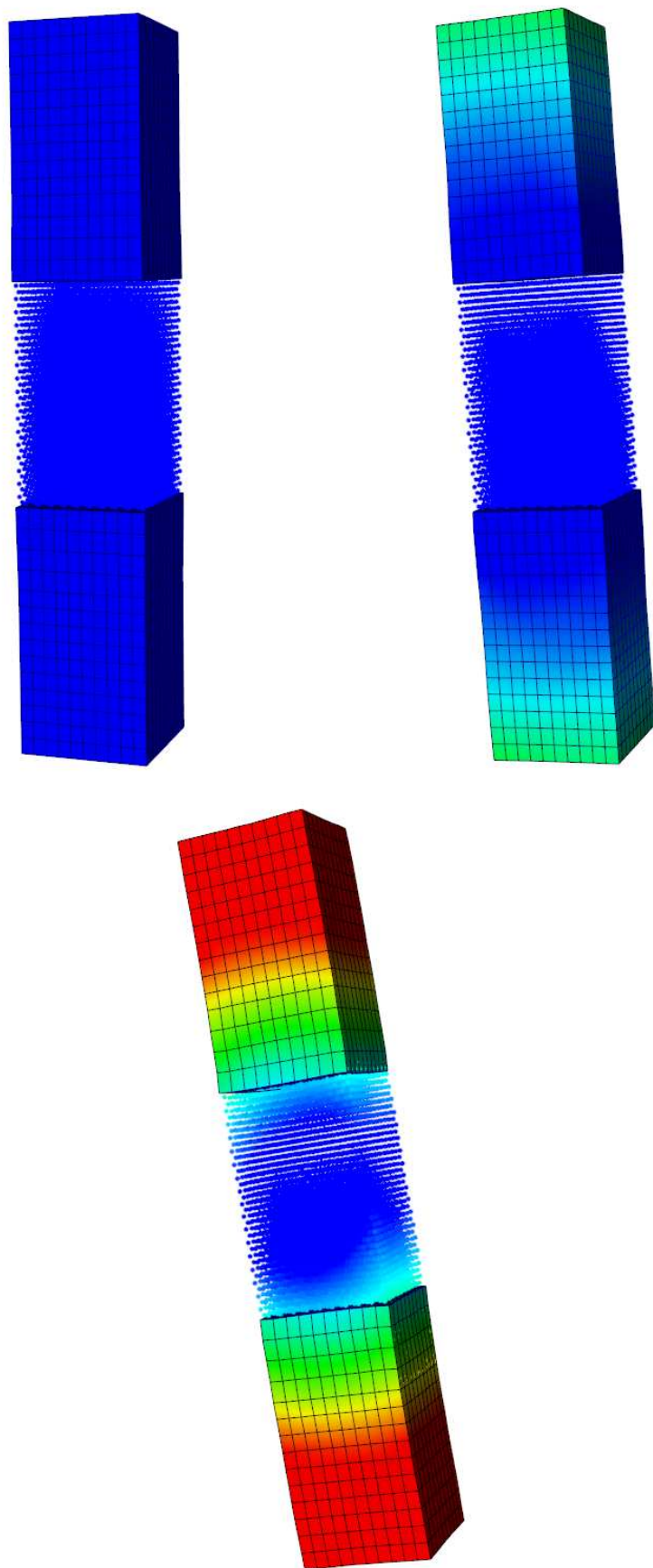
Figure 6.13: *A 3d example of the weak coupling method with constraints.*

Bibliography

[aBKvS90] B. an Beest, G. Kramer, and R. van Santen. Force-fields for Silicas and Alu-minophosphates Based on Ab-initio Calculation. *Phys Rev. Lett.*, 64(16):1955–1958, 1990.

[Abr86] F.F. Abraham. Computational Statistical Mechanics-Methodology, Applications and Supercomputing. *Adv. Phys.*, 35(1):1–111, 1986.

[ACR06] G. Anciaux, O. Coulaud, and J. Roman. High Performance Multiscale Simulation or Crack Propagation. In *Proceedings of the 2006 International Conference on Parallel Processing Workshops (ICPPW'06)*, 2006.

[ACRZ08] G. Anciaux, O. Coulaud, J. Roman, and G. Zerah. Ghost Force Reduction and Spectral Analysis of the 1D Bridging Method. Technical report, INRIA, 2008.

[AD74] S.A. Adelman and J.D. Doll. Generalized Langevin Equation Approach for atom/soild-surface Scattering: Colinear atom/harmonic Chain Model. *J. Chem. Phy*, 61:4242–4245, 1974.

[Ada75] R. Adams. *Sobolev Spaces*. Academic Press, 1975.

[AG05] M. Arndt and M. Griebel. Derivation of Higher Order Gradient Continuum Models from Atomistic Models for Crystaline Solids . *Multiscale Mod. Sim.*, 4(2):531–562, 2005.

[AWG$^+$02] F.F. Abraham, R. Walkup, H. Gao, T.D. de la Rubia, and M. Seager. Simulating Materials Failure by Using up to one Billion Atoms and the World's Fastes Computer. *Proc. Nat. Acad. Sci. USA*, 99(9):5783–5787, 2002.

[Bab73] I. Babuška. The Finite Element Method with Lagrangian Multipliers. *Numer. Math.*, 20:179–192, 1973.

[BABK99] J. Broughton, F. Abraham, N. Bernstein, and E. Kaxiras. Concurrent Coupling of Length Scales: Methodology and Application. *Phys. Rev. B*, 60:2391–2403, 1999.

[BBJ$^+$97] P. Bastian, K. Birken, K. Johannsen, S. Lang, N. Neuss, H. Rentz-Reichert, and C. Wieners. UG - A flexible software toolbox for solving partial differential equations. In *Computing and Visualization in Science*, pages 27–40, 1997.

[BCC$^+$04] P. Bochev, M. Christon, S. Collins, R. Lehoucq, J. Shadid, A. Slepoy, and G. Wagner. A Mathematical Framework for Multiscale Science and Engineering: The Variational Multiscale Method and Interscale Transfer Operators. Technical Report SAND 2004 - 2671, Sandia National Laboratories, 2004.

[BDH96] C. M. Barber, D. P. Dobkin, and H. Huhdanpaa. The Quickhull Algorithm for Convex Hulls. *ACM Trans. Math. Softw*, 22(4):469–483, 1996.

[Bel99] F. Ben Belgacem. The Mortar Finite Element Method with Lagrange Multipliers. *Numer. Math.*, 84(2):173–197, 1999.

[Ber94] J.P Berenger. A Perfectly Matched Layer for the Absorption of Electromagnetic Waves. *J. Comp. Phy*, 114:185–200, 1994.

[BF91] F. Brezzi and M. Fortin. *Mixed and Hybrid Finite Element Methods*. Springer Verlag, Berlin, 1991.

[BH54] M. Born and K. Huang. *Dynamical Theory of Crystal Lattices*. Oxford: Clarendon Press., 1954.

[BM97] I. Babuska and J.M. Melenk. The Partition of Unity Method. *Int. J. Num. Meth. Engrg.*, 40:727–758, 1997.

[BMP94] C. Bernardi, Y. Maday, and A.T. Patera. A new Nonconforming Approach to Domain Decomposition: The Mortar Element Method. In H. Brezis et al., editor, *Nonlinear partial differential equations and their applications. Collège de France Seminar, volume XI. Lectures presented at the weekly seminar on applied mathematics*, 299, pages 13–51. Harlow: Longman, scientific & technical pitman res. notes math. edition, 1994.

[BOK95] T. Belytschko, D. Organ, and Y. Krongauz. A Coupled Finite Element - Element-free Galerkin Method. *Comp. Mech.*, 17:186 – 195, 1995.

[BPO$^+$07] P.T. Bauman, S. Prudhomme, J.T. Oden, H. Ben Dhia, and N. Elkhodja. On the Application of the Arelquin method to the Coupling of Particle and Continuum Methods. Technical report, University Texas at Austin, 2007.

[Bra97] D. Braess. *Finite Element*. Springer, 1997.

[Bre74] F. Brezzi. On the Existence, Uniqueness and Approximation of Saddle-point Problems Arising from Lagrangian Multpliers. *R.A.I.R.O.*, R-2(8):129–151, 1974.

[Bri53] L. Brillouin. *Wave Propagation in Periodic Structures*. Dover Publications, Inc., 2. edition edition, 1953.

[BS89]   L.P. Bos and K. Salkauskas. Moving Least Squares are Backhus Gilbert Optimal. *J. Approx. Theory*, 59:267–275, 1989.

[BvK12]   M. Born and T. von Kármán. Über Schwingungen in Raumgittern. *Phys. Zeit.*, 13:297–309, 1912.

[BvK13]   M. Born and T. von Kármán. Über die Verteilung der Eigenschwingungen. *Phys. Zeit.*, 14:65–71, 1913.

[BX91]   J. H. Bramble and Jinchao Xu. Some Estimates for a Weighted L^2 Projection. *Mathematics of Computation*, 56:463–476, 1991.

[BX03]   T. Belytschko and S. P. Xiao. Coupling Methods for Continuum Model with Molecular Model. *Int. J. Multisc. Comp. Engrg.*, 1(1):115–126, 2003.

[CDBY00]   W. Cai, M. DeKoning, V.V. Bulatov, and S. Yip. Minimizing Boundary Reflection in Coupled-Domain Simulations. *Phys. Rev. Let.*, 85:3213–3216, 2000.

[CFL28]   R. Courant, K. Friedrichs, and H. Lewy. Über die partiellen Differenzengleichungen der mathematischen Physik. *Math. Annalen*, 100:32–74, 1928.

[Cia88]   P.G. Ciarlet. *Mathematical Elasticity; Volume 1: Three Dimensional Elasticity*. North-Holland, Amsterdam, 1988.

[Cle75]   P. Clement. Approximation by Finite Element Functions using Local Regularization. *Rev. Franc. Automat. Inform. Rech. Operat.*, 9(R-2):77–84, 1975.

[CM03]   W.A. Curtin and R.E. Miller. Atomistic/Continuum Coupling in Computational Materials Science. *Mod. Simul. Mater. Sci. Engrg.*, 11:R33–R68, 2003.

[CPW97]   J.S. Chen, C. Pan, and C.I. Wu. Large Defomation Analysis of Rubber based on a Reproducing Kernel Particle Method. *Comp. Mech.*, 19:211–227, 1997.

[CT01]   F. Collino and C. Tsogka. Application of the Perfectly Mateched Absorbing Layer Model to the Linear Elstodynamic Problem in Anisotropic Heterogeneous Media. *Geophys.*, 66(1):294–307, 2001.

[DB02]   P. Deuflhard and F. Bornemann. *Scientific Computing with Ordinary Differential Equations*. Springer, 2002.

[DK08]   T. Dickopf and R. Krause. Efficient simulation of multi-body contact problems on complex geometries: a flexible decomposition approach using constrained minimization. *Int. J. Num. Meth. Engrg.*, DOI: 10.1002/nme.2481, 2008.

[Doe74]   G. Doetsch. *Introduction to the Theory and Application of the Laplace Transformation*. Springer Verlag, 1974.

[EE03]   W. E. and B. Enquist. Multiscale Modeling and Computation. *Notices Am. Math. Soc.*, 50(9):1062–1070, 2003.

[ELVE04]   W. E., X. Li, and E. Vanden-Eijden. Some Recent Progress in Mutlsicale Modelling. In P. Koumoutsakos S. Attiner, editor, *Multiscale Modelling and Simualtion*, volume 39 of *LCSE*. Springer, 2004.

[FBNE98]   F.F.Abraham, J.Q. Broughton, N.Bernstein, and E.Kaxiras. Spanning the Continuum to Quantum Length Scales in a Dynamic Simulation of Brittle Fracture. *Europhys. Lett*, 44(6):783–787, 1998.

[FMH02]   S.F. Fernández-Méndez and A. Huerta. Coupling finite elements and particles for adaptivity: An application to consistntly stabilized convection-diffusion. In M. Griebel and M.A. Schweitzer, editors, *Meshfree Methods for partial differential equations*, volume 26 of *Lecture Notes in Computational Science and Engineering*, pages 117 – 129. Springer-Verlag, Berlin, 2002.

[For77]   M. Fortin. An Analysis of the Convergence of Mixed Finite Element Methods. *RAIRO Anal. Numer.*, 11:341–354, 1977.

[FT02]   G. Friesecke and F. Theil. Validity and Failure of the Cauchy-Born Hypothesis in a Two-Dimensional Mass-Spring Lattrice. *J. Nonlinear Sci.*, 12:445–478, 2002.

[GB07]   P.A. Guidault and T. Belytschko. On the L^2 and H^1 Coupling Techniques for an Overlapping Domain Decomposition Method Using Lagrange Multipliers. *Int. J. Num. Meth. Engrg.*, 70:322–350, 2007.

[GH04]   M. Griebel and J. Hamaekers. Molecular dynamics simulations of the elastic moduli of polymer-carbon nanotube composites. *Computer Methods in Applied Mechanics and Engineering*, 193(17–20):1773–1788, 2004.

[GH06]   M. Griebel and J. Hamaekers. Molecular Dynamics Simulations of the Mechanical Properties of Polyethylene-Carbon Nanotube Composites. In M. Rieth and W. Schommers, editors, *Handbook of Theoretical and Computational Nanotechnology*, volume 9, chapter 8, pages 409–454. American Scientific Publishers, 2006.

[GKZ07]   M. Griebel, S. Knapek, and G. Zumbusch. *Numerical Simulation in Molecular Dynamics*. Springer, Berlin, Heidelberg, 2007.

[GKZC04]   Michael Griebel, Stephan Knapek, Gerhard Zumbusch, and Attila Caglar. *Numerical Simulation in the Dynamics of Molecules. Numerics, Algorithms, Parallelization, Applications. (Numerische Simulation in der Moleküldynamik. Numerik, Algorithmen, Parallelisierung, Anwendungen.)*. Berlin: Springer , 2004.

[HFML04]   A. Huerta, S. Fernández-Méndez, and W.K. Liu. A Comparison of two Formulations to Blend Finite Elements and Mesh-free Methods. *Appl. Mech. Engrg.*, 193:1105– 1117, 2004.

[HFMQ98]   T. Hughes, G. Feijoo, J. Mazzei, and J. Quincy. The Variational Mutiscale Method - A Paradigm for Computational Mechanics. *Comput. Meth. Appl. Mech.*, 166:3–24, 1998.

[Hir88]   C. Hirsch. *Numerical Computations of Internal and External Flows, Vol. 1*. Wiley interscience, 1988.

[Hir90]   C. Hirsch. *Numerical Computations of Internal and External Flows, Vol. 2*. Wiley interscience, 1990.

[HLW02]   E. Haier, C. Lubich, and G. Wanner. *Geometric Numerical Integration*. Springer, 2002.

[HZ98]   H. Hofer and E. Zehnder. *Symplectic Invariants and Hamiltonian Dynamics*. Birkhäuser Verlag, 1998.

[KGF91]   S. Kohlhoff, P. Gumbsch, and H.F. Fischmeister. Crack Propagation in BCC Crystals Studied with a Combined Finite- Element and Atomisitc Model. *Phil Mag A*, 64:851–878, 1991.

[Kit06]   C. Kittel. *Einführung in die Festkörperphysik*. Oldenburg, 2006.

[KLPV01]   C. Kim, R. D. Lazarov, J. E. Pasciak, and P. S. Vassilevski. Multiplier Spaces for the Mortar Finite Element Method in three Dimensions. *SIAM J. Numer. Anal*, 39(2):519–538, 2001.

[Kra09]   D. Krause. A Parallel Approach to Multiscale Simulations in Fracture Mechanics. Master's thesis, Institute for Numerical Simulation, University Bonn, 05/2009.

[KWL05]   E. G. Karpov, G. J. Wagner, and Wing Kam Liu. A Green's Function Approach to Deriving Non-Reflecting Boundary Conditions in Molecular Dynamics Simulations. *Int. J. Num. Meth. Engrg.*, 62(9):1250–1262, 2005.

[LE05]   X. Li and W. E. Variational Boundary Copnditions for Molecular Dynamics Simulatiuons of Solids at Low Temperature. Technical report, University Pennsylvania, 2005.

[LE06]   X. Li and W. E. Variational Boundary Conditions for Molecular Dynamics Simulation of Solids at Low Temperature. *Comm. Comput. Phys.*, 1(1):135–175, 2006.

[LJ24]   J.E. Lennard-Jones. On the Determination of Molecular Fields. II. Form the of State of a Gas. *Proc. Roy. Soc. London A*, 106:463–477, 1924.

[LJL⁺95] W.K. Liu, S. Jun, S. Li, J. Adee, and T. Belytschko. Reproducing Kernel Particle Methods for Strucural Mechanics. *Int. J. Num. Meth. Engrg.*, 38:1655–1679, 1995.

[LJZ95] W.K. Liu, S. Jun, and Y.F. Zhang. Reproducing Kernel Particle Methods. *Int. J. Numer. Meth. Fluids*, 20:1081–1106, 1995.

[LKP06] W.K. Liu, E.G. Karpov, and H.S. Park. *Nano Mechanics and Materials*. Wiley, 2006.

[LLAT06] S. Li, X. Liu, A. Agrawal, and A. To. Perfectly Matched Multisclae Simulations for Discrete Lattice Systems: Extension to Multiple Scales. *Phy. Rev.*, 74(B):045418, 2006.

[LM72] J.-L. Lions and E. Magenes. *Nonhomogeneous Boudary Value Problems and Applications*, volume 1. Springer, 1972.

[LR04] B. Leimkuhler and S. Reich. *Simulating Hamiltonian Dynamics*. Cambridge University Press, 2004.

[LRS96] B. Leimkuhler, S. Reich, and R.D. Skeel. Integration Methods for Molecular Dynamics. In *IMA Volumes in Mathematics and its Applications*, volume 82, pages 161–186. Springer Verlag, 1996.

[LS81] P. Lancaster and K. Salkauskas. Surfaces Generated by Moving Least Squares Methods. *Math. Comp.*, 37:141–158, 1981.

[MD82] M. Mullins and M.A. Dokainish. Simulation of the (001) Plane Crack in α-iron Employing a New Boundary Scheme. *Phil Mag A*, 46:771–787, 1982.

[MH06] F. Magouls and I. Harari. Absorbing Boundary Conditions . *Special issue of Comp. Meth. in App. Mech. Engrg*, 195:352 pp, 2006.

[MT02] R.E. Miller and E.B. Tadmor. The Quasicontinuum Method: Overview, Applications and Current Directions. *Journal of Comp Aided Mat Design*, 9:203–239, 2002.

[MT04] R.E. Miller and E.B. Tadmor. QC Tutorial Guide Version 1.1. Technical report, `http://www.qcmethod.com`, Tutorial (2004).

[Mul84] M. Mullins. Computer Simulation of Fracture Using Long Range Pair Potentials. *Acta metall.*, 32:851–878, 1984.

[Mur81] G. Mur. Absorbing Boundary Conditions for the Finite-difference Approximation of the Time-domain Electromagnetic Field Equations. *IEEE Trans. Electromagn. Compat.*, 23:377–382, 1981.

[Nos84]   S. Nosé. A Unified Formulation of the Constant Temperature Molecular Dynamics Method. *J. Chem. Phys*, 81:511–519, 1984.

[OIea96]   E. Onate, S. Idesohn, and O.C. Zienkiewicz et al. A Stabilized Finite Point Method for Analysis of Fluid Mechanics Problems. *Comp. Methods Appl. Mech. Engrg.*, 139:315–346, 1996.

[PL04]   H.S. Park and W.K. Liu. An Introduction and Tutorial on Multiple Scale Analysis in Solids. *Comp. Meth. Appl. Mech. Eng.*, 193:1733–1772, 2004.

[PS85]   F. Preparata and M. Shamos. *Computational Geometry*. Springer, New York, 1985.

[QV99]   A. Quarteroni and A. Valli. *Domain Decomposition Methods for Pratial Differential Equations*. Oxford Science Publications, 1999.

[Rah64]   A. Rahman. Correlations in the Motions of Atoms in Liquid Argon. *Phys Rev.*, 136:A405–A411, 1964.

[RB98]   R.E. Rudd and J.Q. Broughton. Coarse-Grained Molecular Dynamics and the Atomic Limit of Finite Elements. *Phys. Rev. B*, 58:5893–5896, 1998.

[RB05]   R.E. Rudd and J.Q. Broughton. Corase-grained Moelcular Dynamics: Nonlinear Finite Elements and Finite Temperature. Technical report, Livermore, 2005.

[SABW82]   W.C. Swope, H.C. Anderson, P.H. Berens, and K.R. Wilson. A Computer Simulation Method for the Calculation of Equilibrium Constants for the Formation of Physical Clusters of Molecles: Application of Small Water Clusters. *J. Chem. Phys*, 76:637–649, 1982.

[Sch70]   H. A. Schwarz. Gesammelte mathematische Abhandlungen. *Vierteljahrsschrift der Naturforschenden Gesellschaft Zürich*, 15:272–286, 1870.

[Sch03]   M. A. Schweitzer. *A Parallel Multilevel Partition of Unity Method for Elliptic Partial Differential Equations*. Number 29 in LNCSE. Springer, 2003.

[SGHH78]   J. Sinclair, P.C. Gehlen, R.G. Hoagland, and J.P. Hirth. Flexible Boundary Conditions and Nonlinear Geometric Effects in Atomic Dislocation Modelling. *J. Appl. Phys*, 49(7):3890–3897, 1978.

[She68]   D. Shepard. A two-dimensional Function for Irregularly Spaced Data. In *ACM National Conference*, pages 517–524, 1968.

[Sin71]   J. Sinclair. Improved Atomistic Model of a bcc Dislocation Core. *J. Appl. Phys*, 42(13):5321–5329, 1971.

[Sri97]   M. Sringborg. *Density-Functional Methods in Chemistry and Materials Science*. Wiley research series in Theoretical Chemistry, 1997.

[Ste70]   E. Stein. *Singular Integrals and Differentiability Properties of Functions*. Princeton University Press, 1970.

[TL05]   A.C. To and S. Li.   Perfectly matched multiscale simulation.   *Phy Rev. B*, 72:035414–1 – 8, 2005.

[Tsy98]   S. V. Tsynkov. Numerical Solution of Problems on Unbounded Domains. A Review . *Appl. Numer. Math.*, 27:465–532, 1998.

[TW05]   A. Toselli and O. Widlund. *Domain Decomposition Methods*. Springer, 2005.

[TZCT92]   R. Thomson, S.J. Zhou, A.E. Carlsson, and V.K. Tewary. Lattice Imperfections Studied by Use of Lattice Green's Function. *Rhys. Rev. B, Condens Matter*, 46(17):10613–10643, 1992.

[Ver67]   L. Verlet.   Computer Expermiments on Classical Fliuds I: Thermodynamical Properties of Lennard Jones Molecules. *Phys Rev.*, 159:98–103, 1967.

[WL01]   G.J. Wagner and W.K. Liu.   Hierarchical Enrichment for Bridging Scales and Mesh-free Boundary Conditions. *Int. J. Num. Meth. Engrg.*, 50:507–524, 2001.

[WL03]   G.J. Wagner and W.K. Liu.   Coupling of Atomistic and Continuum Simulations Using a Bridging Scale Decomposition. *J. Comp. Phy.*, 190:1261–1289, 2003.

[Wlo82]   J. Wloka. *Partielle Differentialgleichungen*. Tuebner Verlag Stuttgart, 1982.

[XB04]   S.P. Xiao and T. Belytschko. A Bridging Domain Method for Coupling Continua with Molecular Dynamics. *Comp. Meth. Appl. Mech. Engrg.*, 193:1645–1669, 2004.

[XCP02]   X.Blanc, C.LeBris, and P.Lions. From Molecular Models to Continuum Mechanics. *Arch. Ration. Mech. Anal.*, 164(4):341–381, 2002.

[YL06]   J. Z. Yang and X. Li. Comparative Study of Boundary Conditions for Molecular Dynacmis Simulations of Solids at Low Temperature. *Rhys. Rev. B*, 73:224111, 2006.